NORTHWESTERN UNIVERSITY

Nanostructured Membrane Catalysis

A DISSERTATION

SUBMITTED TO THE GRADUATE SCHOOL

IN PARTIAL FUFILLMENT OF THE REQUIREMENTS

For the degree

DOCTOR OF PHILOSOPHY

Field of Chemistry

By

Hao Feng

EVANSTON, ILLINOIS

December 2007

ABSTRACT

Nanostructured Membrane Catalysis

Hao Feng

This thesis summarizes our research efforts on the application of the nano-structured anodic aluminum oxide (AAO) membrane in heterogeneous catalysis. Procedures for growing the AAO membrane in the center of an aluminum disc have been developed by appropriately masking the disk's perimeter during the anodization and etching steps. The remaining aluminum ring connects seamlessly to the AAO and serves as a support for the membrane. The supported AAO membrane can be sealed in a flow reactor so that the nanopores on the membrane function as a parallel array of tubular reactors. Coating catalytically active materials onto the walls of the nanopores turns the AAO membrane into a novel catalytic system. In the cyclohexane oxidative dehydrogenation (ODH) reaction, the membrane catalytic system demonstrates advantages over the conventional powder bed in terms of overcoming bypass and diffusion limitations, reducing over oxidation, and inhibiting undesired gas phase reactions.

The ordered one-dimensional nanopores make the AAO membrane an ideal substrate for

fabrication of catalysts by atomic layer deposition (ALD). The catalytic performances of vanadium oxide (VOx) catalysts deposited on the membranes by ALD and by incipient wetness impregnation are compared in the ODH of cyclohexane. The ALD VOx show higher activity than the impregnated VOx, which reflects the better dispersion of the catalytic species as synthesized by ALD. In the same range of VOx loadings, distinct catalytic activities resulting from different structures of the catalytic sites are more evident on the samples prepared by multiple cycles of ALD, implying that the form of the supported catalyst can be better controlled by applying the ALD technique.

The ODH of cyclohexane is studied in detail over the ALD synthesized VOx catalysts. At low loadings of the catalyst, the supported VOx are mostly in the isolated state; the polyvanadate domains are formed as the vanadium content increases. In the cyclohexane ODH reaction, the polyvanadate sites are shown to be more active than the monovanadate sites; while the isolated VOx are more selective to the olefin. The performance of various VOx catalysts is explained by the different chemical properties of the catalytic sites due to their structural differences.

I express my most sincere gratitude to …

.. Professor Peter C. Stair, my advisor, for providing me the opportunity to join this research project and for his guidance and support throughout my PhD study. His vision, wisdom and experience helped me learn how to be a qualified researcher. His kindness and consideration helped me go though the hard times when I was facing life determining decisions.

.. Dr. Hsien-Hau Wang for giving me guidance and help at the beginning phase of the project, and for his care and concern about my life.

.. Professor Harold Kung and Mayfair Kung for their help with heterogeneous reactions. I learned a lot about designing reaction systems, installing pipelines, interpreting catalysis data and catalysis lab safety regulations from them.

.. Dr. Michael Pellin, Dr. Larry Curtiss, Dr. Christopher Marshall, and Dr. Lennox Iton for contributing excellent ideas and meaningful discussions about the project.

.. Dr. Guang Xiong for teaching me running heterogeneous catalysis experiments.

.. Dr. Jeffrey Elam and Dr. Joseph Libera for pleasant collaborations on the ALD catalyst synthesis and XRF characterization.

.. Dr. Yurong (Catherine) Han for teaching me the AAO synthesis and characterization techniques.

.. Professor Randall Snurr and Dr. Simon Albo for collaboration on the numerical simulation work.

.. Professor Tobin Marks and Dr. Aswini Dash for collaboration on the vanadium cluster compound synthesis and contribution of ideas and useful discussions in the poisoning experiment.

.. Dr. Zili Wu, Dr. Hack-sung Kim and Dr. Stephanie Mucherie for their share of experiment data on catalyst characterizations and on butane and propane ODH.

.. Professor Richard Van-duyne, Professor Eric Weitz, and Professor Kenneth Poeppelmeier for attending my examination board.

.. all members of the Stair group for their help and care during my life at Northwestern University.

.. my wife Yi Zhang and my parents for their ongoing support and motivation.

.. the Chemistry Department and the Institute of Catalysis and Surface Science of Northwestern University for the financial support.

.. the ASL, NUANCE, and KECK facilities at Northwestern University and the EMC and APS facilities at Argonne National Lab for allowing me to use their state-of-the-art instruments.

Table of Contents

Abstract 2

Acknowledgements 4

Table of Contents 6

List of Figures 10

List of Tables 16

Chapter 1. Background 17

1.1 Nanostructured Catalytic Membrane 17

1.2 Fabrication of the AAO Membranes by ALD 20

1.3 Application of the Nanostructured Catalytic Membrane in Oxidative Dehydrogenation Reactions 24

1.3.1 Selective Oxidation of Alkanes to Produce Oleins 25

1.3.1.1 Redox catalysis 28

1.3.1.2 Non-redox catalysis 30

1.3.1.3 Noble metal catalysis 31

1.3.2 The ODH of Cyclohexane 31

1.4 Aim of the Work 33

Chapter 2. Experimental Details 34

2.1 Overview 34

2.2 Materials Used 34

2.3 Membrane Synthesis 35

2.4 Catalyst Preparation 39

2.5 Catalytic Measurements 40

2.6 Poisoning Experiment 42

2.7 Characterization 44

2.7.1 Characterization on the AAO membrane 44

2.7.2 Characterization on the VOx catalyst 46

Chapter 3. Properties of the Nanostructured Catalytic Membranes 48

3.1 Overview 48

3.2 Discussions 48

3.2.1 The Nano-scale Structure of the AAO Membrane 48

3.2.2 Effects of Preparation Conditions 52

3.2.3 Impurities Incorporated in the AAO Membrane 57

Chapter 4. Building Nano Reactor Arrays 64

4.1 Overview 64

4.2 Discussions 65

4.2.1 The AAO Membrane Embedded in Aluminum Ring Support 65

4.2.2 Catalytic Performance: Membrane VS Powder 69

4.2.3 Performance Function of the Nano Reactor Arrays 74

Chapter 5. Catalytic Performances of Vanadium Oxides Supported on the AAO Membranes 80

5.1 Overview 80

5.2 Discussions 81

5.2.1 The VOx supported on the AAO membranes 81

5.2.2 Catalytic properties of the VOx supported on the AAO membranes 87

Chapter 6. Structure-Function Relationship of the Vanadium Oxide Catalysts Supported on the AAO Membrane 98

6.1 Overview 98

6.2 Discussions 99

6.2.1 Composition and structure of the ALD VOx catalysts 99

6.2.2 Analyses on the catalytic activity 104

6.2.3 Analyses on selectivity and reaction paths 111

6.2.4 Effects of the support 128

Chapter 7. Other Topics Related to Nanostructured Catalytic Membrane Research 132

7.1 Catalytic Performances of the Vanadium Containing Organometallic Clusters Grafted on AAO Membranes 132

7.1.1 Introduction 132

7.1.2 Results and Discussions 133

7.2 Asymmetric Catalytic Stripes inside the Nanopores 137

7.2.1 Introduction 137

7.2.2 Experimental, Results and Discussions 139

Chapter 8. Counting the Active Sites through Partially Poisoning the Catalyst in a Heterogeneous System 143

8.1 Introduction 143

8.2 Discussions 144

Chapter 9. Summary 154

References 161

Vita 166

List of Figures

Chapter 1

Fig 1.1 The schematic picture and SEM image of the AAO membrane……....**18**

Fig 1.2 (a). The push-through flow mode and the sweep flow mode in a membrane reactor. (b). Different pore structures and catalysts locations……**19**

Fig 1.3 The ALD of alumina……..**21**

Fig 1.4 ALD fabrication on the AAO membrane: tuning the pore size…….**22**

Fig 1.5 Elements and Compounds that can be coated by ALD……..**24**

Fig 1. 6 Fabrication of the AAO membrane by ALD…….……**24**

Fig 1.7 The ODH of propane over VOx supported on Al_2O_3……..…...**28**

Fig 1. 8 Effects of VOx surface density on ODH rates…….…..……**29**

Fig 1.9 The cyclohexane ODH reaction network…….……..…...**32**

Chapter 2

Fig 2.1 Preparation of the free standing AAO membranes…….**37**

Fig 2.2 (a). The dissembled anodization cell. (b). Anodization of the aluminum disc. (c). photo of the AAO/aluminum ring support……...…….**38**

Fig 2.3 The membrane reactor configuration and cyclohexane ODH reaction system……..**42**

Fig 2.4 The poisoning experiment setup…….**43**

Chapter 3

Fig 3.1 Schematic picture of the nanopores on the AAO Membrane…….**49**

Fig 3.2 The SAXS pattern and 1-D Q value curve obtained from the AAO membrane……**51**

Fig 3.3 The linear correlation between the cell size and anodization potential……..……**53**

Fig 3.4 The AAO membrane made with oxalic acid and sulfuric acid solution……..……..**53**

Fig 3.5 The regularity of nanopores on the membrane……..…….**57**

Fig 3.6 XRD pattern of the AAO membrane……..…….……**58**

Fig 3.7 Raman spectrum of the AAO membrane (prepared with oxalic acid solution) and that of the aluminum oxalate powder…….……**59**

Fig 3.8 Raman spectra of the AAO membranes prepared with oxalic acid and sulfuric acid solution……..……..**59**

Fig 3.9 The TGA of the AAO prepared with oxalic acid and sulfuric acid solutions…….……**60**

Fig 3.10 The Raman spectra of the AAO membrane (prepared with oxalic acid solution) after calcinations at different temperatures…….**61**

Fig 3.11 The XPS of the AAO membrane synthesized with sulfuric acid solution……**62**

Fig 3.12 The EPR spectra of the AAO membranes……...…….**63**

Chapter 4

Fig 4.1 SEM pictures of the AAO/aluminum boundaries on the front (anodized) side……...…..**66**

Fig 4.2 SEM pictures of the AAO/aluminum boundaries on the backside…….....**67**

Fig 4.3 The configuration of the AAO/Aluminum connection…….……..**67**

Fig 4.4 The supported AAO membrane sealed in a VCR fitting as a gasket…….....**68**

Fig 4.5 The conductance of the AAO membrane measured with oxygen and helium……...…**69**

Fig 4.6 The catalytic performance comparison between the sealed membrane and the grinded membrane……...…….**71**

Fig 4.7 Comparison between the membrane catalytic system and the powder bed……..…….**74**

Fig 4.8 The mass balance in an elementary section of the nanopore…….……..……...**77**

Fig 4.9 The dependence of conversion on residence time (1/flow rate)……..……...**79**

Chapter 5

Fig 5.1 The UV-Vis absorption spectra of the ALD and the wet impregnated VOx supported on the AAO membranes……...……**85**

Fig 5.2 The conversion curves and the product distribution charts of 1 cycle, 2 cycles, and 4 cycles of the ALD VOx supported on the AAO membranes……..……**89**

Fig 5.3 The conversion curves and the product distribution charts of the monolayer, 2 layers, and 4 layers of the wet impregnated VOx supported on the AAO membranes……..…….....**90**

Fig 5.4 The TOF of the VOx supported on the AAO membranes…….……**91**

Fig 5.5 The reaction rates (cyclohexane conversions) at different concentrations of cyclohexane and oxygen…….……...…..**95**

Fig 5.6 The Arrenhius plots of the ALD and the impregnated VOx supported on the AAO membranes……..**97**

Chapter 6

Fig 6.1 The vanadium surface densities at different cycles of the ALD loading……..…**100**

Fig 6.2 V surface density: ICP results vs XRF results……..……**100**

Fig 6.3 The UV-Vis absorption spectra of the ALD VOx……...……..**103**

Fig 6.4 The edge energies of the ALD VOx supported on the AAO membranes compared to those of the reference compounds measured by Gao and Wachs…….....**104**

Fig 6.5 The conversions of the ALD VOx supported on the AAO membranes in the ODH of cyclohexane…….....**105**

Fig 6.6 The TOF of the membrane supported ALD VOx samples at 450°C……**107**

Fig 6.7 The Arrhenius plots of the ALD VOx supported on the AAO membranes……..**111**

Fig 6.8 The product distribution charts of the ALD VOx supported on the AAO membranes in the ODH of cyclohexane……..…..**113**

Fig 6.9 The cyclohexane ODH reaction diagram: the C-H breaking process and the C-C breaking process……..**114**

Fig 6.10 The C_6H_{10} selectivity versus C_6H_{12} conversion curve of the ALD VOx supported on the AAO membranes……**116**

Fig 6.11 The C_6H_{10} yield versus C_6H_{12} conversion curve of the ALD VOx supported on the AAO membranes…….....**116**

Fig 6.12 The C_6H_{10} yield versus C_6H_{12} conversion curves of the selected ALD VOx samples measured at different temperatures and at different reagent flow rates……...**117**

Fig 6.13 The conversions of C_6H_{12}, C_6H_{10} and C_6H_6 under the same experiment conditions over the 2-cycle ALD VOx supported on the AAO membrane……...……..….**121**

Fig 6.14 The conversions of C_6H_{12}, C_6H_{10} and C_6H_6 under the same experiment conditions over the 8-cycle ALD VOx supported on the AAO membrane……**122**

Fig 6.15 The cyclohexane ODH selectivity pattern over the 2-cycle ALD VOx supported on the AAO membrane. a.) The estimated cyclohexane ODH selectivity pattern based on the 100% consecutive path assumption. b.) The actual cyclohexane ODH selectivity pattern measured from the reaction……**124**

Fig 6.16 The cyclohehxane ODH selectivity pattern over the 2-cycle ALD VOx supported on the AAO membrane a.) The estimated cyclohexane ODH selectivity pattern showing only the products from the consecutive path. b.) The actual cyclohexane ODH selectivity pattern showing contributions from both the sequential path and parallel paths……..**125**

Fig 6.17 The cyclohehxane ODH selectivity pattern over the 8-cycle ALD VOx supported on the AAO membrane. a.) The measured cyclohexane ODH selectivity pattern. b.) The selectivity pattern showing contributions from both the sequential path and parallel paths……**126**

Fig 6.18 The TOF and the Arrhenius plots of the 2 cycles of ALD VOx supported on the ALD Al_2O_3, TiO_2, and Nb_2O_5 fabricated AAO membranes……..**129**

Chapter 7

Fig 7.1 Organometallic V clusters and their grafting onto the AAO membrane……..…..**133**

Fig 7.2 The conversion and selectivity of V clusters supported on the ALD fabricated AAO membranes at 450 °C in the ODH of cyclohexane…….**134**

Fig 7.3 The conversion and selectivity of 1 ML of $V_4(\mu\text{-}O)_6Cp_4$ cluster supported on the TiO_2 fabricated AAO membrane in the ODH of cyclohexane…….....…**136**

Fig 7.4 Simulation results on the fraction of hits at different locations of the pore walls……**139**

Fig 7.5 Control the direction of reactant flow through the membrane reactor…….……....**140**

Fig 7.6 Effects of the reactant flow direction on the conversion of a membrane sample with asymmetrically loaded catalytic stripe…….……...**141**

Chapter 8

Fig 8.1 The proposed poisoning mechanism of the supported VOx…….....**145**

Fig 8.2 The change in catalytic activity after a dose of poison injection…….……**146**

Fig 8.3 The titration poisoning curve on 12C ALD VOx…….…….....**147**

Fig 8.4 Logarithm of the titration poisoning curve where a linear relationship is evident…....**149**

Fig 8.5 The titration poisoning curve on the $V_4(\mu\text{-}O)_6Cp_4$ cluster…….....……**150**

Fig 8.6 The change in selectivity during the poisoning process…….....**153**

Fig 8.7 The changes in yields to different products during the poisoning process……...…**153**

List of Tables

Chapter 5

Table 5.1 The loadings of ALD VOx measured by XRF……..…….**83**

Table 5.2 The edge energies of the ALD and the impregnated VOx supported on the AAO membranes…….…….**85**

Table 5.3 The activation energies of the wet impregnated and ALD VOx supported on the AAO membranes…….…….**97**

Chapter 6

Table 6.1 The loadings of the VOx measured by XRF and ICP.……**100**

Table 6.2 The edge energies of the ALD VOx supported on the AAO membranes……..……**104**

Table 6.3 The selectivity in the oxidation reaction of C_6H_{10} and C_6H_6 over the 2-cycle ALD VOx supported on the AAO membrane…….……..**111**

Table 6.4 The selectivity in the oxidation reaction of C_6H_{10} and C_6H_6 over the 8-cycle ALD VOx supported on the AAO membrane……...……..……**122**

Chapter 7

Table 7.1 Activation energies of V clusters in the ODH of cyclohexane…….……**134**

Chapter 1

1. Background

1.1 Nanostructured Catalytic Membrane

The porous anodized aluminum oxide (AAO) membrane features a highly ordered array of straight nanopores (Fig 1.1). For the last half a century this material has been widely used as micro filters, anti corrosion barrier layers and as substrates for various coatings. [1-4] In recent years, the AAO membrane has found many more applications in the nano fabrication field because the ordered nanopores form an ideal template for synthesizing a variety of nano structures. [5-7] However, the application of the AAO membrane as the framework for catalysts remains an intriguing but little investigated area. The functionality of a heterogeneous catalyst depends critically on its structure over a range of length scales. [8, 9] At the length scale of 10's to 1000's of nanometers, the dimensions and topology of the catalyst pore structure can influence reagent flow, the sequencing of catalytic active sites, and the contact time between reagents and catalyst. [10] Conceptually, the AAO membrane consists of an assembly of identical pores having nanometer dimensions that span a flow reactor so as to produce an array of nanoreactors. With this assembly, each reagent molecule must traverse an identical pore and, ideally, each diffusion path can be engineered through control over the pore diameter, wall composition, and length. This results in more uniform and tunable contact times than are

possible with a conventional fixed bed powder catalyst.

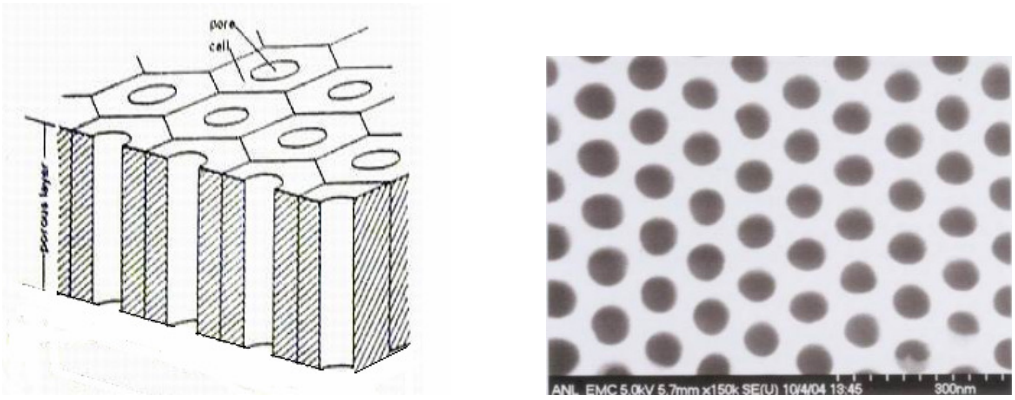

(a) **(b)**

Fig 1.1 The schematic picture (a) [11] and SEM image (b) of the AAO membrane

Other than the finer control over the diffusion path and the contact time, this catalytic system also provides a number of additional possibilities. Another feature of this membrane catalytic system is the possibility to study the influence of reagent delivery to the membranes on catalytic performance. For example, with an asymmetric reactor it is possible to deliver two reagents on opposite sides of the membrane structure or to sweep reactants or products away from the entrance and exit of the membrane (as pictured in Fig 1.2-a) in order to control the flow of molecules that enter and exit the membrane. Catalytic results from such experiments may be a valuable test of theoretical predictions regarding the location of catalytic transformations in the pores. Furthermore, the influence of the flow pattern in the nanopores on the catalytic performance can also be studied. Using atomic layer deposition (ALD), the sizes and shapes of the nanopores can

be precisely tuned. By controlling the preparation conditions, it is even possible to synthesize asymmetric membranes with pores of different diameters and compositions open on the two sides. [12] Since the dimensions of the nanopores significantly influence the flow pattern of the reagents inside the pores, a measure of control over the catalytic properties of the membrane system can be achieved. [13] We can also investigate how the spatial location of the catalytically active materials in the pores influences the catalytic performance. For example, it is possible, using ALD diffusion techniques, to locate the catalytic material at the entrance or exit to the pores or even to arrange the catalytic material as a series of bands down the pore. Similarly, the formation of a controlled sequence of different catalytic materials is a topic of interest. Schematic pictures of some catalytic structures of interest are depicted in Fig 1.2-b.

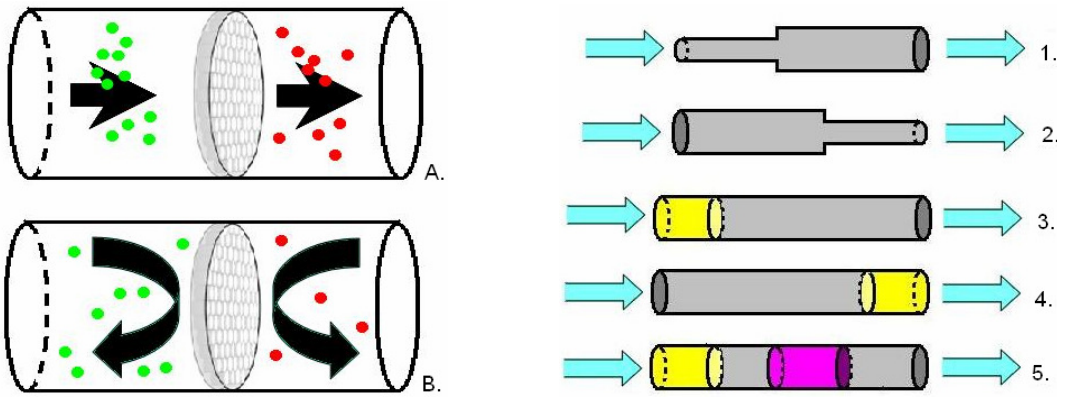

(a) **(b)**

Fig 1.2 (a). The push-through flow mode (A) and the sweep flow mode (B) in a membrane reactor. (b). Different pore structures and catalysts locations: asymmetric pores (1 & 2); catalyst

located near the entrance (3) and the exit (4); controlled sequence of different catalysts along the pore (5).

1.2 Fabrication of the AAO Membranes by ALD

The open, one-dimensional channel structure of the AAO membrane facilitates the deposition of coatings and catalytically active materials. One good example is the application of the atomic layer deposition (ALD) in fabricating the AAO membranes. Atomic layer deposition (originally named atomic layer epitaxy, ALE) is a novel film deposition technique based on the chemical reactions between reactive molecular precursors and the substrate. [14-16] In similarity to chemical vapor deposition (CVD), elements composing the film are introduced in the forms of molecular precursors. For ALD applications, the precursors are delivered separately; each deposition cycle is composed of two (or more) gas-surface interactions that are self-limiting, that is, in each elementary step the deposition stops once all the surface functional groups have been consumed. After each cycle of deposition, the surface functional groups will be regenerated so that the next deposition cycle is ready to be applied. With this ALD technique, films of the desired compositions and thickness can be coated by a repetitive sequence of single layer deposition cycles. An example of ALD process is shown in Fig 1.3, in which trimethyl aluminum (TMA) and water are used as the precursors to coat alumina film on the substrate.

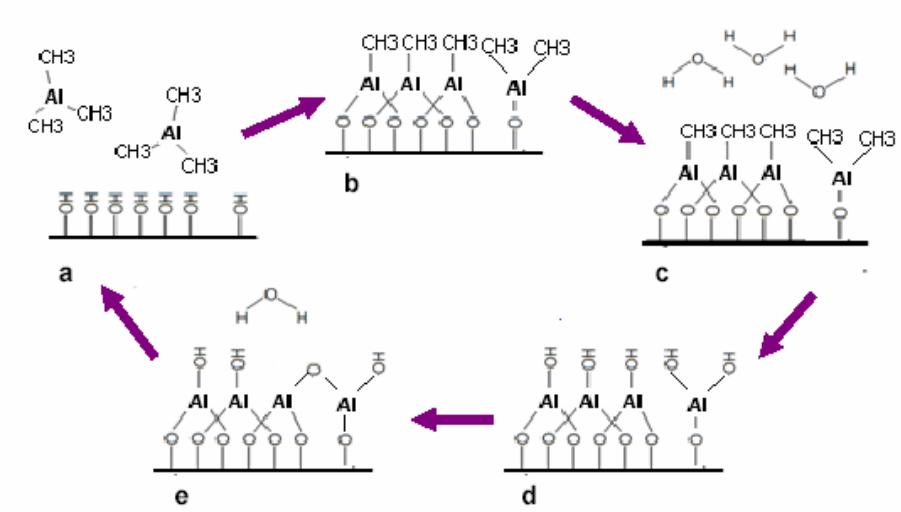

Fig 1.3 The ALD of alumina

a. The hydroxyl terminated surface is exposed to the TMA precursor.

b. The TMA molecules react with the surface hydroxyls. The reaction stops when all –OH sites are consumed.

c. The $–CH_3$ terminated surface is exposed to water vapor.

d. The H_2O molecules react with the $–CH_3$ sites. The reaction stops when all $–CH_3$ sites are consumed.

e. Cross-link of adjacent $–Al(OH)_2$ sites. The cycle is complete and the surface functional groups are regenerated.

Traditionally this powerful deposition technique has been used in the coating of flat surfaces; its application in the catalysis field is usually limited by the diffusion problems in coating powder supports with very small irregular pores. [17] However, the straight nanopores on the AAO membranes facilitate the diffusion of precursor molecules into the

channels; therefore the ALD technique can also be used to fabricate these membranes. By coating multiple cycles of ALD alumina, the pore size on the AAO membrane can be precisely controlled. Fig 1.4 displays the SEM images of the surface and cross-section of the AAO membrane before and after ALD coating. As we can see from these pictures, all the pores on the membrane are evenly shrunk from 40 nm to 10 nm after coating 10 nm of alumina. Besides, the alumina coating on the pore walls is extremely uniform throughout the entire length of the channel.

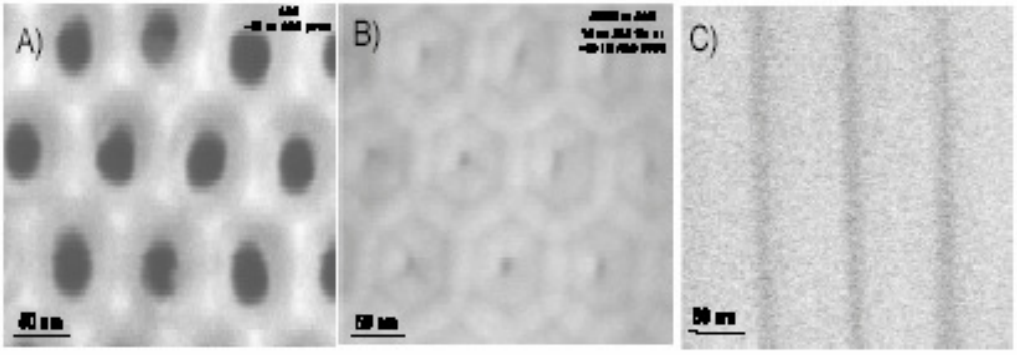

Fig 1.4 ALD fabrication on the AAO membrane: tuning the pore size

A) Plan view SEM image of surface of the original 40 nm AAO material.

B) Plan view SEM image of the surface of the 40 nm AAO material coated with 15 nm of alumina.

C) Cross sectional view of 40 nm AAO material coated with 15 nm of alumina taken from the center of the AAO membrane (note that the coating is uniform despite the high aspect ratio)

Binary reaction sequences applicable for ALD have been developed to coat a wide variety of materials including oxides, nitrides, sulfides and metals, [18-20] which provides us a lot of flexibility in fabricating the AAO membrane using the ALD technique. On the other hand, the membrane catalytic system provides a perfect platform for testing the catalytic performance of structures synthesized by ALD. Fig 1.5 lists the elements and compounds discovered so far that can be coated by doing ALD. [21] With the combination of AAO and ALD, we are able to precisely control the pore size and shape, the pore wall composition, and the catalyst distribution in the membrane catalytic system. The ALD fabrication of the AAO membrane usually includes three sequential steps (depicted in Fig 1.6): 1.) Coat alumina to cover the impurities and to tailor pore size; 2.) Coat support materials such as TiO_2 or Nb_2O_5 to change the surface properties (optional); 3.) Coat catalytically active materials such as vanadium oxides. The catalytic properties of these ALD fabricated AAO membranes will be discussed in detail in later chapters.

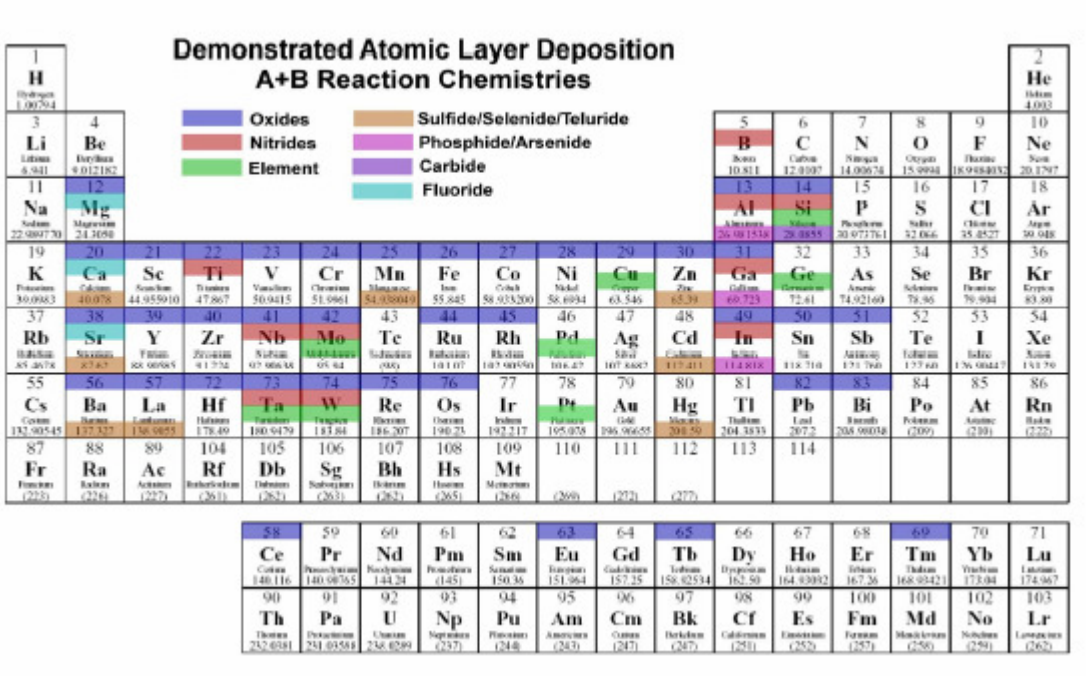

Fig 1.5 Elements and Compounds that can be coated by ALD

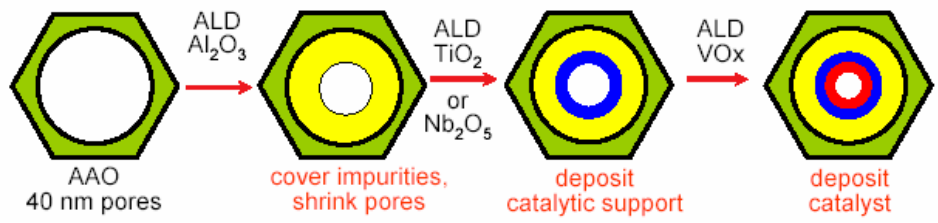

Fig 1. 6 Fabrication of the AAO membrane by ALD

1.3 Application of the Nanostructured Catalytic Membrane in Oxidative Dehydrogenation Reactions

The array of nanoreactors on the AAO membrane make a promising, highly selective

catalytic system for some sequential reactions. When the reactants flow through the nano-pores, the limited thickness of the film may dramatically reduce the contact time between reactants and catalyst so that undesired over reactions can be limited to a great extent. The oxidative dehydrogenation of alkanes to olefins is a sensitive probe for the performance of the nanoreactor arrays because the partial oxidation products are easily oxidized to oxygenated products, which are thermodynamically more stable. [22-24] Presumably, the application of the membrane catalytic system in these reactions can effectively separate the partial oxidation products (olefins) before the thermodynamic equilibrium is reached.

1.3.1 Selective Oxidation of Alkanes to Produce Olefins

Due to their higher chemical activities, the unsaturated hydrocarbons are more desirable feedstock than alkanes in a lot of chemical industrial processes. For example, the production of polymers and other synthetic materials use olefins as the starting materials. With the steady increasing demand for these new synthetic materials, the need for light olefins follows the same trend. Currently the worldwide production of light olefins mainly relies on two commercial processes: thermal cracking (pyrolysis or steam cracking) and catalytic dehydrogenation. [25-26, 30] The majority of today's olefin capacity is produced from thermal cracking of petroleum hydrocarbons, usually liquefied petroleum gas (LPG) and naphtha. Since these cracking reactions are usually carried out with steam, the process is commonly called steam cracking or pyrolysis. The products of these

reactions may vary largely, depending on the feedstock and the conditions of the cracking operation. The main products of steam cracking are ethane and propylene, with limited amounts of higher olefins and aromatics. Because of the presences of various byproducts, the separation of resulting product mixtures is a very complex and costly process. Catalytic thermal dehydrogenation reactions can also be used in the attainment of olefins (especially propylene and butane) from alkanes. The commonly used catalysts in these reactions are noble or heavy metal catalysts such as platinum or chromium. However, these reactions are highly endothermic therefore they are often equilibrium limited. Dehydrogenation reactions have to be carried out at temperatures as high as 700 – 800 °C depending on the alkane feed, where the side reactions are difficult to control and the catalysts deactivate rapidly due to the coke formations. [27]

On the other hand, the oxidative dehydrogenation (ODH) of alkanes to the corresponding olefins is a promising method due to the thermodynamically favorable (exothermic) nature and the resistance to catalyst deactivation. [23, 24] However, the major problem of the ODH reactions is that the partial oxidation reactions always have to compete with the more thermodynamically favored total oxidation reactions. Since both the partial oxidation reactions and the total oxidation reactions share some common mechanistic features, the major challenge in the catalytic system design is to favor the partial oxidation routes over the total oxidation routes. Usually the catalytic oxidation reaction network is represented as consecutive reactions in which the partial oxidation products

react further to produce the deeper oxidation products. [28] Therefore, to get a high yield to the partial oxidation product, the catalytic system has to be able to effectively separate the initial products before the thermodynamic equilibrium is established.

Take the ODH of propane for an example,

$$C_3H_8 + 1/2O_2 \longrightarrow C_3H_6 + H_2O \quad \Delta H = -86.3 \text{ kJ/mol}$$

When this reaction is carried out, propane and propylene can also be over-oxidized to CO, CO_2 and other oxygenated products. Consequently, it is hard to achieve a high selectivity to propylene, especially at high conversions. Although a lot of efforts have been made to try to realize this process, the maximum propylene yield in propane ODH reported in the literature is no more than 30%, which is not yet satisfactory for industrial applications. [29] Up to date, the commercialized ODH processes are limited to the oxidation of ethylbenzene to styrene and that of butane to maleic anhydride. The common feature of these two reactions is that the weakest C-H bond in the product is harder to break than those in the reactant, which effectively prohibits the over oxidations.

Generally three types of materials were investigated for the purpose of developing better ODH catalysts: redox catalysts, non-redox catalysts, and noble metal coated monolith. [30, 40] The basic properties of these three types of catalysts are briefly discussed as follows.

1.3.1.1 Redox catalysis

For ODH reactions, the most intensively studied catalytic materials are transition metal containing redox catalysts. A lot of research has been carried out on the ODH of low alkanes. [24, 29] Vanadium oxides (VOx) anchored on different types of supports (MgO, TiO_2, Al_2O_3, etc.) were probably the most studied catalysts. These reactions follow a typical Mars-Van Krevelen mechanism, where the hydrocarbon is oxidized by the lattice oxygen in the metal oxide (the catalytic site) in the first step and then the reduced metal oxide is re-oxidized by gas-phase oxygen in a subsequent step (Fig 1.7). [31, 32]

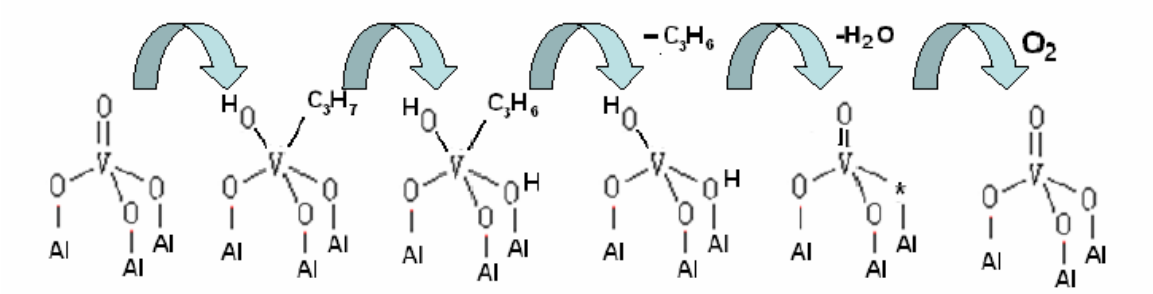

Fig 1.7 The ODH of propane over VOx supported on Al_2O_3

The different alkanes showed different activities, depending on the strength of the weakest C-H bond, implying that the rupture of the C-H bond is the rate-determining step of this reaction. This deduction is consistent with the results of isotopic tracer studies of ODH pathways on VOx catalysts. [33]

In the alkane ODH reactions it is generally believed that the type of support is the most important factor in determining the catalytic behavior of the supported VOx, in that

dramatic differences in catalytic activity have been observed over similar loadings of VOx supported on different types of substrate. [34-36] The large difference in activity could be due to the different acidity, dispersion, or oxidation capability of the VOx species formed on these substrates. [34, 37] In addition, Iglesia et. al. showed that the performance of the vanadia catalysts could also be affected by the surface coverage and/or the domain size of the catalytic species. [34] As is shown in Fig 1. 8, except for effects of the support, the propane ODH rates are also largely influenced by the surface density of the VOx species. Higher vanadium surface densities or larger VOx domains appear to have promotion effects on the catalytic activity.

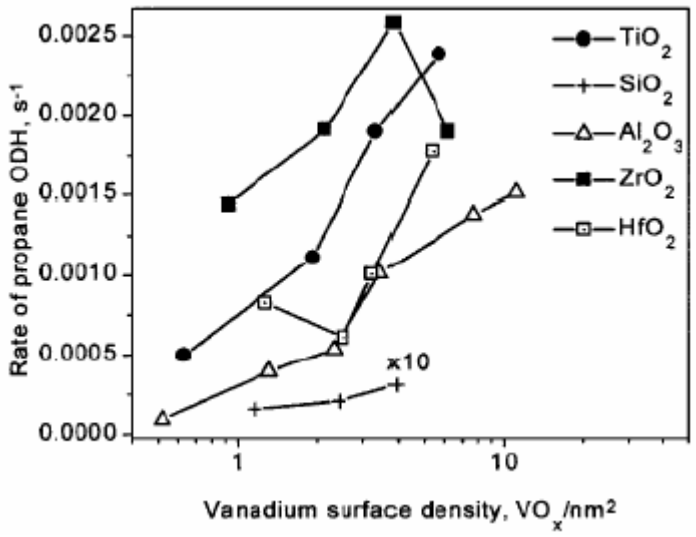

Fig 1. 8 Effects of VOx surface density on ODH rates [34]

Since the breaking of the first C-H bond in alkene molecules is usually much easier; alkenes generally react much faster than alkanes over redox catalysts. This fact makes it a

very hard task to find a suitable redox catalyst for ODH reactions. [26, 38] In order to avoid contact of oxygen with the partial oxidation product, a method has been reported to carry out the reaction in a cyclic mode, where the lattice oxygen oxidizes the hydrocarbon in one cycle, and in the subsequent cycle the reduced catalytic site was re-oxidized by the gas phase oxygen. [39] The practice of the membrane catalysis is also aimed at reducing the contact of the olefin with the redox catalysts to prevent over oxidations.

3.1.2 Non-redox catalysis

The ODH of ethane was mostly studied over non-redox type catalysts such as alkali promoted alkali-earth oxides and rare-earth oxides. [26, 30, 41] Propane ODH with non-redox catalysts was less studied, however the best propylene yield reported in literatures (~30%) was achieved over these non-redox catalysts. The olefin product in the ODH of propane with non-redox catalysts is not limited to propylene; ethylene is another major product from this reaction. In these reactions, it is believed that non-catalytic homogeneous reactions also contribute to the olefin formation. [41] However, at this point it is not quite evident whether the catalytic or non-catalytic reaction has more important contributions to the yield of propylene. Burch and Crabb, and Cavani and coworkers compared catalytic and non-catalytic reactions of propane respectively and concluded that the proper combination of heterogeneous and homogeneous reactions gives the best yields to the olefin products. [41, 42]

1.3.1.3 Noble metal catalysis

Although known to be very good total oxidation (combustion) catalysts, noble metals can also be used in selective oxidations: at low oxygen concentration and very short contact times, alkanes can be converted to olefins with high selectivity over these catalysts. The product spectrum is similar to those obtained over non-redox catalysts. [30] The mechanism of this process is described as an initial total oxidation of alkanes until 100% oxygen conversion, accompanied by a large amount of heat generation and a corresponding further thermal cracking of the remaining alkanes. [43, 44] In practice Pt coated monolith are used under very high flow conditions in the ODH of ethane, where contact times are as short as one millisecond. An ethylene selectivity of 80% can be achieved at 60% ethane conversion using such short contact time reactors. [45]

1.3.2 The ODH of Cyclohexane

In contrast to the intensive work on light alkanes, the ODH reaction of cyclohexane has been very little explored. In this reaction cyclohexane is first converted to cyclohexene and then further oxidized to benzene and oxygenated products such as CO and CO_2. The reaction network and the enthalpy change corresponding to the formation of the three products are presented in Fig 1.9. Usually benzene is not considered as a useful product from this reaction since industrially cyclohexane is mostly made from the hydrogenation of benzene. The valuable product from this reaction is cyclohexene, which is an intermediate in the production of adipic acid, the monomer for Nylon 6, 6. [46] A traditional

way to produce cyclohexene is by dehydration of cyclohexanol, which is obtained from the oxidation of cyclohexane in the liquid phase. [47] A direct conversion from cyclohexane to cyclohexene through a heterogeneously catalyzed process is highly desirable but no catalytic system has been found so far that is able to obtain a meaningful yield to cyclohexene.

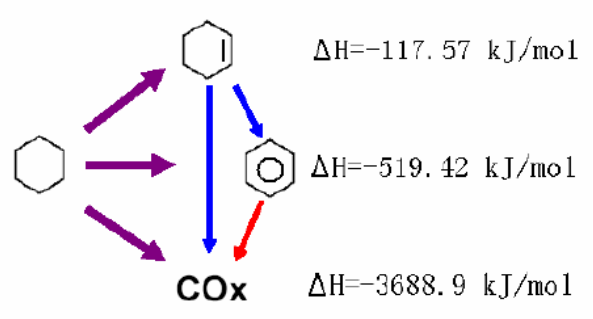

Fig 1.9 The cyclohexane ODH reaction network

Lopez and coworkers studied the performance of different groups of catalysts in this reaction, including silica and niobia supported vanadia, V, Fe, and Ce phosphates, and protonic and transition metal exchanged ZSM-5 zeolites, finding out that the major product of this reaction is either benzene or COx. [48] More explorations on this reaction are necessary so that the cyclohexane oxidation process can be further understood and an efficient catalyst towards a high yield to cyclohexene can possibly be developed. Besides, there is another benefit to study the catalytic dehydrogenation of cyclohexane, compared to propane, in terms of separating the effect of multiple C-H bond breaking reactions and C-C or O-insertion reactions. With propane COx is the inevitable result of breaking three or more C-H bonds. However this is not the case for cyclohexane. For cyclohexane ODH,

the activity of the catalyst is still likely to be determined by C-H bond activation in a CH_2 group, however, this step is unlikely be what determines the product selectivity between hydrocarbons and COx, since benzene is the result of breaking one C-H bond on each methylene group. Because benzene is a relatively stable product which preserves all of the C-C bonds, the selectivity toward benzene vs. COx may be a measure of the catalysts' propensity for C-C bond activation. In another words, a catalyst that is very active only for breaking C-H bonds will make benzene but not COx; while the same catalyst will make COx from propane.

1.4 Aim of the Work

The goal of this thesis is to construct a membrane catalytic system based on the nanostructured AAO membrane, to try to investigate the use this system to achieve higher yield to the partial oxidation product in ODH reactions, to test the properties of the novel catalytic structures synthesized by the combination of AAO and ALD, and to explore the reaction kinetics and mechanism (pathway) in the ODH of cyclohexane. Some other explorations related to the understanding and application of the membrane catalytic system, such as properties of the asymmetric catalytic stripes, and poisoning experiments for the purpose of counting the active sites in a gas/solid heterogeneous system, are also described.

Chapter 2

2. Experimental Details

2.1 Overview

This chapter details the methods and procedures of AAO membrane synthesis, vanadium oxides catalyst preparation and testing, and characterization techniques used to study the properties of the membrane and the catalyst.

2.2 Materials Used

AAO Membrane Synthesis:

Aluminum Sheets (Alfa Aesar, ultra pure, 99.98%), Oxalic Acid (Fisher, 99.9%), Hydrochloric Acid Solution(Fisher, 60%), Phosphoric Acid (Fisher, 99.8%), Chromium Oxide (Fisher, 99.9%), Cupric Chloride (Fisher, 99.8%), Ethyl Alcohol Solution (VWR, 95%), Acetone (VWR, 99.9%), Hydrochloric Acid Solution (VWR, 37%), Sulfuric Acid (VWR, 99.5%), Aluminum Oxalate (Alfa Aesar, 99.9%).

Catalyst Preparation and Testing:

Ammonium Meta Vanadate (Fisher, 99.9%), Sodium Vanadium Oxide (Fisher, 99.9%), Vanadium (V) Oxide (Fisher, 99.95%), Cyclohexane (VWR, 99.8%), Cyclohexene (Fisher, 99.9%), Benzene (VWR, 99%), Silicon Carbide (Alfa Aesar, 1micron particles,

99.99%), Silica Chips (99.9%, 14-30 mesh), Quartz Wool, Helium (UHP, Airgas), Oxygen (UHP, Airgas), Hydrogen (UHP, Airgas), Methane/Helium 1.00/99.00 Mixture (Matheson), Hexamethyldisiloxane (Fisher, 99.95%).

2.3 Membrane Synthesis

The procedures to prepare the free-standing AAO membrane are described as follows. First, a piece of cleaned high purity aluminum sheet was electro-polished in 10% perchloric acid/ethanol (v/v) solution with a current density higher than 100mA/cm^2. This sheet of aluminum was used as the anode in an electro-chemistry cell where the cathode is a piece of pure platinum. The porous alumina membranes can be made in oxalic acid, sulfuric acid, or phosphoric acid solution, depending on the desired pore size and pore to pore separation.[6] To obtain the membranes with most regular pores, the applied anodization potential is normally ranged between 15 and 25 volts for sulfuric acid solution, 25 and 40 volts for oxalic acid solution, and greater than 100 volts for phosphoric acid solution. A standard two step anodization procedure was applied to get a highly ordered hexagonal pattern of pores. [49] To obtain the best regularity, the thickness of the membrane grown in the first step anodization has to be at least 20 microns. This membrane was then dissolved in hot phosphoric acid solution, leaving a regular hexagonal pattern of dents on the surface of aluminum. During the second anodization, one side of the aluminum sheet was covered by a layer of removable polymer (usually a type of nail polish) so that the membrane would only grow from the other side. In order

to get the membrane with desired thickness, the duration of the second anodization is carefully controlled. After the anodization, the membrane grown on the aluminum sheet was protected by coating the polymer layer on it, and the protective coating on the other side of the aluminum sheet was removed. The un-anodized side of the aluminum sheet was exposed to an $HCl/CuCl_2$ etching solution. When the etching is complete, the membrane was left in 5% phosphoric acid for a proper period of time to dissolve the bottom alumina barrier layer. Finally the protective polymer coating was peeled off and the free standing membrane was obtained. The schematic picture of these procedures is presented in Fig 2.1. Due to the limitations of the free standing membranes (unsealable, fragility, and low productivity), these membranes were mostly used for characterization purposes. A new technique was developed to prepare the AAO membrane embedded in an aluminum ring support, which is primarily used in catalysis experiments.

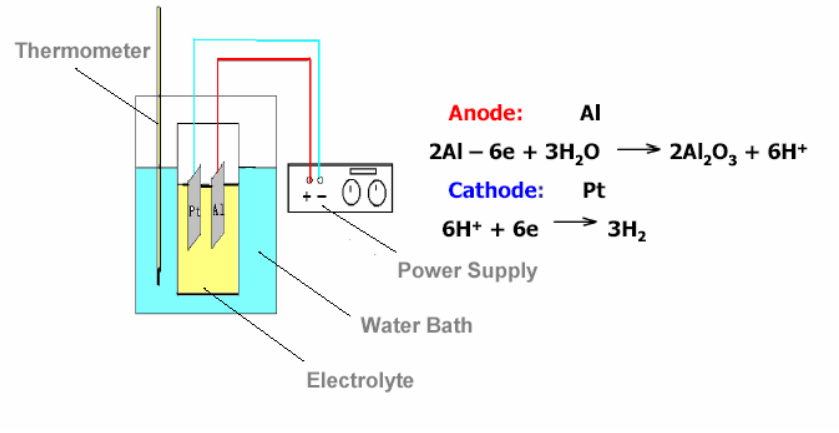

(a).

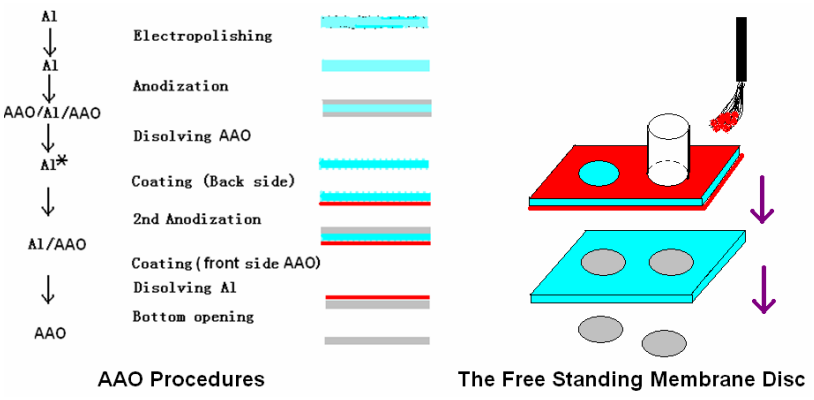

(b).

Fig 2.1 Preparation of the free standing AAO membranes. **(a).** The AAO setup. **(b)** .The membrane synthesis procedures.

To prepare the AAO membrane embedded in an aluminum ring support, a special cell was designed to mask part of the surface of aluminum during the anodization (Fig. 2.2). The cell is made of two pieces of Teflon, between which rests an aluminum disk of the proper size. On one piece of teflon (the front piece) a hole is drilled so that the central region on one side of the aluminum disc is exposed. The two Teflon pieces can be pressed together tightly using Teflon screws. Two O-rings of different sizes are used to provide firm seals so that central region of the front side is in contact with the electrolyte during anodization. Electrical contact to the back side of the disk is established by a copper cup and a metal rod buried in the back piece of teflon that connects to the external circuit.

The method of growing the AAO membranes embedded in the aluminum ring mostly follows the above procedures. The aluminum sheets were cut into disks that fit into the

anodization cell. These discs were anodized for 24 hrs in a 0.3M oxalic acid solution at a constant potential of 40V at 3 °C. The AAO membranes prepared in such conditions are 70 microns thick and have an average pore diameter of about 40 nm. After the anodization, the un-anodized back side of the aluminum disk (except for the supporting ring) was dissolved in a 37% HCl/ 10% $CuCl_2$ (1/4 v/v) solution. In this step, the disk is turned around in the anodization cell to expose the aluminum lying beneath the AAO membrane for etching. This back side of the membrane was treated in 5% phosphoric acid at 30 C° for 70 minutes to remove the barrier layer on the bottom of the AAO structure so that both ends of the channels were open. A photograph of the as-prepared AAO membrane mounted in the aluminum ring is shown in Fig. 2.2(c). The durability of these fragile membranes has been greatly enhanced with the supporting aluminum ring.

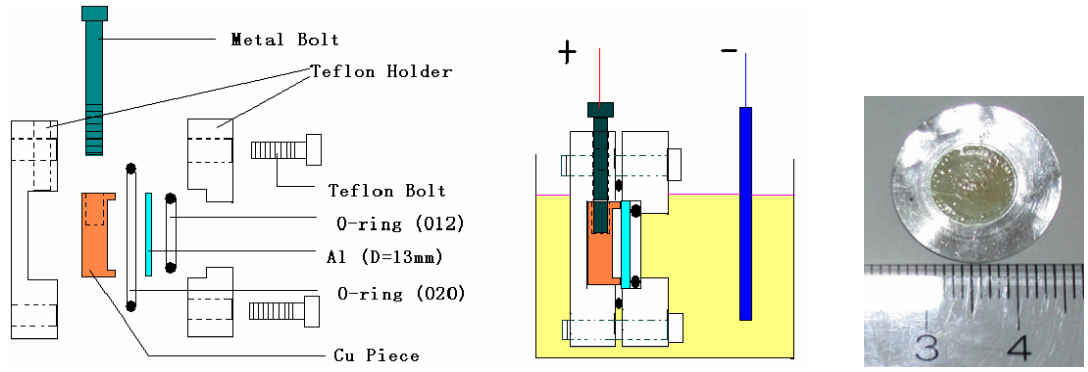

(a) **(b)** **(c)**

Fig 2.2 (a). The dissembled anodization cell. (b). Anodization of the aluminum disc. (c). A photo of the AAO/aluminum ring support.

2.4 Catalyst Preparation

To cover the impurities incorporated into the membrane structure during the anodization and to change the type of support, the AAO membranes were coated with 1nm of Al_2O_3 or other metal oxides such as TiO_2 or Nb_2O_5 by ALD before any catalyst was loaded.

Three different ways were applied to load vanadium oxides (VOx) onto the AAO membranes: incipient wetness impregnation, atomic layer deposition (ALD), and grafting of organometallic clusters. When the impregnation method was used, an aqueous solution of NH_4VO_3 was dropped onto one side of the membrane and at the same time a slight vacuum was applied from the other side to draw the solution through the nanopores and to help facilitate the evaporation of the liquid. To ensure a complete wetness of the pore walls by the liquid, a solution dilute enough (3.2×10^{-3} mol/l) was used so that the volume of the solution was much greater than that of the membrane. The precursor solution was dropped from the two sides of the membrane alternately and the dropping and drying procedures could be repeated several times until a desired amount of the catalyst was introduced. The membranes were dried at 150°C for 1 hr and then calcined in oxygen at 500 °C for 5 hrs before carrying out the catalysis experiments. During the ALD process, VOx was deposited in an integral number of sub-monolayer cycles using vanadium oxytriisopropoxide /hydrogen peroxide and water as the precursors. [50] Different cycles (1 to 24) of VOx were put down onto the membranes to make a series of samples with

different loadings of the catalyst. After coating the catalytic materials by ALD, the samples were tested directly in the catalysis experiments without further treatments. When the first run of the catalysis testing is complete, these ALD samples were calcined in oxygen at 500 °C for 2 hrs and then re-tested under the same conditions. The method of grafting the vanadium containing organometallic clusters onto the AAO membranes is similar to incipient wetness impregnation. Since these organometallic clusters are air and water sensitive, the grafting was carried out in a glove box. An adequate amount of the cluster compound (Cp_2V, Cp^*_2V, $V_4(\mu\text{-}O)_6Cp_4$ or $V_4(\mu\text{-}O)_6Cp_4^*$) was dissolved in toluene. The solution was then dropped from both sides of the membrane alternatively. Once in contact with the surface, the cluster compounds will react with the surface hydroxyls and be attached to the pore walls. After the solution dried, the membrane was exposed to air and then calcined in oxygen at 500 °C for 5 hrs.

2.5 Catalytic Measurements

The Catalytic experiments were carried out in a flow reactor modified from a standard Swagelok VCR fitting, in which the AAO membrane was sealed inside (Fig 4.4 and Fig 2.3-a). The reactor was coated with 1nm of Al_2O_3 by ALD to avoid the possible interference from reactions catalyzed by the metal reactor itself. The fitting was carefully fastened to a point where the upstream pressure became stable and no leak could be detected as the flow of the reactants was pushed through. Quartz chips (14-30 mesh) were used to fill the empty spaces in the reactor to minimize the possible gas phase reactions.

The vapor of cyclohexane was introduced into the reaction system (Fig 2.3-b) from a bubbler with a controlled stream of helium flowing through. Oxygen (99.99%) was used as the oxidant and a mixture of methane and helium (1.00:99.00) was used as the balance gas. In most of the cyclohexane ODH experiments, the reactant gas was composed of 1% cyclohexane, 2% oxygen, and 97% balance gas. The reactions were carried out in a temperature range between 400°C and 480°C at atmospheric pressure. Reaction products were analyzed by a HP 6890 gas chromatography equipped with a flame ionization detector (FID) and a thermal conductivity detector (TCD) for probing the organic and the inorganic products respectively. Methane was used as an internal standard to convert signals between the two detectors. (The conversion of methane has been found to be zero under the experiment conditions of the catalysis tests.) The published values of the response factors for the FID and TCD were used to correct the peak areas obtained from the two detectors.

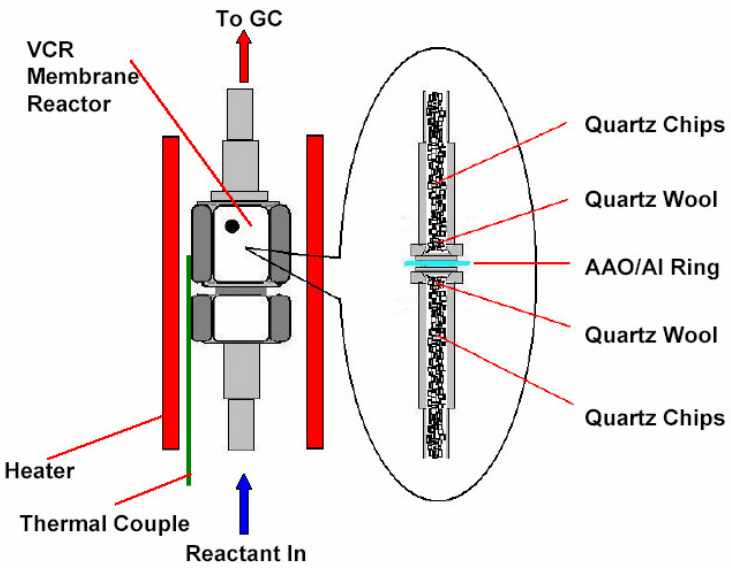

a.

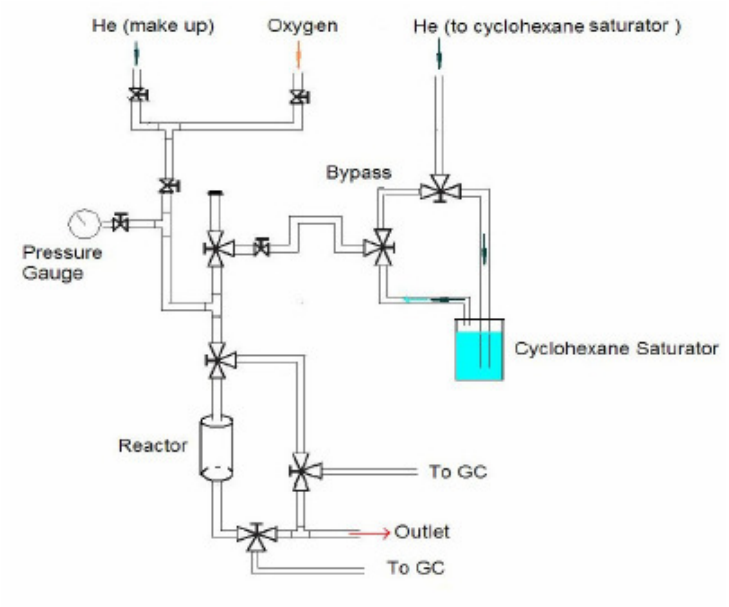

b.

Fig 2.3 The membrane reactor configuration (a) and cyclohexane ODH reaction system (b)

2.6 Poisoning Experiment

A titration poisoning method is used to determine the number of active sites in the membrane catalytic system. The poisoning experiment involves the introduction of an inhibitor, which interacts with the active species at a certain stoichiometric ratio and thus makes part of the catalytic sites inactive. The number of active sites can be counted by relating the amount of the introduced poison and the reduction in the catalytic activity.

In the poisoning experiment, hexamethyldisiloxane is used as the inhibitor compound to react with the supported vanadium oxide catalyst in the ODH of cyclohexane. Its stability has to be tested prior to the poisoning experiment under the conditions of the heterogeneous reaction. The experiment is carried out in the sealed membrane flow

reactor. The vanadium oxide catalysts are loaded onto the membrane by ALD or by grafting of the $V_4(\mu\text{-}O)_6Cp_4$ cluster. The reaction conditions (reactant compositions, temperatures and flow rates) are kept the same as those used in the catalysis testing. The poison compound is introduced into the membrane reactor by a syringe through a septum injection port located next to the reactor (Fig 2.4). The total amount of the poison used to deactivate the catalyst is based on the estimation of the total number of active sites in the membrane sample. Normally a small fraction of the total amount is used in each injection so that a poisoning curve similar to a titration curve can be obtained. After each poison injection, the activity of the catalyst is continuously monitored until it does not change any further.

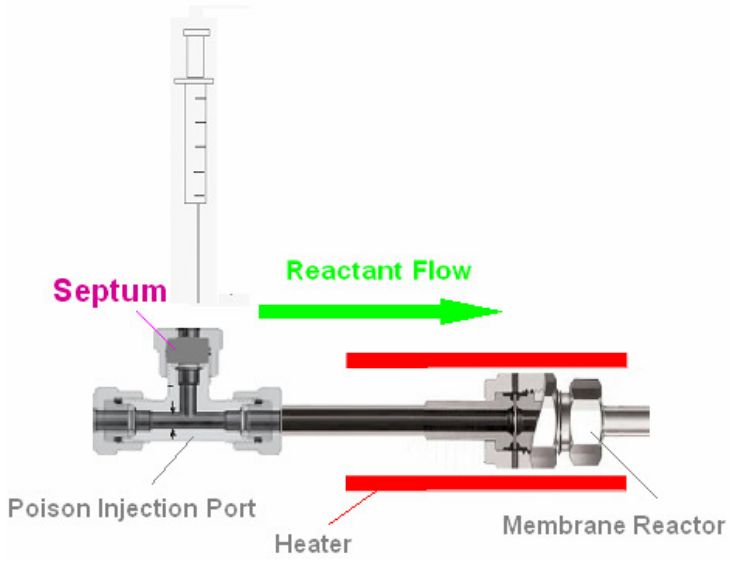

Fig 2.4 The poisoning experiment setup

2.7 Characterization

2.7.1 Characterization on the AAO membrane

SEM

A Hitachi S4700 Field Emission Scanning Electron Microscope (SEM) was used to study the surface topology and structure of the AAO membranes. No conductive coating was applied to the membranes so that the structural and chemical properties of the membranes can be best maintained. To reduce the charging build up on the insulating alumina membrane samples, low accelerating voltage (<5 kV) was used at the ultra-high resolution. The upper secondary electron detector was used in order to get more topology information.

XRD

X-ray diffraction was applied to probe the atomic structure of the AAO membrane. X-ray powder diffraction data was obtained with a Rigaku Dmax powder diffractometer using the Cu $K\alpha_1$ radiation. X-ray diffraction data was measured at ambient temperature in the range of $2\theta = 10\ ^\circ$ to $60\ ^\circ$ with a step range of $0.05\ ^\circ$.

SAXS

Small Angle X-ray Scattering was used to characterize the meso-scale structure of the AAO membrane. The measurements were taken with the Advanced Photon Source (APS)

Small Angle X-ray Diffraction Beam Line at Argonne National Lab. The diffraction data was obtained in the Q range of 0.003 $Å^{-1}$< Q < 0.03 $Å^{-1}$with an exposure time of t = 30s. The SAXS pattern was analyzed by IGOR Pro software combined with 2D → 1D data reduction macros.

XPS

The X-ray Photoelectron Spectra were taken on some AAO membrane samples prepared in sulfuric acid solution to determine the amount of sulfur incorporated into the membrane structure. The measurement was conducted on a Physical Electronics model 548 XPS system.

Raman

The Raman spectra of the AAO membranes were measured using a UV-Raman instrument built at Northwestern University. The Raman spectra were excited at 244 nm generated by an argon ion laser (Lexel 95 SHG). The laser power at the sample is 4 mW, and a typical spectrum collection time is 20 min. These spectra were compared to those of the aluminum oxalates powder measured under the same conditions.

TGA

The Thermal Gravimetric Analysis on the AAO membrane samples were taken with a Q50 TGA instrument. During the measurement the temperature was ramped from room

temperature up to 1000 °C at a speed of 20 °C/min in a nitrogen atmosphere.

EPR

EPR studies were carried out to investigate the nature of the different kinds of impurities incorporated into the AAO membrane. The measurement was carried out in a continuous wave (CW) mode at microwave frequencies, using a Bruker EMX spectrometer. The samples were exposed to microwave radiation of constant frequency while sweeping the external magnetic field B until resonance condition was fulfilled.

2.7.2 Characterization on the VOx catalyst

XRF

The X-ray Fluorescence Spectroscopy was used as a non-destructive way to characterize the amount of vanadium oxide catalyst supported on the AAO membrane. The measurements were taken with an Oxford ED2000 instrument at Argonne National Laboratory using a "semi-quantitative fundamental parameters" method. These XRF results were calibrated with the results from ICP measurements.

ICP-AES

The ICP-AES characterizations of vanadium content were performed on some of the membrane samples to provide a calibration for the XRF data. A Varian Vista-MPX instrument was used for the measurements. To prepare the samples for the ICP

characterizations, the membranes were removed from the aluminum ring and dissolved in 10% phosphoric acid solution. The primary atomic emission wavelength of vanadium at 292.4 nm was used for analysis.

UV-Vis

The UV-Vis spectra of the catalysts were measured with a Cary 500 UV-Vis-NIR spectrometer. Since the AAO membranes are virtually transparent films, it is very convenient to measure the transmission spectra of the VOx species supported on them. The measurements were taken in a double beam configuration with a piece of blank AAO membrane used as the reference.

Chapter 3

3. Properties of the Nanostructured Catalytic Membranes

3.1 Overview

In this chapter, the physical, structural and chemical properties of the AAO membranes related to their application in heterogeneous catalytic reactions are discussed. Effects of the preparation conditions on the properties of the AAO membranes are also described in detail.

3.2 Discussions

3.2.1 The Nano-scale Structure of the AAO Membrane

Unlike most other porous materials, the AAO membrane is unique in its highly ordered hexagonal pattern of nanopores and the uniformity in the pore size and shape (Fig 3.1). The pores on the membrane are straight and perpendicular to the surface; there is no interconnection, merging, or separation among the channels. The formation of the ordered hexagonal patter of nanopores during the anodization is probably related to the tension generated on the interface of alumina and aluminum due to the volume expansion when aluminum is anodized, since naturally the honeycomb like hexagonal configuration turns out to be a most stable structure capable of undertaking a lot of lateral force. [51] This excellent uniformity in the pore size and shape is meaningful for catalysis studies.

First, it makes it much easier for us to estimate the surface area of this material just by doing simple mathematical calculations. Because the surface area of the AAO membrane is pretty low (~ 5 m^2/g), it is hard to perform a direct measurement on it using traditional gas adsorption methods. Furthermore, since all the channels on the membrane are the same, in a heterogeneous catalytic reaction presumably every reactant molecule will have an identical diffusion path in the catalytic layer, which leads to more uniform and tunable contact times than are possible with a conventional fixed bed powder catalyst.

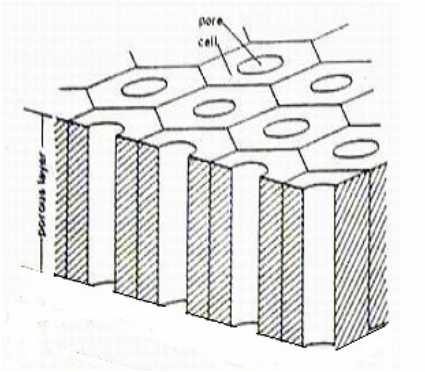

Fig 3.1 Schematic picture of the nanopores on the AAO Membrane [11]

The most straightforward way to characterize the morphology of the membrane is by SEM, which allows us to directly measure the pore size, the pore to pore distance, and the film thickness. (Fig 3.4) Small Angle Xray Scattering (SAXS) is an alternative tool used to characterize the porous structure on the AAO membrane. Information about the film regularity and the average pore to pore distance can be obtained from the diffraction pattern. Fig 3.3 displays a typical SAXS pattern obtained from an AAO membrane sample and the corresponding "Q value curve" generated by the analyzing software,

where the Q value represents the length of the diffraction vector in the reciprocal space. The Q values at intensity peaks are expressed as:

$$(\frac{Q}{2\pi})^2 = (h^2 + k^2 + 2hk\cos\gamma^*)^2 a^{*2} \quad \text{(h, k = 0, 1, 2…)} \qquad 3.1$$

In this expression, a* is related to a, the distance between the centers of adjacent pores, by the following equation:

$$a^* = \frac{1}{a\sin\gamma} \qquad 3.2$$

For the 2D hexagonal pattern, $\gamma = 60°$, $\gamma^* = 180° - 60° = 120°$, then equation 3.1 becomes:

$$Q^2 = (h^2 + k^2 + hk)^2 a^{*2} \qquad 3.3$$

Each peak in the curve represents the diffraction intensity due to a certain pore to pore distance (corresponding to a certain set of h and k values). The first (strongest) peak in the Q value curve represents the distance between the two adjacent pores, where h, k = 0, 1 or 1, 0 respectively. The second peak is corresponding to the distance between the two pores positioned next adjacent to each other (h, k = 1, 1) and the third peak represents the distance between the two pores on the main diagonal of the hexagon (h, k = 0, 2 or 2, 0). The sharpness of these peaks reflects the regularity of the hexagonal pattern of the pores on the membrane. Sharper peaks indicate a more regular hexagonal porous structure.

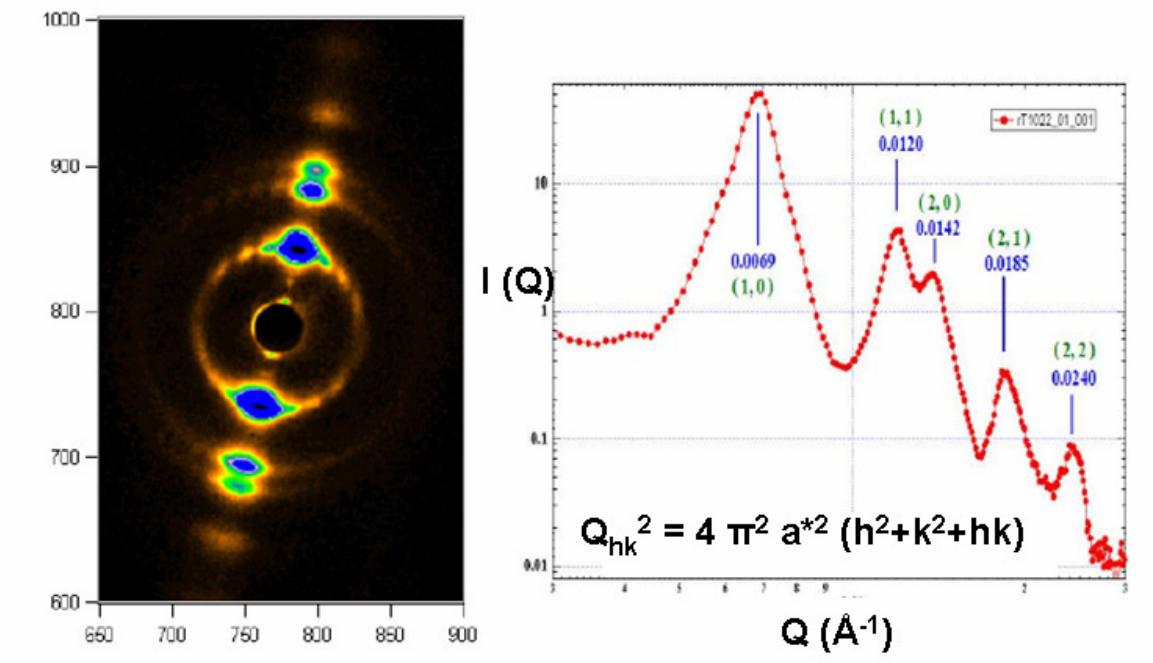

Fig 3.2 The SAXS pattern and 1-D Q value curve obtained from the AAO membrane

The average pore to pore distance can be calculated from equation 3.3 using the Q value of any peak on the curve. This calculated average pore to pore distance (105 Å) is in excellent agreement with the result of the direct measurement from the SEM image (110 Å).

The SAXS measurement was also carried out at extreme heating conditions, in which the membrane was heated up to 1000°C by an infrared furnace attached to the sample holder. During the heating and cooling process, little change in the diffraction patterns was observed. This result demonstrates the satisfactory thermal stability of the nanoporous structure on the AAO membrane.

3.2.2 Effects of Preparation Conditions

It is well known that the structure of the membrane can be tuned by varying the preparation conditions such as the anodization potential, the current density, the type and concentration of the electrolyte, the reaction temperature and the duration of anodization. By adjusting these parameters, the AAO membranes with different porosity, pore diameter, and thickness can be made.

The anodization potential is the most important factor in determining the morphology of the AAO membrane in that both the pore to pore distance and the pore diameter are closely related to the potential applied. [6] Fig 3.3 shows the linear correlation between the cell size (pore to pore distance) and the anodization potential over a wide voltage range. The basic reason for this is that the thickness of the barrier layer (a layer of alumina formed between the electrolyte and Al metal during the anodization) is proportional to the potential applied [51]; while this thickness largely determines the pore to pore distance and the pore size.

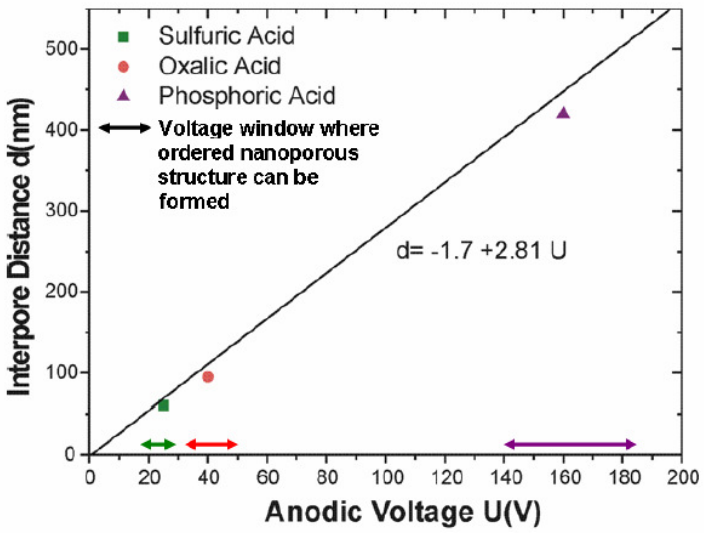

Fig 3.3 The linear correlation between the cell size and anodization potential

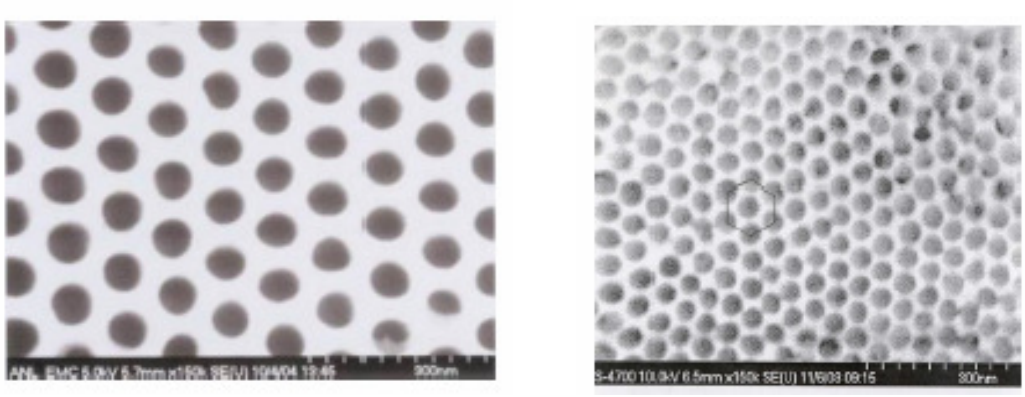

(a) **(b)**

Fig 3.4 The AAO membrane made with (a) oxalic acid and (b) sulfuric acid solution

The current density (J) determines the rate of film growth. Since the half reaction on the anode is:

$$Al - 3e + 1.5H_2O \longrightarrow 0.5Al_2O_3 + 3H^+$$

the Al_2O_3 generated on the anode can be calculated from the number of electrons pass through it. From Faraday's law:

$$Q = \frac{3Fm}{M} \qquad 3.4$$

where Q stands for the total current through the circuit, F is the Faraday constant, m denotes the mass of the aluminum sheet and M stands for the molar mass of aluminum, the thickness of the alumina film (h) can be expressed with the area of the anode (A); and the density of alumina (ρ):

$$h = \frac{V}{A} = \frac{m}{\rho A} = \frac{QM}{3F\rho A} \qquad 3.5$$

Then the rate of the film growth is:

$$v = \frac{dh}{dt} = \frac{M}{3F\rho} \times \frac{dQ}{Adt} = \frac{M}{3F\rho} \times J \qquad 3.6$$

The current density on the anode depends on the potential, the conductivity of the solution, and the temperature. Therefore parameters such as the anodization temperature and the type and concentration of the electrolyte may affect the film growth rate through influencing the current density on the anode.

The anodization temperature is normally kept as low as possible because the current becomes smaller at a lower temperature and a corresponding lower film growth rate facilitates the formation of the ordered hexagonal porous structure. Other than this factor, the chemical etching of the pore walls in the electrolyte is greatly accelerated with the increasing temperature [52]. The etching of the pore walls is a natural process independent of the field-assisted dissolution of the bottom barrier layer. It limits the maximum thickness of the membrane because the porous structure will be completely etched away

if exposed to the acidic electrolyte for a long enough period of time, which depends on the etching capability of the solution. For example, in 15% sulfuric acid solution, the maximum film thickness is no more than 160 microns; while in 0.3M oxalic acid solution where the chemical etching effect is much smaller, a film as thick as 400 microns can be made.

The type and concentration of electrolyte affects the quality of the AAO membrane in three aspects. First, for each type of electrolyte there is a window of anodization potential within which the highly ordered hexagonal pattern of pores can be obtained (Fig 3.3). Therefore, the 0.3M oxalic acid solution is usually used to prepare the membrane with 40 nm pores at 40 volts while the 15% sulfuric acid solution is used to make membranes with 18 nm pores at 20 volts. Secondly, the current density on the anode is greatly influenced by the type and concentration of electrolyte. Consequently the film growth rate is closely related to these conditions. Finally, due to the anion incorporation during the anodization, the chemical composition of the membranes prepared in different electrolytes is slightly different, which may lead to different results when they are being characterized.

In most of the literature describing the AAO synthesis, it is stated that during the anodization the aluminum sheet should be placed parallel to the anode and should face it in order to get a most regular pattern of pores. However, this may not be necessary since

the electric field in the electrolyte which determines the formation of the AAO membrane is distributed evenly on the entire surface of the submerged aluminum plate. A simple experiment was designed to test the possible effect of the position on the anode on the regularity of the nanopores. In this test a very small part of the platinum sheet (the cathode) is submerged in the 0.3M oxalic acid electrolyte and a long sheet of aluminum (the anode) is submerged in the solution from another spot (Fig 3.5). With this configuration the different parts on the aluminum sheet are greatly different in terms of their relative positions to the cathode. After the second step anodization at 40 V for 24 hours, the membranes formed on the different locations of the anode are carefully compared. It turns out that the patterns of nanopores formed in all the tested locations are all very regular. Therefore the relative location of the electrodes does not seem to influence the regularity of the porous structure. This finding has a practical value since in the design of the AAO membrane mass-production device the position of each piece of aluminum disc relative to the cathode is not critical.

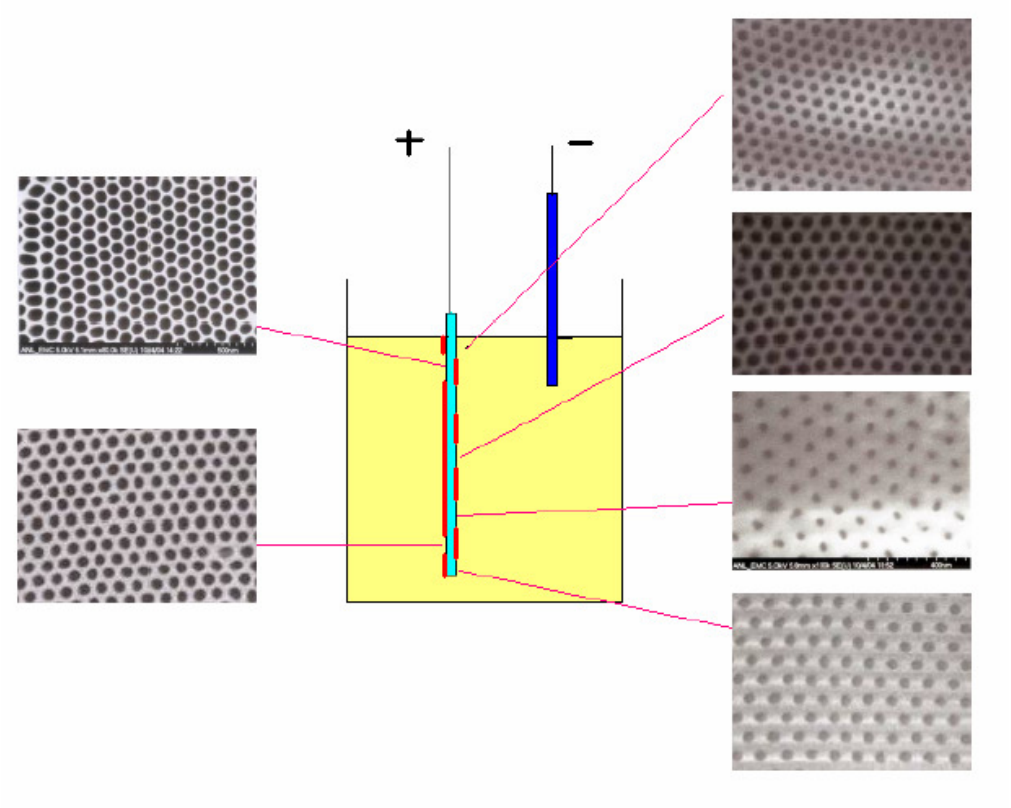

Fig 3.5 The regularity of nanopores on the membrane grown at different regions of the anode

3.2.3 Impurities Incorporated in the AAO Membrane

The impurities found in the AAO membranes are due to the incorporation of anions from the electrolyte during the anodization. Partly because of the incorporation of these impurities, the anodic alumina does not have a long range ordered crystal structure. Fig 3.6 shows the XRD pattern of the AAO membrane prepared with the oxalic acid solution. No sign of any specific crystal structure is detectable.

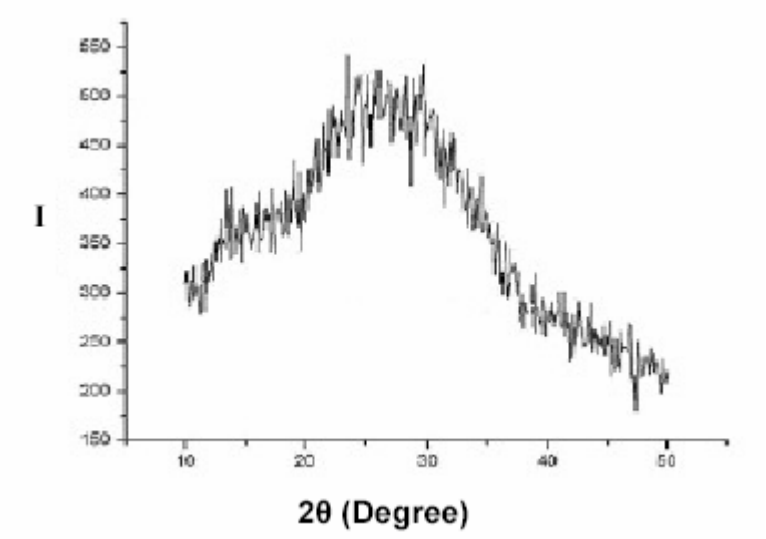

Fig 3.6 XRD pattern of the AAO membrane

As has been mentioned before, the impurities incorporated in the AAO membranes are determined by the type of electrolyte used to synthesize the membranes. These incorporated anions show strong bands in the Raman spectra measured from the AAO membranes. [53] Fig 3.7 compares the Raman spectrum of the membrane prepared with oxalic acid solution and that of the pure aluminum oxalate powder after calcination in air at 550 °C. Most of the peaks appearing in the spectrum of the membrane can be attributed to the incorporated oxalates. In the Raman spectrum of the membrane prepared with sulfuric acid solution (Fig 3.8), the peaks at 1056 and 1615 cm^{-1} are attributed to incorporated sulfates.

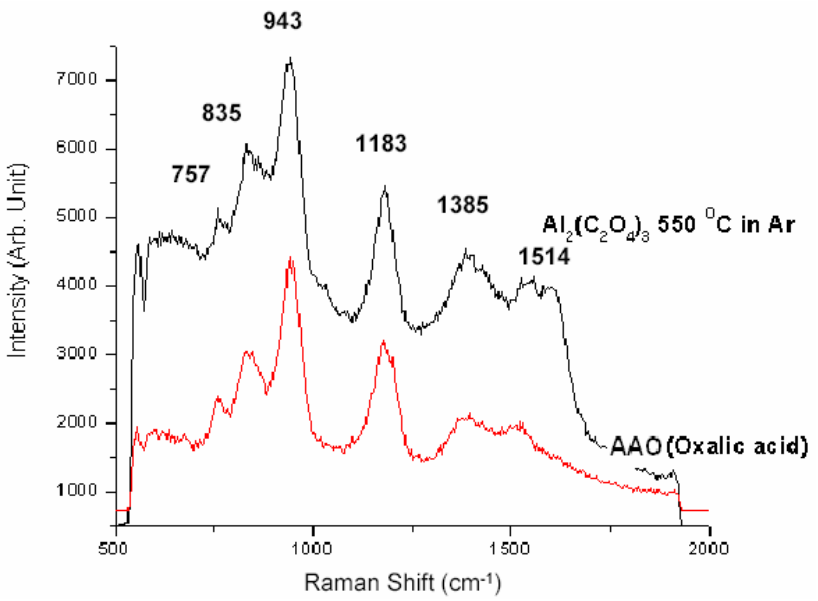

Fig 3.7 Raman spectrum of the AAO membrane (prepared with oxalic acid solution) and that of the aluminum oxalate powder

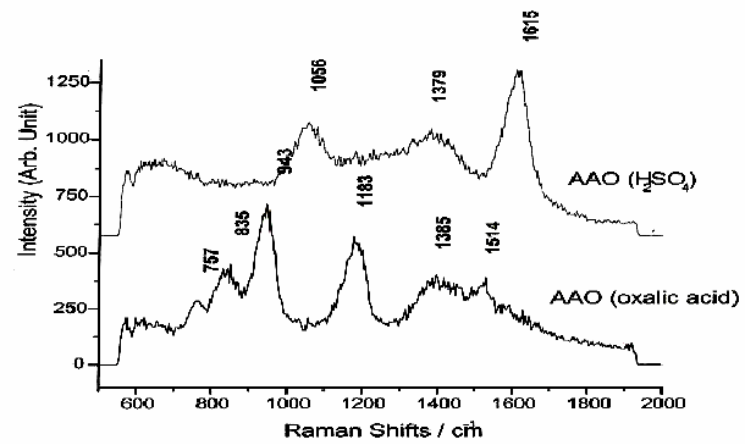

Fig 3.8 Raman spectra of the AAO membranes prepared with oxalic acid and sulfuric acid solution

Thermogravimetric Analyses are performed on the AAO membranes to monitor the process of dehydration and the decomposition of the impurities. The results show that the dehydration takes place slowly at temperatures above RT while the impurities decompose

at very high temperatures. As is shown in the TGA curve obtained from the AAO membrane made with oxalic acid solution (Fig 3.9-a), the slow decrease in the sample mass with the elevated temperature is due to the dehydration and the sharp slump of the curve starting at around 850 °C corresponds to the decomposition of oxalates. Fig 3.10 shows the Raman spectra of the same membrane sample taken after calcination at different temperatures. [53] The bands from the incorporated oxalates remain in the spectra until a calcination temperature as high as 900 °C is reached. The loss of mass corresponding to the impurity decomposition is about 5% for the membrane prepared with oxalic acid. After calcination at 900 °C the crystal structure of the membrane begins to change to α alumina while the hexagonal porous nanostructure is still maintained. As for the membrane synthesized with sulfuric acid solution, the TGA curve (Fig 3.9-b) shows that the sulfates start to decompose at around 930 °C.

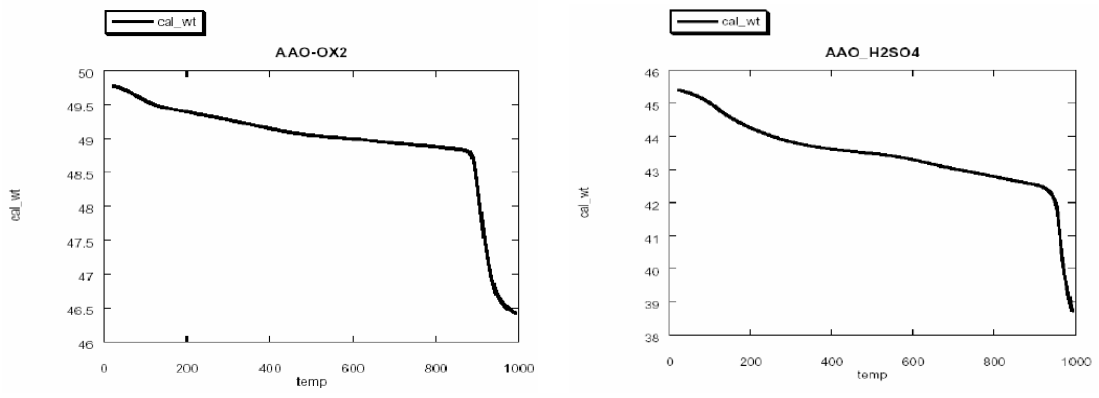

(a) **(b)**

Fig 3.9 The TGA of the AAO prepared with (a) oxalic acid and (b) sulfuric acid solutions

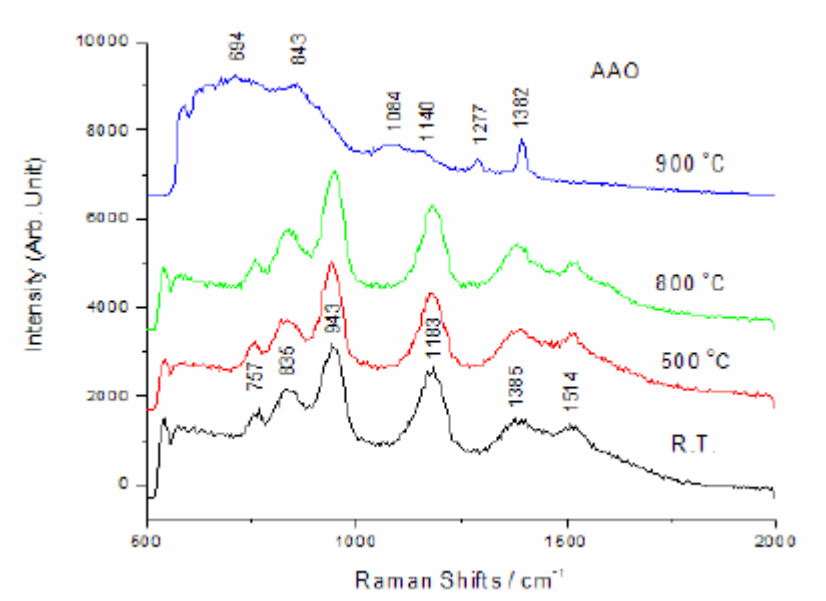

Fig 3.10 The Raman spectra of the AAO membrane (prepared with oxalic acid solution) after calcinations at different temperatures.

XPS is used to quantitatively measure the sulfur content in the AAO membrane made with sulfuric acid solution, because the TGA measurement was unable to give this result due to the limitation of the instrument used. In the XPS spectrum (Fig 3.11) the two peaks at 1055 and 1075 eV are assigned to sulfur. The integration of these peaks shows that in this sample the number of sulfur atoms is approximately 3-4% of that of the oxygen atoms. This result indicates that approximately 8-10 %(wt.) of the membrane structure is made of sulfates.

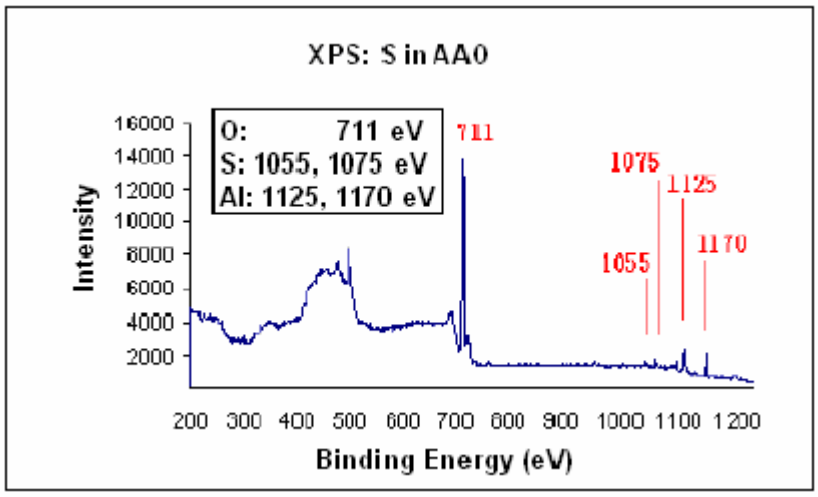

Fig 3.11 The XPS of the AAO membrane synthesized with sulfuric acid solution

The anodic oxidation process appears to produce some oxygen vacancies in the AAO membranes. These oxygen vacancies are partially charged and consequently generate signals in EPR spectra (Fig 3.12). [54] It appears that the presence of these oxygen vacancies is dependent on the type of electrolyte used during the anodization, in that no EPR signal is found on the membrane synthesized in sulfuric acid solution. Additionally, calcination at high temperatures can effectively reduce the strength of the EPR signal from the AAO membrane prepared in the oxalic acid solution, which seems to be related to the decomposition of the incorporated oxalates. Consequently, it was assumed that the EPR signals observed from AAO membranes are actually from the incorporated impurities. However, no EPR signal has been observed from the pure aluminum oxalate powder. In addition, it turns out that the decrease in the EPR signal from the membrane as a result of the heat treatment occurs at temperatures much lower than the decomposition temperature of the incorporated oxalates – higher temperatures only increase the rate of

disappearance. Therefore the reduction in the EPR signal after high temperature treatments probably reflects an annealing process of the oxygen vacancies in the AAO membrane. Currently the origin of these oxygen vacancies in the AAO membrane has not been clarified.

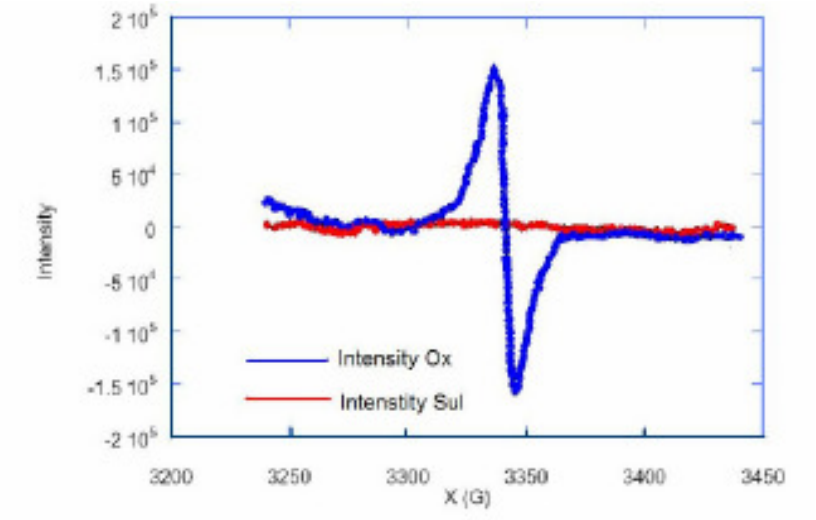

Fig 3.12 The EPR spectra of the AAO membranes

Since both the incorporated impurities and the possible presence of the oxygen vacancies in the AAO membrane might influence the catalytic properties of the support, all the membranes are coated with 1nm of Al_2O_3 (or other metal oxides) by ALD before catalyst loading and testing.

Chapter 4

4. Building the Nano Reactor Arrays

4.1 Overview

This chapter reports our preliminary results on the application of the nano-structured anodic aluminum oxide (AAO) membrane in heterogeneous catalysis. Procedures for growing the AAO membrane in the center of an aluminum disc have been developed by appropriately masking the disk's perimeter during the anodization and etching steps. The remaining aluminum ring connects seamlessly to the AAO and serves as a support for the membrane allowing convenient handling. The supported AAO membrane can be sealed, gas tight, in a flow reactor so that the nanopores on the membrane function as a parallel array of tubular reactors. Coating catalytically active materials onto the walls of the nanopores turns the AAO membrane into a novel catalytic system. In the oxidative dehydrogenation (ODH) reaction of cyclohexane, the membrane catalytic system demonstrates advantages over the conventional powder bed in terms of overcoming bypass and diffusion limitations, reducing over oxidation, and inhibiting undesired gas phase reactions. These nanoreactors function more like mixed flow reactors rather than plug flow reactors, in that Knudsen diffusion has a larger contribution to the mass transport inside the nanopores than does mass flow.

4.2 Discussions

4.2.1 The AAO Membrane Embedded in Aluminum Ring Support

During the catalysis experiment a gas tight seal between the AAO membrane system and the flow reactor is required to ensure that the reactants must flow through the nanopores in the membrane and gas bypass is eliminated. With our AAO/Al ring assembly a crack or gap at the boundary between the AAO and the supporting aluminum ring is the most likely location for gas bypass. Therefore this region was examined with SEM. As seen in Fig 4.1 and Fig 4.2, the morphology of the boundary regions on the front side (the anodized side) looks quite different from the backside (the etched side). On the front side, the AAO layer becomes thinner as it approaches the edges; at the boundary an alumina layer of several microns thick joins the aluminum on the ring. In this boundary region, aluminum can be found buried under the thin layer of AAO and the whole configuration is similar to a frozen lake where the ice shell becomes thinner as it approaches the shoreline and finally pushes against the rocks on the shore. Additionally, the pattern of the pores near the front side edge is not as regular as that in the center of the membrane. On the backside, however, the actual boundaries seem to be completely covered by the aluminum and there is no noticeable difference in the regularity of the patterns between the pores near the boundaries and in the center of the membrane. Generally speaking, the transition from AAO membrane to aluminum ring support is seamless; there is no evidence of cracking along the AAO/aluminum boundary. Based on the above observations, a schematic picture of the cross-sectional view of the connection between

the AAO membrane and the aluminum ring is drawn in Fig 4.3.

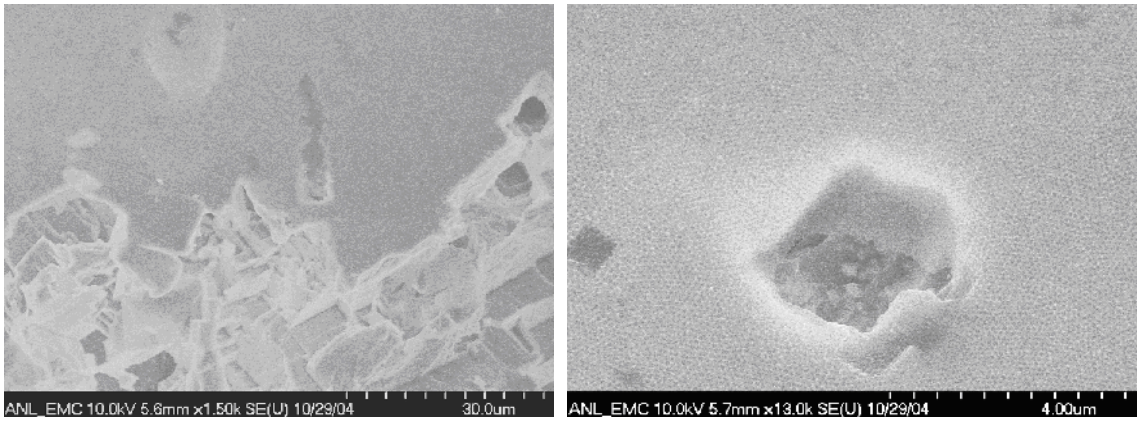

(a) **(b)**

Fig 4.1 SEM images of the AAO/aluminum boundaries on the front (anodized) side. (a). The AAO/aluminum interface. The flat layer in the upper part of the picture is the AAO. (b). A defect point (a hole) on the AAO near the interface. Aluminum is visible under a very thin layer of AAO.

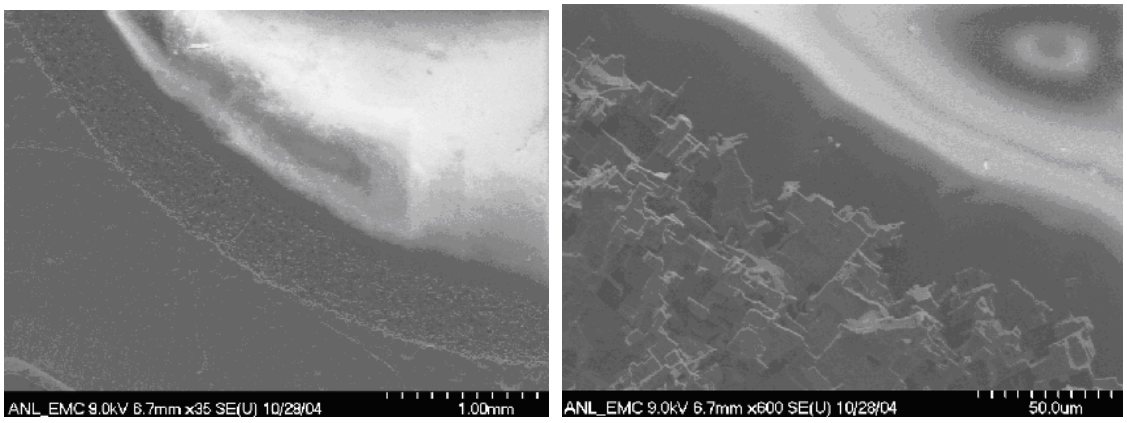

(a) **(b)**

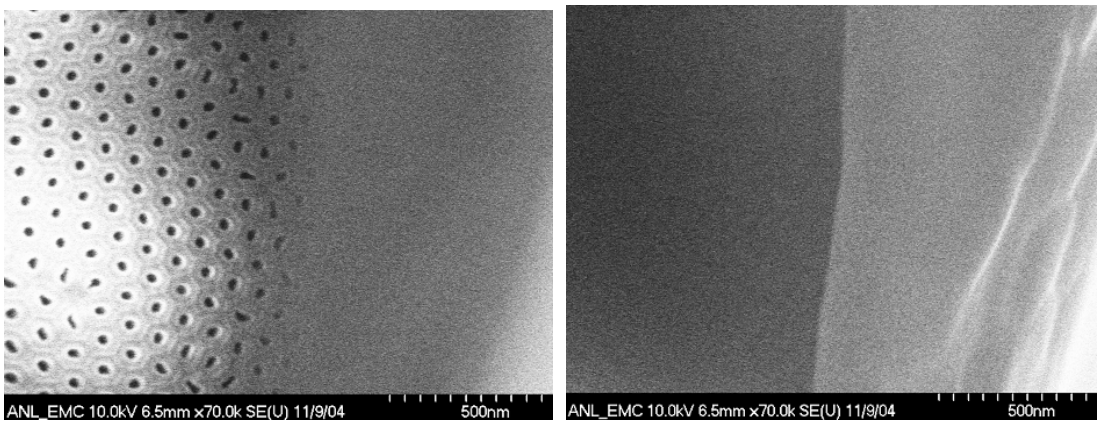

(c) **(d)**

Fig 4.2 SEM images of the AAO/aluminum boundaries on the backside (the etched side) of the membrane. (a) & (b), low magnification images of the AAO/aluminum interface. (c) & (d), high magnification pictures of the interface when the beam is focused on the AAO (c) and aluminum (d).

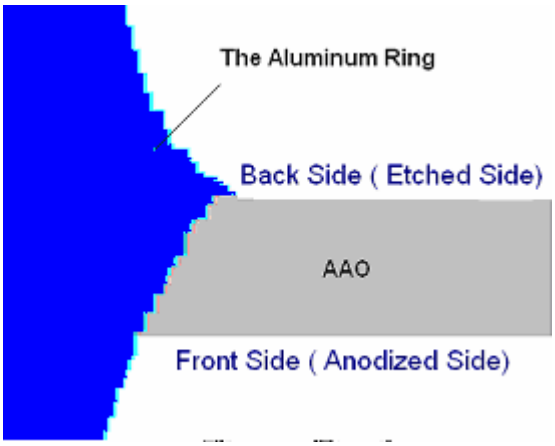

Fig 4.3 The configuration of the AAO/Aluminum connection

The mounted AAO membrane can be sealed in a standard Swagelok face seal adaptor (VCR fitting), in which two metal glands are tightly held against the aluminum ring to

form a gas tight seal (Fig 4.4). The adaptor is carefully fastened until no leak can be detected as flowing gas is purged through the fitting. A pressure drop due to the resistance of the nanopores to the flow of gas is present across the membrane, which serves an indicator of the membrane integrity. This pressure drop is related to the size and shape of the nanopores and the density, viscosity, and flow rate of the gas. Plotting the pressure drop versus the flow rate gives the conductance of the AAO membrane. The curves for oxygen and helium plotted in Fig 4.5 are linear in the pressure range between 1.0 to 5.0 Psi. The conductance measured for helium (0.235 ml/s/Psi) is nearly three times that measured for oxygen (0.78 ml/s/Psi). Both extrapolate to zero at the origin. Detailed analysis of the gas flow through these nanopores and its relation to the pore size has been discussed elsewhere. [55]

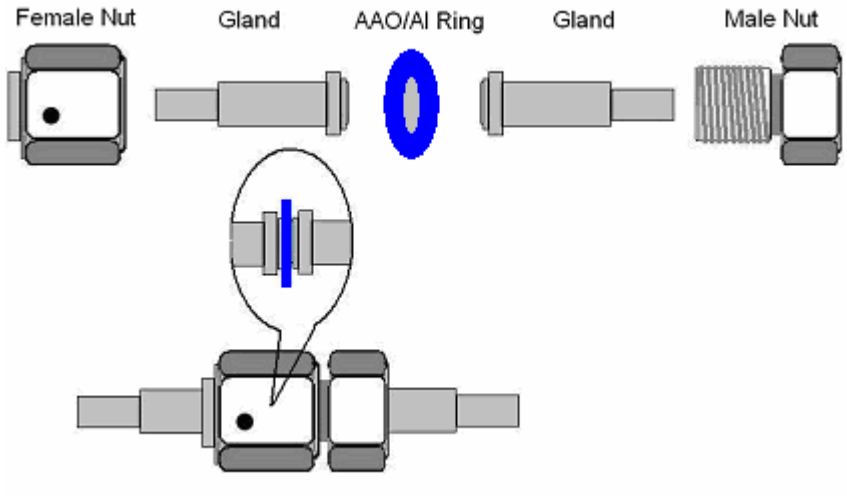

Fig 4.4 The supported AAO membrane sealed in a VCR fitting as a gasket.

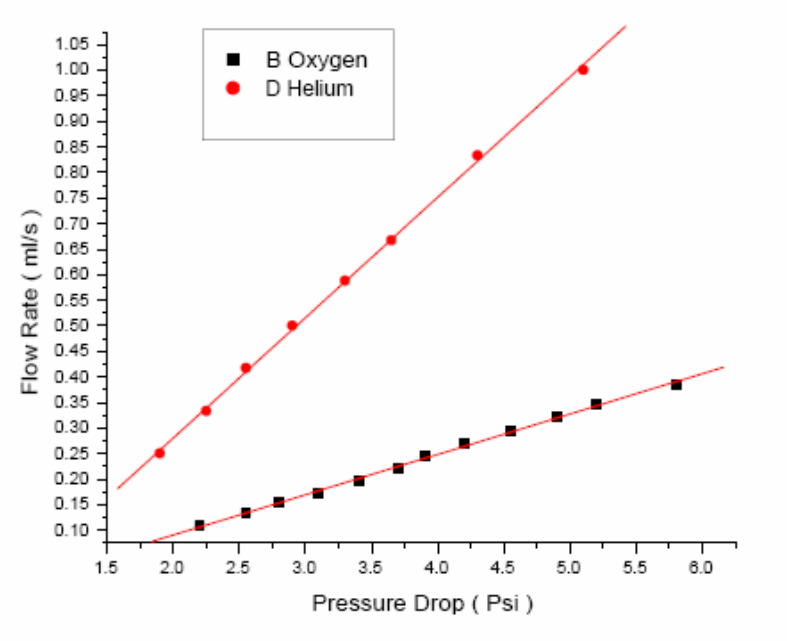

Fig 4.5 The conductance of the AAO membrane measured with oxygen and helium

To check the mechanical and structural stability of the AAO membrane under the conditions of the catalytic reaction, the membrane sealed in the VCR fitting was heated at 500 °C for several hours in flowing oxygen. After the test, no leak from the fitting was detected, and no cracks were found either on the AAO membrane or at the AAO/aluminum boundaries. In our experience a 70-microns-thick membrane can withstand a relative pressure of up to 11 Psi.

4.2.2 Catalytic Performance: Membrane VS Powder

The performance of the membrane catalytic system and a conventional powder bed was compared by conducting a catalytic reaction experiment on an intact membrane sealed in

the VCR flow reactor and on the same membrane material crushed into a powder. The samples used in these tests were prepared by coating the AAO membranes with two ALD cycles of VOx. The vanadium surface concentration on these samples is approximately 5.7V/nm^2 according to the XRF measurements (calibrated by the ICP results). Catalytic results on the membrane samples are reproducible with no evidence of deactivation. After these tests the membrane was ground into a fine powder and mechanically mixed with SiC, an inert dilute used to increase the total volume of the catalytic layer. Since ALD produces an extremely even dispersion of the catalytic species, VOx particles are not formed on the surface of the AAO membrane, which means that the process of grinding the membrane into the powder should not change the structure or chemical properties of the VOx catalyst or the number of the active sites. The powder mixture was loaded into the VCR flow reactor to produce a densely packed bed approximately 1 mm thick. The catalytic reaction was performed under the same experimental conditions used for the intact membrane. The results from the membrane and the powder bed are compared in Fig 4.6.

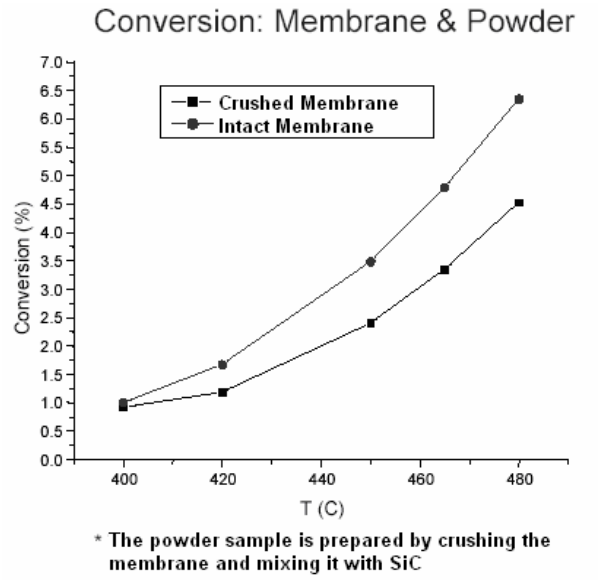

a.

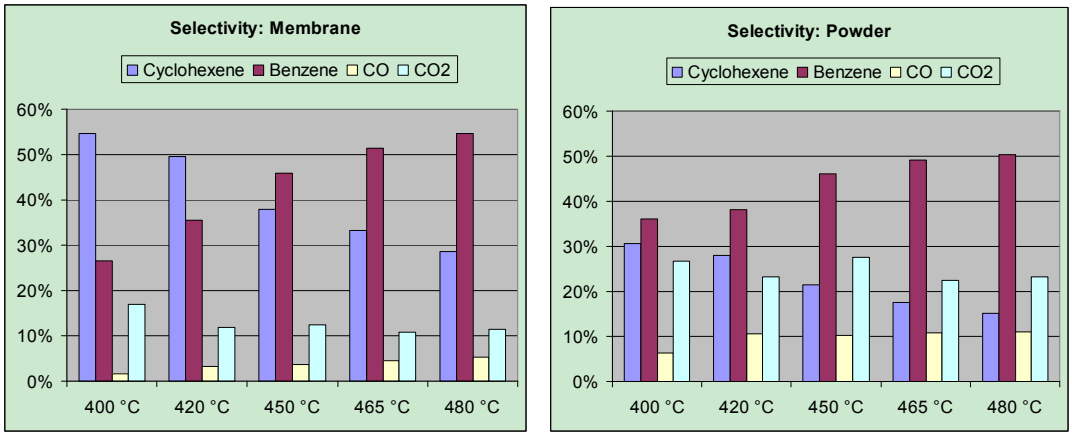

b.

Fig 4.6 The catalytic performance comparison between the sealed membrane and the grinded membrane: (a). conversion; (b). selectivity

It is interesting to note that the membrane system shows better activity than the powder bed. The higher activity of the membrane system is probably related to the configuration of the nanoreactor arrays in which each single reactant molecule must flow through the

catalytic pores. The schematic pictures drawn in Fig 4.7 compare the situation when the reaction is carried out in the powder bed and in the membrane reactor. In the membrane case, reactant molecules cannot avoid contact with the catalytic surface. However, in the powder bed, since the reactant is not forced into the pores of the catalyst particles, some of the reactant molecules may bypass the catalytic particles and have no chance to react. Furthermore, the configuration of the nanoreactor arrays helps make full use of all the catalytic species because in the force-through mode each reactant molecule has to travel through the entire length of the pore to leave the catalytic layer. This configuration guarantees that all the catalysts are accessible to the reactant, including those located deep in the pores and consequently harder to reach by random diffusion into catalyst support particles.

The results in Fig. 4.6 show that a much better selectivity to cyclohexene is achieved with the membrane system as compared to the powder bed. With the sealed AAO membrane, the selectivity to the deep oxidation products, CO and CO_2, is relatively low at all measured temperatures and conversions. In contrast, a much larger fraction of the reactant is converted to COx over the powder catalyst. The selectivity to benzene is similar in both configurations. These results are consistent with our expectation that the membrane reduces the residence time of the partial oxidation product (cyclohexene) in the catalytic layer and avoids deep oxidation. In the powder system, because the reactant (or the partial oxidation product) may diffuse into several porous catalyst particles before

leaving the catalytic layer, the total residence time may be very long for some molecules; in the membrane system the reactant typically diffuses through a single pore. Consequently, for a fraction of the reactant, the total residence time in the powdered catalytic layer may be much longer than in the sealed membrane, which will results in higher selectivity to the deep oxidation products in the powder bed.

Besides the effects of the limited contact times, the membrane system may also be capable of prohibiting the direct conversion from cyclohexane to COx by reducing the gas phase combustion reactions. Since the selectivity toward benzene and COx are uncorrelated, it appears that COx is formed directly from cyclohexane or cyclohexene rather than a consecutive path through benzene as an intermediate. Indeed, experiments have shown that benzene has low reactivity toward COx formation. The production of the COx species is very likely to come from the surface enhanced homogeneous reactions due to the desorption of the reactive intermediates from the catalytic surface. These intermediates are in the form of alkyl radicals and their reactions with molecular oxygen in the gas phase will lead to the formation of the COx. [56] The gas phase reactions will mainly take place in the void volumes of the catalytic layer since other spaces of the reactor have been filled with quartz chips, which have been shown to be able to effectively quench free radicals and inhibit homogeneous reactions. [24] In the membrane system, because the diameter of the nanopores is less than the mean free path of the reactant molecules, collisions between the reactant molecule and the pore walls are much

more frequent than those between the reactants themselves in the gas phase. In these collisions with the pore walls, the potential for homogeneous free radical reactions may be effectively quenched due to readsorption or radical transfer processes. However, in the powder bed with inert diluents, where the void spaces between the particles are much larger, homogeneous reactions may occur, contributing to the higher COx yield in the powder bed.

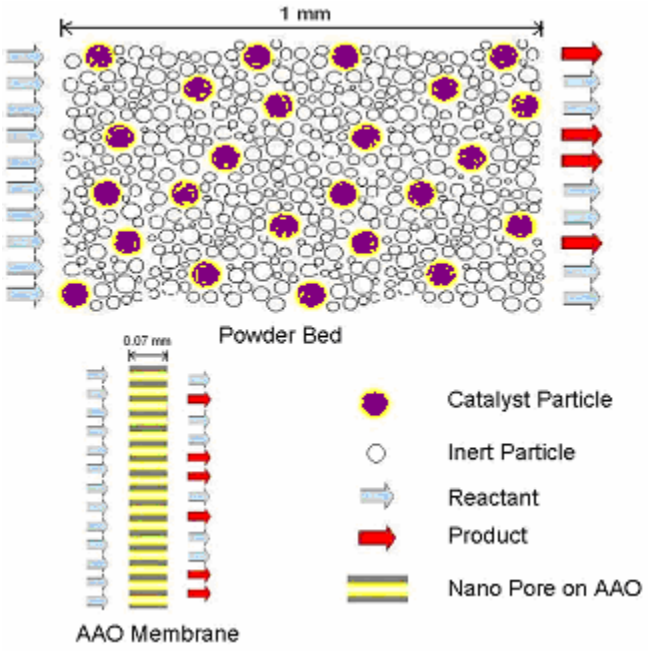

Fig 4.7 Comparison between the membrane catalytic system and the powder bed

4.2.3 Performance Function of the Nano Reactor Arrays

A most remarkable feature of the membrane catalytic system is that the reactants must flow through the nanopores in the AAO membrane, which makes each of these pores

function as a nanoscale reactor. Since the nanopore in the membrane has the shape of a long straight tube, it is natural to view each pore in relation to a plug flow reactor. However, because the dimensions of these nanoreactors are so small, diffusion also has to play an important role in the mass transfer. A plug flow with dispersion model may be appropriate for analyzing the mass transfer in the nanopore. [57] In an elementary section of the nanopore pictured in Fig 4.8, if u denotes the linear velocity of the reactant flow (m/s), C_A is the concentration of the reactant, l denotes the length of the tube, S is the cross sectional area of the channel, D is the diffusion constant (m^2/s) and k is the chemical reaction rate constant, the reactant entering the elementary section by mass flow is expressed as:

$$C_A(x) \times u \times S \qquad 4.1$$

The reactant entering the section by diffusion is:

$$-D\left(\frac{dC_A}{dl}\right)_{l=x} \times S \qquad 4.2$$

Similarly, the reactant leaving this elementary section by mass flow and by diffusion can be expressed as:

$$C_A(x+dx) \times u \times S \qquad 4.3$$

and

$$-D\left(\frac{dC_A}{dl}\right)_{l=x+dx} \times S \qquad 4.4$$

The reactant consumed in this section of nanopore due to the surface reaction is:

$$k \times C_A(x) \times 2\pi r \times dx \qquad 4.5$$

The mass balance equation in this elementary section of nanopore means that the disappearance of the reactant in this elementary section, which is equal to the sum of the differences between the reactant entering and leaving this section by mass flow and by diffusion, is due to the chemical reaction on the surface of the pore walls. Therefore this equation can be expressed as:

$$-D\left(\frac{dC_A}{dl}\right)_{l=x} \times S + C_A(x) \times u \times S + D\left(\frac{dC_A}{dl}\right)_{l=x+dx} \times S - C_A(x+dx) \times u \times S$$

$$= k \times C_A(x) \times 2\pi r \times dx \qquad 4.6$$

or

$$u\left(\frac{dC_A}{dl}\right) - D\left(\frac{d^2C_A}{dl^2}\right) + k'C_A = 0 \quad (k' = \frac{2k}{r}) \qquad 4.7$$

The three terms in the equation 4.7 represents the contributions from mass flow, diffusion and chemical reaction, respectively. In this equation the chemical reaction is assumed to be a first order reaction, whose rate is proportional to the concentration of the hydrocarbon reactant. In fact, it will be shown in the next chapter that the ODH of cyclohexane behaves very similar to a first order reaction at low conversions.

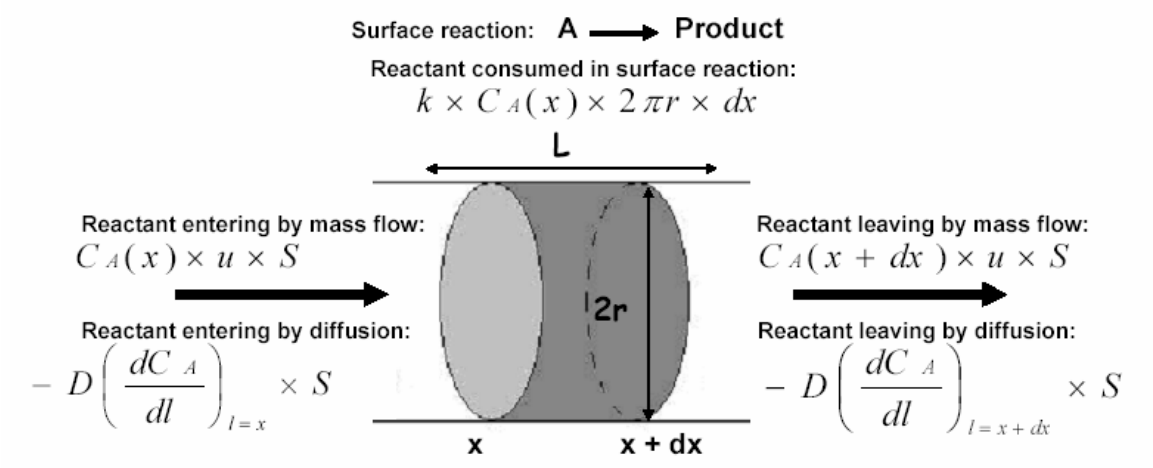

Fig 4.8 The mass balance in an elementary section of the nanopore

In dimensionless form where z = L/l, τ = L/u (the residence time), the above equation becomes:

$$\frac{D}{uL}\left(\frac{d^2C_A}{dz^2}\right) - \frac{dC_A}{dz} - k'\tau C_A = 0 \qquad 4.8$$

In this equation, the coefficient of the first term D/uL determines the contribution from diffusion on the reactor performance or how much the system deviates from the plug flow model. When the D/uL value is less than 0.01, the reactor is very similar to a plug flow reactor; while its performance transforms to more of a mix flow reactor as the D/uL value becomes larger. In the nanopores on the AAO membrane where the mean free path of the reactant molecule is much longer than the diameter of the pores, Knudsen diffusion is the predominant diffusion mode. [13] The Knudsen diffusion constant can be estimated as:

$$D_k = \frac{2}{3} r \sqrt{\frac{8RT}{\pi M}} \qquad 4.9$$

, in which r is the radius of the pore and M is the molar mass of the molecule. In most of our experimental conditions (T~700K, v = 10ml/min), the D_k value is estimated to be approximately 1.1×10^{-5} m^2/s, and the corresponding D/uL coefficient is around 14. This D/uL value implies that Knudsen diffusion has a significant contribution to the mass transfer in the nanopores, therefore a large deviation from the plug flow model is expected. The nanoreactor arrays are very likely to function more like mixed flow reactors rather than plug flow reactors. For both types of reactors, the conversion should be almost proportional to the residence time when it is low enough. In one experiment of cyclohexane ODH on a membrane coated with 1 cycle of VOx by ALD, the reactant residence time in the nanopores was adjusted by changing the flow rate of the balancing helium. (While the concentration of cyclohexane in the nanopores is not changed.) The conversions obtained at different flow rates are presented in Fig. 4.9. As expected, at higher flow rates a linear correlation between the conversion and the residence time (1/flow rate) was observed. At lower flow rates or longer residence times, the curve deviates from the straight line, which may be due to a decrease in reaction rate at higher hydrocarbon conversions (lower reactant concentrations). This result shows that the performance of these nanoreactor arrays can be predicted through analysis of the physical model and controlled by adjusting the experiment settings. More catalysis experimental results focused on understanding the properties of these nanoreactor arrays will be

described in chapter 7.

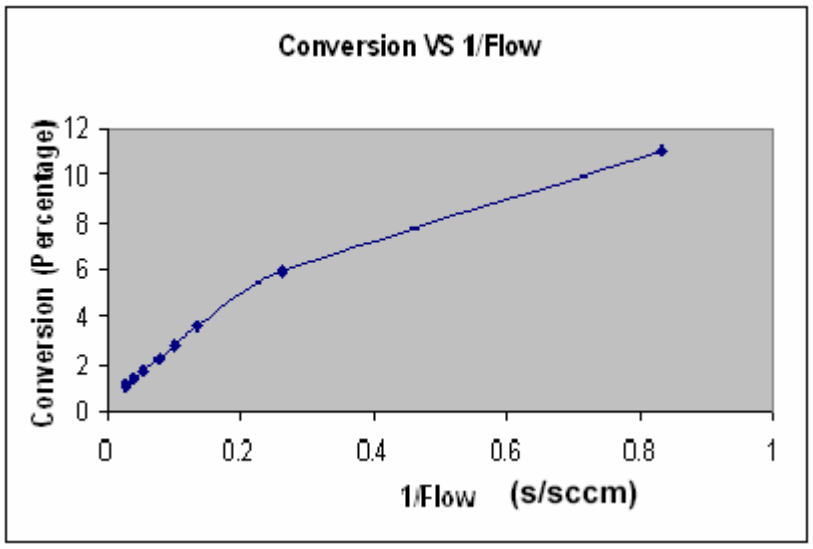

Fig. 4.9 The dependence of conversion on residence time (1/flow rate)

Chapter 5

5. Catalytic Performances of Vanadium Oxides Supported on the AAO Membranes

5.1 Overview

In this chapter the catalytic performance of vanadium oxides supported on the AAO membranes is studied. The catalysts deposited on the membranes by ALD and by incipient wetness impregnation are characterized by XRF and UV-Vis spectroscopy. In the ODH of cyclohexane, all the ALD VOx samples show higher TOF (normalized by the number of V centers) than the impregnated VOx samples, which reflects the better dispersion of the catalytic species on the surface as synthesized by ALD. In the same range of VOx loadings, distinct catalytic activities resulting from different structures of the catalytic sites are more evident on the samples prepared by multiple cycles of ALD, implying that the form of the supported catalyst can be better controlled by applying the ALD technique. In the ODH of cyclohexane catalyzed by supported ALD VOx, the determined reaction rate equation and the activation energies are comparable to kinetics data reported for VOx supported on γ-alumina. These results indicate that the ALD technique can be applied as an alternative approach to synthesize supported catalysts.

5.2 Discussions

5.2.1 The VOx supported on the AAO membranes

The surface area of the AAO membrane is calculated from direct measurements on the nanoporous structure made by SEM. The AAO membrane is unique in its highly ordered hexagonal pattern of nanopores and the uniformity in the pore size and shape. Therefore a calculation of the total surface area of the membrane can be made based on the information about the pore density, the average pore diameter, and the thickness of the membrane. From the calculation, each piece of the as-prepared AAO membrane (40nm pores, 110nm pore-to-pore separation, and 70 μm thickness) has a total surface area of about 0.053 m^2. Since a piece of such membrane weighs about 9 mg, the surface area of this material is approximately 5 m^2/g.

It is know that the AAO membranes are not made of pure alumina in that anions in the electrolyte, such as oxalates or sulfates, are incorporated into the alumina framework during the anodization process. TGA measurements show that the decomposition temperatures of these incorporated impurities are as high as 890 – 950 °C. Since this temperature range exceeds the melting point of the supporting aluminum ring, calcination is not a feasible way to remove those impurities. To avoid the possible interference from the impurities in the catalytic reactions, the membranes were usually coated with 1nm of Al_2O_3 by ALD to completely cover the incorporated anions. In blank tests on the AAO membranes under the conditions of the catalysis experiments, the membranes with ALD

alumina coatings show much less and more stable background reactions (0.1 - 0.5% conversions from 400 to 480°C) than those without the coatings. With the ALD coating, the diameter of the nanopores on the AAO membrane is reduced from 40 nm to 38nm. The corresponding reduction in the total surface area is only about 5%.

It is well established that the incipient wetness impregnation of the vanadium containing precursors and the subsequent calcinations can form a two-dimensional layered structure of supported VOx on the surface of alumina, titania, and niobia. [34, 37] The monolayer loading of VOx depends on the type of support. On γ alumina, this loading is reported to be 13μmol/m^2 or roughly 8 V/nm^2. [34] On the pore walls of the AAO membrane, the layer of ALD coated alumina has been shown to be amorphous. Since the surface of the amorphous alumina has a lot of structural similarities to the γ alumina, [58] the value of 8 V/nm^2 is adopted as the monolayer loading when introducing VOx onto the AAO membranes by the incipient wetness impregnation method. The amount of VOx loaded by ALD is measured by the non-destructive XRF technique. The detected vanadium contents of the ALD samples are listed in Table 5.1. In obtaining the XRF results, the vanadium surface concentrations are calculated based on the measured weight percentage of the VOx species, and the total weight and the surface area of the AAO membranes. Since in the XRF measurements no accurate calibration has been carried out because of the difficulty of obtaining a series of homogeneous powder samples, which are of the same composition as the AAO membrane and supported with a known amount of VOx,

results of the ICP measurements are used to provide a calibration for these XRF data. The calibration is made by comparing the XRF and ICP data measured on the same samples, from which an almost linear function is found to correlate the two sets of data. This method is described in detail in the next chapter. The calibrated vanadium surface concentration data are also listed in Table 5.1.

VOx Sample	Weight Percentage (V_2O_5 wt %)	Surface Concentration Measured by XRF (V/nm^2)*	Calibrated Surface Concentration (V/nm^2)
ALD 1 cycle	0.18%	3.5	2.8
ALD 2 cycles	0.41%	8.0	6.4
ALD 4 cycles	0.73%	14.3	11.4

* The V surface concentration is calculated from the measured amount of supported V and the surface area of each membrane.

Table 5.1 The loadings of ALD VOx measured by XRF

The vanadium species coated by each cycle of ALD is much less than the assumed monolayer loading, which means that a single cycle of the VOx ALD does not cover the entire surface. This is likely due to the steric constraints imposed by the vanadia precursor or perhaps because of the limited density of surface hydroxyls on the AAO membrane. Additionally, the lower vanadium surface concentrations on the ALD samples

indicate that there cannot be significant micro-porosities in the AAO membrane. If there were a lot of micro-pores in the membrane structure, they would have been coated during the ALD process and consequently the VOx loading by ALD would have been significantly higher than that by wet impregnation. However, this phenomenon is not found in the comparison between the VOx loadings by the incipient wetness impregnation and by the ALD.

Because of the electronic transitions between the ligand and the metal center, a large and broad band can usually be observed in the UV-Vis spectra of the supported VOx catalysts. In these spectra, the absorption edge energy (E_g) can be used to determine the state of the VOx species since it has been shown to be related to the number of V-O-V bond or the domain size of the catalytic site. [36] Fig 5.1-a displays the transmission UV-Vis spectra of the membranes loaded by ALD and the impregnated VOx. On these samples, the spectra measured before catalytic reaction show little difference to those measured after the reactions and subsequent calcination. The edge energies were determined from the x-intercept of the linearized near edge region in the absorption versus hυ curve where hυ is the incident photon energy (Fig 5.1-b). The obtained E_g values of the two types of samples are listed in Table 5.2 for comparison.

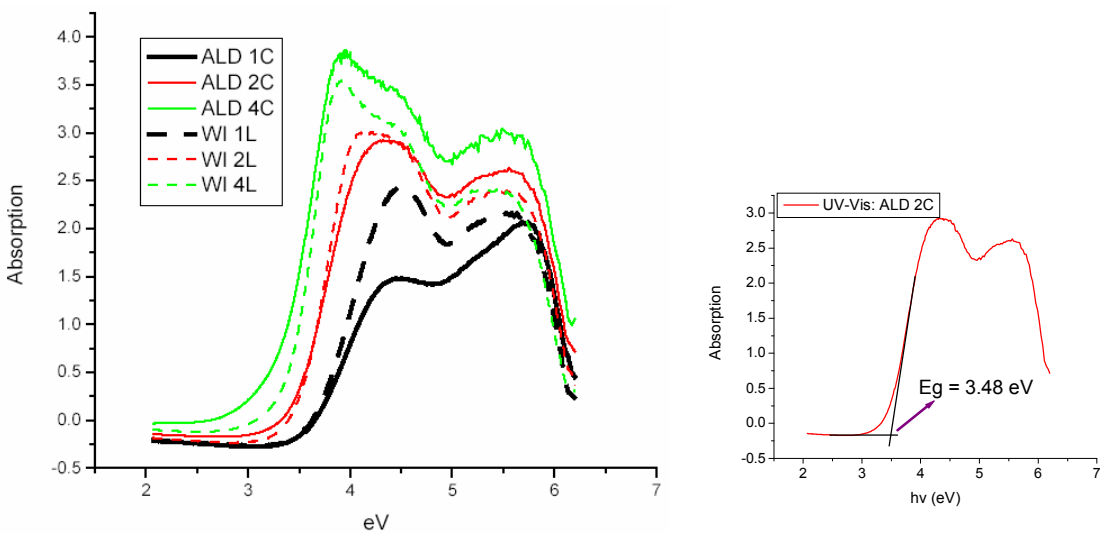

a. **b.**

Fig 5.1 The UV-Vis absorption spectra of the ALD and the wet impregnated VOx supported on the AAO membranes. a.) The UV-Vis spectra of the ALD and W.I. VOx samples. b.) The determination of E_g from the UV-Vis spectrum of the 2-cycle ALD VOx sample.

Sample	E_g (eV)
ALD 1C	3.64
ALD 2C	3.48
ALD 4C	3.33
W.I. 1 L	3.69
W.I. 2 L	3.52
W.I. 4 L	3.37

Table 5.2 The edge energies of the ALD and the impregnated VOx supported on the

From the above spectra we find that the edge energies of both the ALD and the impregnated VOx samples show red shifts as the loading increases. The change in the edge energy is due to the change in the local structure of the V^{5+} center with the increased loading of the catalyst. Generally speaking, the isolated VOx sites, which are formed at a low loading of the catalyst, show higher edge energy in the UV-Vis absorption spectrum; polyvanadate domains, which are formed at higher loadings, have lower edge energies. The detailed analyses of these edge energy values with relation to the specific structures of the VOx sites are discussed in the next chapter. Interestingly, despite the large difference in VOx loadings between the two types of samples, the edge energies of the 1-cycle, 2-cycle, and 4-cycle ALD samples are close to their 1-layer, 2-layer, and 4-layer wet impregnated counterparts, indicating that the predominant forms of the VOx sites are nearly the same on each pair of the membranes having the similar edge energy. Additionally, although the change in the loading between the wet impregnated samples is much greater, the change in the adsorption edge energy on these samples is similar to or even smaller than that between the ALD samples. These phenomena probably reflect the different qualities of the two types of catalyst loading methods. It is well known that the ALD technique enables an extremely even coating of the catalytic species on the surface. [59] In contrast, the incipient wetness impregnation and the following calcinations cannot guarantee a perfect dispersion of the catalytic species, and consequently particles of V_2O_5

may be formed even at loadings much lower than the theoretical monolayer. [36,87] Correspondingly, in some areas of the surface, the vanadium density (or the average VOx domain size) has to be smaller. During the impregnation process, due to the condensation of the precursor solution near the boundary of the alumina membrane and the aluminum ring, layers of crystalline V_2O_5 are very likely to be formed in these regions. However, in the UV-Vis transmission spectroscopy measurements, only the transparent alumina membrane embedded in the center of the aluminum ring is exposed to the beam and is characterized, where the vanadium surface density is most likely to be lower. It is worth mentioning that the surface area of the porous alumina membrane is much higher than the area of the boundary region, which means that it is the portion of the VOx species dispersed on the alumina membrane that does the chemistry in the catalysis experiments.

5.2.2 Catalytic properties of the VOx supported on the AAO membranes

Both the catalytic reactions and the non-catalytic gas phase reactions may contribute to the cyclohexane conversion under the conditions of the ODH reaction. In the blank test carried out on a piece of AAO membrane coated with only 1nm of Al_2O_3, very tiny conversions (0.1~0.5%) due to the background reactions are found under the conditions of the catalysis tests. These background reactions have been subtracted from the catalysis test results when evaluating the performance of the catalysts.

The catalysis test results on the membranes with the ALD VOx are presented in Fig 5.2.

These experiments are carried out in a temperature range between 400°C and 480°C at a constant reactant flow rate of approximately 10cc/min. Each of these measurements has been taken multiple times and nice reproducibility has been achieved. The samples tested freshly (immediately after the ALD VOx loading) and those re-tested after the calcination in oxygen show little difference in catalytic performance. Therefore the calcinations do not seem to affect the catalytic properties of the VOx sites supported on the AAO membranes. The major detectable products of the cyclohexane ODH reaction are cyclohexene, benzene, CO, and CO_2. These products and the un-reacted cyclohexane account for $100 \pm 0.5\%$ of the carbon balance compared before and after the reaction. For each specific sample, the selectivity to cyclohexene goes down while the selectivity to benzene goes up as the conversion increases with the reaction temperature. However, the selectivity to COx (CO and CO_2) stays almost constant in spite of the change in temperature and conversion. Comparing the membrane samples with different loadings, the conversion becomes higher with the increased loading of the catalyst, accompanied by the lower selectivity to cyclohexene and the higher selectivity to benzene. In all the cases, the cyclohexane conversion and the selectivity to cyclohexene always go in opposite directions. These observed trends reflect a typical hydrocarbon sequential oxidation path where the alkane is first oxidized to the alkenes, which are then further oxidized to the more stable deep oxidation products. Benzene is a special partial oxidation product in this reaction in that it is quite stable and cannot be easily further oxidized; therefore it makes the major product at high conversions.

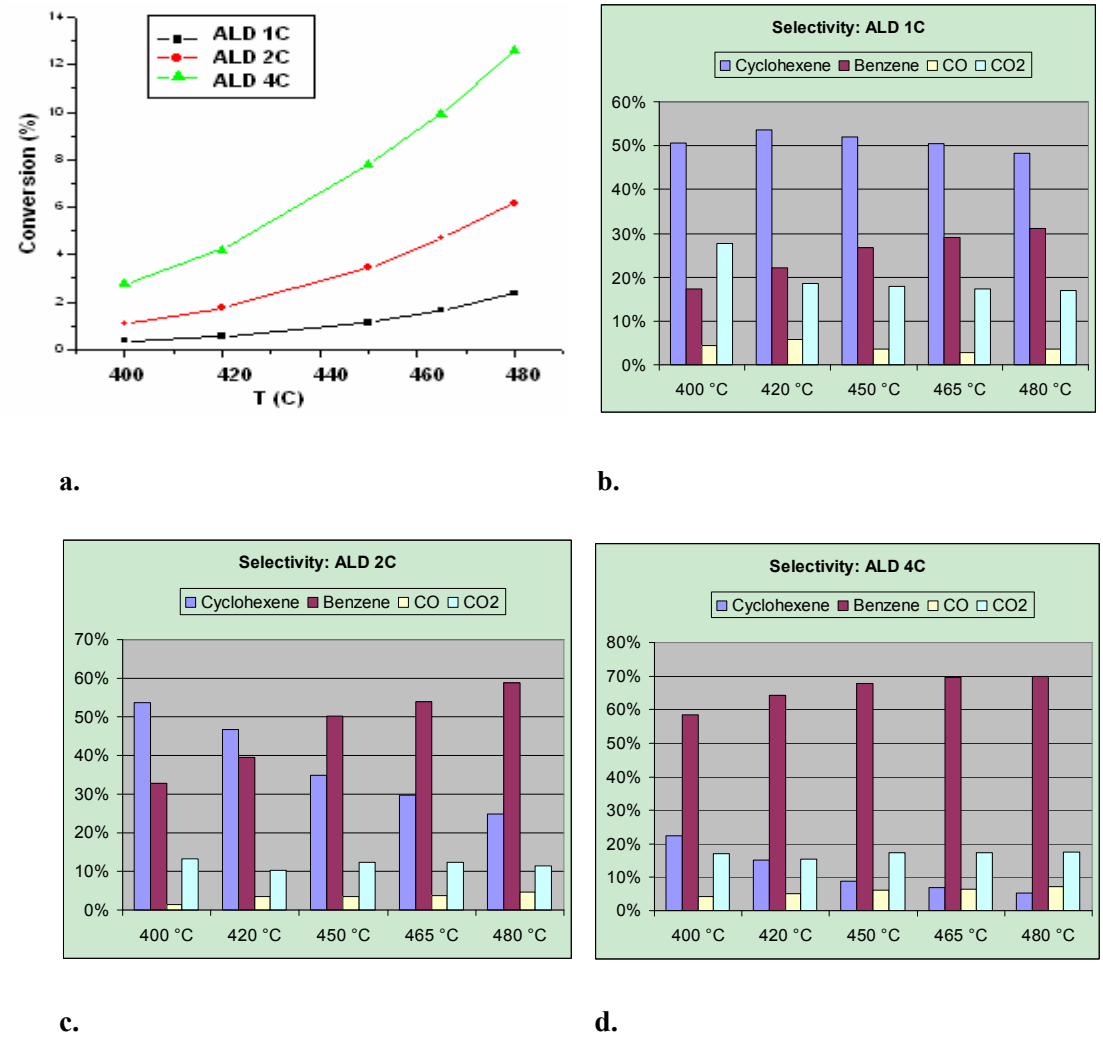

Fig 5.2 The conversion curves (a.) and the product distribution charts of (b.) 1 cycle, (c.) 2 cycles, and (d.) 4 cycles of the ALD VOx supported on the AAO membranes

Fig 5.3 displays the catalysis experimental results on the membranes with the wet impregnated VOx tested under the same reaction conditions. The conversion and selectivity measured from these samples show similar trends as those observed with the ALD samples. For each of the wet impregnated VOx sample, its conversion/selectivity

pattern looks close to its ALD counterpart that has the similar absorption edge energy in the UV-Vis spectrum. The match in the catalysis results provides additional support to the statement that the structures of the catalytic sites are nearly the same on each pair of such membranes.

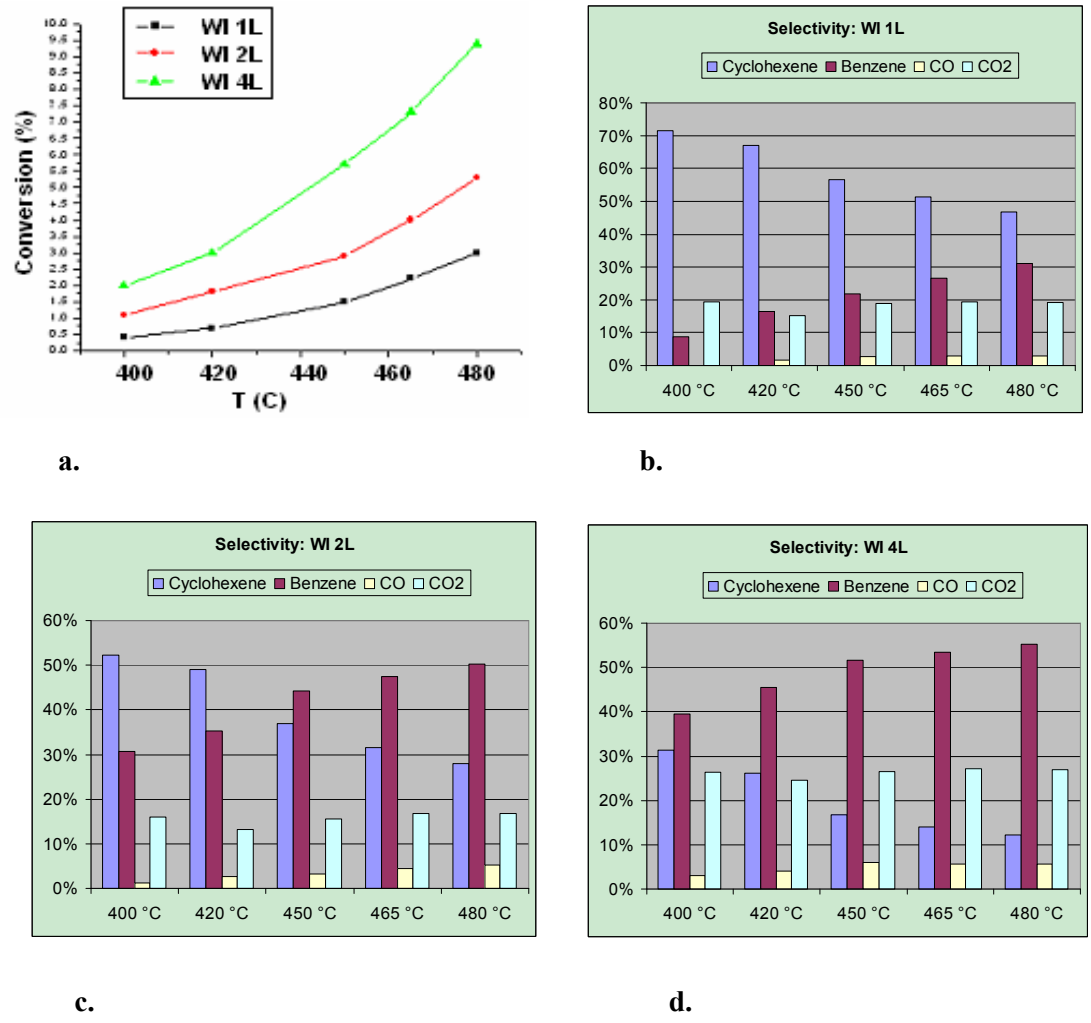

Fig 5.3 The conversion curves (a.) and the product distribution charts of the (b.) monolayer, (c.) 2 layers, and (d.) 4 layers of the wet impregnated VOx supported on the AAO membranes

The TOF of the VOx catalysts supported on the AAO membrane is calculated based on

the total number of the supported vanadium atoms. Fig 5.4 compares the TOF of the wet impregnated and the ALD VOx samples. The wet impregnated samples have remarkably lower TOF than the ALD samples. This result is not too surprising since with the ALD technique the distribution of VOx on the surface is very uniform so that all the vanadium species has a good chance to be exposed and thus made available for the surface reaction. In contrast, the incipient wetness impregnation and the following calcinations do not allow much control over the distribution of VOx on the surface so particles of V_2O_5 may be present somewhere on the surface. As a consequence, part of the vanadium species is buried under the surface layer and made inaccessible to the surface reaction, which will result in a lower TOF normalized by the total amount of the supported vanadium species.

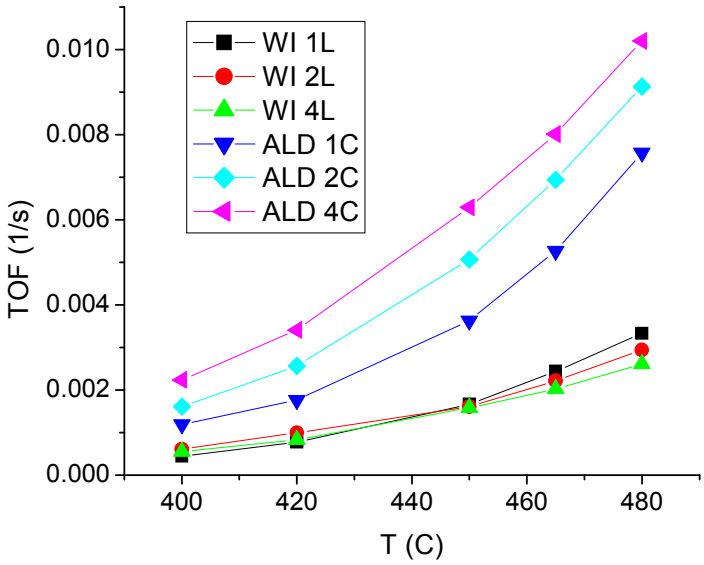

Fig 5.4 The TOF of the VOx supported on the AAO membranes

It is interesting to notice that the TOF of ALD VOx increases with the increasing loading

of the catalyst. This phenomenon reflects the different activities of the catalytic sites formed by different cycles of the VOx ALD. Analyses on the UV-Vis spectra suggest that the VOx species formed by one cycle of ALD is mostly in the isolated state; the V-O-V bond connecting two adjacent V centers begins to form and gradually becomes predominant on the surface as more cycles of VOx are put down by ALD. Due to their different structural and chemical properties such as reducibility, surface hydroxyl density, and the separation between adjacent V centers, the polyvanadate domains turn out to be more active than isolated monovanadate sites in the ODH of cyclohexane. More discussions about this structure-function relationship of the VOx catalysts in the cyclohexane oxidation reaction are reported in the next chapter. Unlike the ALD samples, the wet impregnated samples show little change in the TOF with the different VOx loading. Since these samples have similar UV-Vis absorption edge energies compared to the corresponding ALD samples, any effect on the catalytic activity due to the change in the form or structure of the VOx should also be in effect with them. However, during the wet impregnation process, due to the lack of control over the dispersion of the supported VOx, at higher loadings more V_2O_5 crystals are likely to be formed on the surface, causing more vanadia to be inaccessible to the surface reaction. The consequent reduction in the TOF could counteract with the activity promotion effect and make it unnoticeable. The differences in the TOF between the wet impregnated and ALD samples demonstrate the excellence of the ALD technique in making a uniformly dispersed catalytic layer on the surface even at relatively high loadings of the catalyst.

Since the dispersed VOx species have much greater contribution to the catalytic activity than the crystalline V_2O_5, we can assume that only the former form of the VOx is catalytic while the latter one has almost no contribution to the reaction. From the rising catalytic activity with increasing loading of ALD VOx we know that these VOx coated onto the membranes by a few cycles of the ALD are in the highly dispersed form. Estimations on the percentage of the dispersed VOx species among all the VOx supported on the wet impregnated membranes (including the dispersed and crystallized VOx) can be made by comparing the TOF of the wet impregnated and the ALD samples that possess similar catalytic sites. The calculation procedure is shown as follows:

$$\begin{aligned}\text{Dispersed VOx \%} &= \frac{\text{Conversion}_{\text{W.I.}}}{\text{Conversion}_{\text{ALD}} \times (\text{Loading}_{\text{W.I.}} / \text{Loading}_{\text{ALD}})} \times 100\% \\ &= \frac{\text{Conversion}_{\text{W.I.}} / \text{Loading}_{\text{W.I.}}}{\text{Conversion}_{\text{ALD}} / \text{Loading}_{\text{ALD}}} \times 100\% \\ &= \frac{\text{TOF}_{\text{W.I.}}}{\text{TOF}_{\text{ALD}}} \times 100\%\end{aligned}$$

Because the absorption edge energy in the UV-Vis spectrum is considered an indicator of the structure of the supported VOx domains, the above comparison can be made between the pair of ALD and impregnated samples that have a similar edge energy. According to the UV-Vis spectra of the wet impregnated and ALD samples, the edge energies of the monolayer, 2-layer, and 4-layer wet impregnated VOx samples are close to those of the 1-cycle, 2-cycle, and 4-cycle ALD samples respectively. Consequently, using the TOF data plotted in Fig 6 we find that 46% of the VOx is highly dispersed on the membrane

with the monolayer loading of the catalyst by impregnation; and this percentage drops to 34% and 26% on the membranes with 2 layers and 4 layers of the impregnated VOx. These calculation results are in agreement with our deduction that more V_2O_5 crystal is formed on the membrane with a higher loading of VOx by impregnation. It is worth noticing that these TOF ratios do not change much with the temperature: for each impregnated sample, the variation in the calculated percentage of the dispersed VOx is within 2% at all tested temperatures. To some extent, this excellent consistency in the calculation results support the feasibility and accuracy of the estimation method.

The rate of the heterogeneous catalytic reaction is usually influenced by many factors such as the surface kinetics (including the surface chemical reaction and the adsorption and desorption process), the pore diffusion resistance, and the film mass transfer. In the membrane catalytic system where the reactants are continuously pushed through the nanopores, the diffusion resistance will not significantly affect the reaction rate. Also, since the conversions are low enough in most of our experiments, the mass transfer and the concentration of the products are not likely to significantly influence the reaction rate. In most cases it is good enough to use the simplest available correlating rate expression, hence the exponential rate equation, to represent the surface reaction. Therefore the rate equation of the cyclohexane ODH reaction can approximately be expressed as $r_{(cyclohexane)} = - k [C_6H_{12}]^a [O_2]^b$. The reaction orders with respect to cyclohexane and oxygen were determined by measuring the conversions (the reaction rates) at the different

concentrations of one reactant while holding that of the other constant. From the conversion curves of a catalytic membrane sample loaded with 2 cycles of the ALD VOx (Fig 5.5), we find that the reaction rate increases linearly with increasing concentration of cyclohexane while it remains almost constant at all oxygen concentrations (unless the O_2 partial pressure gets very close to 0). Therefore the dehydrogenation reaction is nearly first order for cyclohexane and is zero order for oxygen. This result is consistent with the reported reaction orders in the ODH of propane and butane over supported VOx. [36, 60] The resultant rate equation is in agreement with the Mars-van Krevelen redox mechanism, in which it is believed that lattice oxygen in the catalytic site is responsible for the dehydrogenation process; while gas phase oxygen only serves as a reservoir of the oxidant that continuously replenishes the consumed lattice oxygen on the surface. [35]

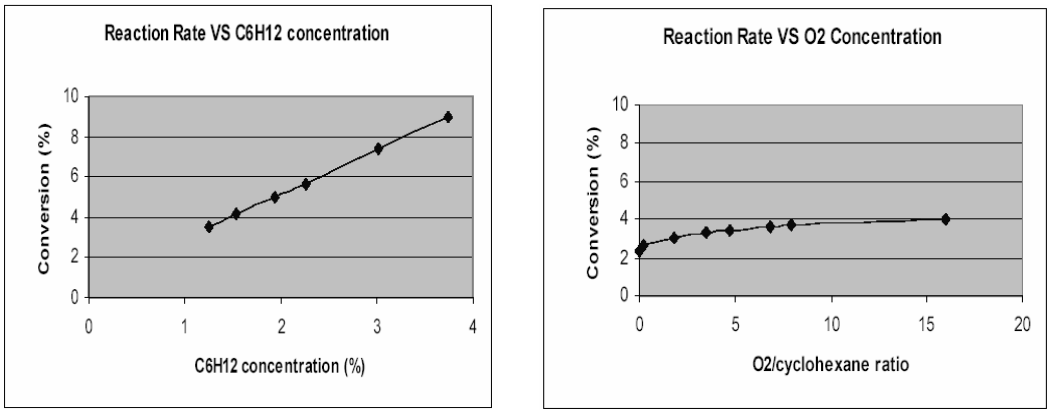

a. **b**.

Fig 5.5 The reaction rates (cyclohexane conversions) at different concentrations of (a.) cyclohexane and (b.) oxygen

The reaction activation energies are obtained from Arrenhius plots (Fig 5.6) using the conversion data over the temperature range of 400 to 480 °C. Since the ODH reaction rate shows a linear dependence on the concentration of cyclohexane, the reaction rate data at zero conversion, which are determined by dividing the percentage of the un-reacted cyclohexane, are used in the Arrenhius plots. As are listed in Table 5.3, the activation energies ranged between 81 and 107 kJ/mol for the wet impregnated samples and between 80.3 and 98 kJ/mol for the ALD samples. For both the ALD and the wet impregnated samples, the activation energy generally becomes lower at a higher loading of the catalyst. This trend agrees with our conclusion that the polymeric forms of VOx domains are more reactive than the isolated form in the ODH of cyclohexane. The activation energies measured in our system are consistent with those of γ-alumina supported VOx reported by Lopez and coworkers in studies of the same reaction. [48] Therefore, neither the AAO scaffold nor the ALD loading technique seems to greatly influence the chemical properties of the supported VOx, which implies that the ALD technique can possibly be widely used as an alternative method to synthesize conventional supported catalysts.

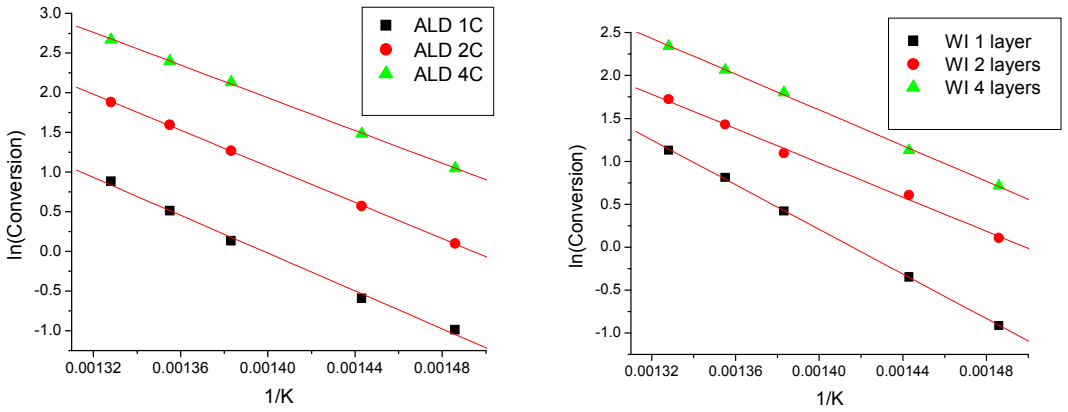

a. **b.**

Fig 5.6 The Arrenhius plots of (a.) the ALD and (b.) the impregnated VOx supported on the AAO membranes

Sample	Ea (kJ/mol)
W.I. 1 layer	106.6
W.I. 2 layers	80.6
W.I. 4 layers	82.4
ALD 1 cycle	98.1
ALD 2 cycles	92.0
ALD 4 cycles	80.3

Table 5.3 The activation energies of the wet impregnated and the ALD VOx supported on the AAO membranes

Chapter 6

6. Structure-Function Relationship of the Vanadium Oxide Catalysts Supported on the AAO Membrane

6.1 Overview

In this chapter the structure-function relationship of the vanadium oxide catalysts is investigated. The catalysts are synthesized by coating different cycles of VOx onto the AAO membranes by ALD. At low loadings of the catalyst, the supported VOx are mostly in the isolated state; the polyvanadate domains are gradually formed as the vanadium content increases. In the cyclohexane ODH reaction, the polyvanadate sites are shown to be more active than the monovanadate sites. On the other hand, the isolated VOx are more selective to the olefin than the polymeric VOx. By comparing the ODH of cyclohexane and the oxidations of cyclohexene and benzene, we find that both the sequential path and the parallel path (the direct conversion from cyclohexane to benzene) exist in the oxidation process of cyclohexane. The formation of benzene may go through either the sequential path or the parallel paths, depending on the structure of the VOx catalyst. The catalytic properties also show strong dependence on the type of support in that the VOx supported on the ALD TiO_2 and Nb_2O_5 fabricated membranes are much more active but not as selective to cyclohexene as those supported on Al_2O_3. The performance of the various VOx catalysts is explained by the different chemical

properties of the catalytic sites due to their structural differences.

6.2 Discussions

6.2.1 Composition and structure of the ALD VOx catalysts

The amount of the catalyst loaded by VOx ALD is measured by both XRF and ICP techniques. As has been discussed in the previous chapter, these two elemental analysis techniques are complementary to each other: the XRF method is convenient and non-destructive; while the ICP results are stable and accurate. Therefore, the ICP data are used as a calibration to standardize the XRF results. The vanadium surface concentrations measured by both techniques are listed in Table 6.1.

VOx Sample	Weight Percentage (V_2O_5 wt %) (XRF)	V Surface Concentration by XRF (V/nm^2)*	V Surface Concentration by ICP (V/nm^2)*
ALD 1 cycle	0.18%	3.5	2.9
ALD 2 cycles	0.41%	8.0	N.A.
ALD 4 cycles	0.73%	14.3	8.9
ALD 8 cycles	0.97%	18.9	14.2
ALD 12 cycles	1.04%	20.3	16.3
ALD 18 cycles	1.73%	33.9	25.8

***** The V surface concentration is calculated from the measured amount of supported V and the surface area of each membrane.

Table 6.1 The loadings of the VOx measured by XRF and ICP

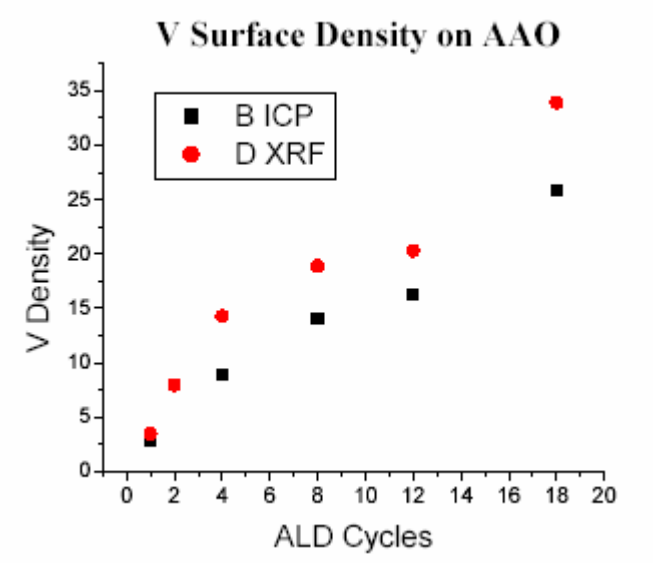

Fig 6.1 The vanadium surface densities at different cycles of the ALD loading

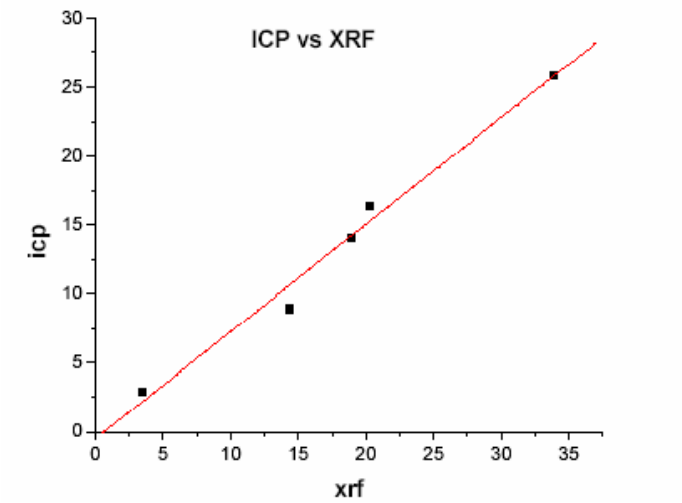

Fig 6.2 Vanadium surface density: ICP results vs XRF results

Fig 6.1 displays the results of XRF and ICP measurements of the VOx surface densities on the AAO membranes. The curves representing the results from the two techniques match reasonably well, except that the ICP always shows a little lower V surface density. Fig 6.3 plots the ICP results vs the XRF results measured from the same samples. A good linear correlation can be found between the two sets of data, which can be used as a calibration line to quantify the results of the XRF measurements.

It is interesting to notice that the amount of vanadium loaded by ALD does not increase linearly with the number of ALD cycles. As is displayed in Fig 6.1, both XRF and ICP results show that more vanadium was put onto the surface in the first few cycles and less was added in the subsequent cycles. Since the ALD of VOx is a self limiting process determined by the surface hydroxyl groups, the change in vanadium loading by each cycle of ALD may indicate the different densities of surface hydroxyls. As more cycles of VOx are coated, the surface gradually changes from alumina to vanadia. It seems that the latter surface has a lower hydroxyl group density than the former one. The presence of the surface hydroxyl groups might influence the catalytic behavior of VOx in the ODH reactions. This effect will be discussed in more detail later.

Fig 6.3 displays the UV-Vis spectra of the membranes loaded with ALD VOx. The edge energies were determined from the x-intercept of the linearized near edge region in the absorption versus hυ curves where hυ is the incident photon energy. The obtained E_g

values are listed in Table 6.2 and plotted in Fig 6.4-b. As has been mentioned in the previous chapter, these E_g values are believed to be useful in elucidating the local structure of V^{5+} centers. Gao and Wachs reported an approximately linear correlation between the edge energy and the number of V-O-V covalent bonds around the central V^{5+} cations based on measurements of some standard compounds. [61] Their results are plotted in Fig 6.4-a and are used as the reference to be compared to the measured edge energies of VOx supported on the AAO membranes.

The edge energies of the ALD VOx samples show red shifts as the loading increases. The 1 cycle ALD VOx sample has an edge energy of 3.64 eV, which corresponds to the isolated tetrahedrally coordinated VO_4 species according to the E_g values of the reference compounds. This result is quite reasonable for the first cycle of ALD VOx loaded onto the membrane: in the first ALD cycle, the vanadium species are bonded to the surface through reactions with the surface hydroxyl groups (Al-OH) so that only the V-O-Al bonds are present on the surface. As more cycles of VOx are coated, the V-O-V bond will be formed in the reaction between the regenerated surface hydroxyls (the V-OH groups) and the organometalic precursors from the gas phase, resulting in the gradual increase in the average VOx domain size and the corresponding decrease in the edge energy. The lowest edge energy is obtained on the membrane with the highest loading of VOx. Even for the sample with the highest loading (24 Cycles of ALD VOx), the E_g value (2.72 eV) is still much higher than that of the V_2O_5 crystal, indicating that at high loadings the ALD

VOx have fewer V-O-V bonds than V_2O_5, therefore the two-dimensional layered structure is probably still the predominant form of VOx on the surface. Recent UV-Raman studies on this series of ALD samples show no sign of crystalline V_2O_5 formation on the surface of the AAO membranes even at a VOx loading as high as 28 V/nm^2. These spectroscopy results demonstrate the excellence of the ALD technique in making an ultra even distribution of the catalytic materials on the surface.

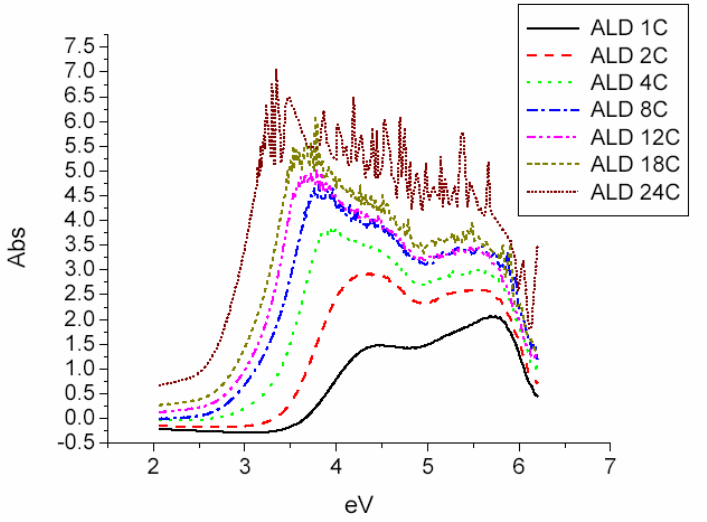

Fig 6.3 The UV-Vis absorption spectra of the ALD VOx supported on the AAO membranes

Sample	$E_g^{\#}$ (eV)
ALD 1C	3.64
ALD 2C	3.48
ALD 4C	3.33
ALD 8C	3.17

ALD 12C	3.11
ALD 18C	3.04
ALD 24C	2.72

Table 6.2 The edge energies of the ALD VOx supported on the AAO membranes.

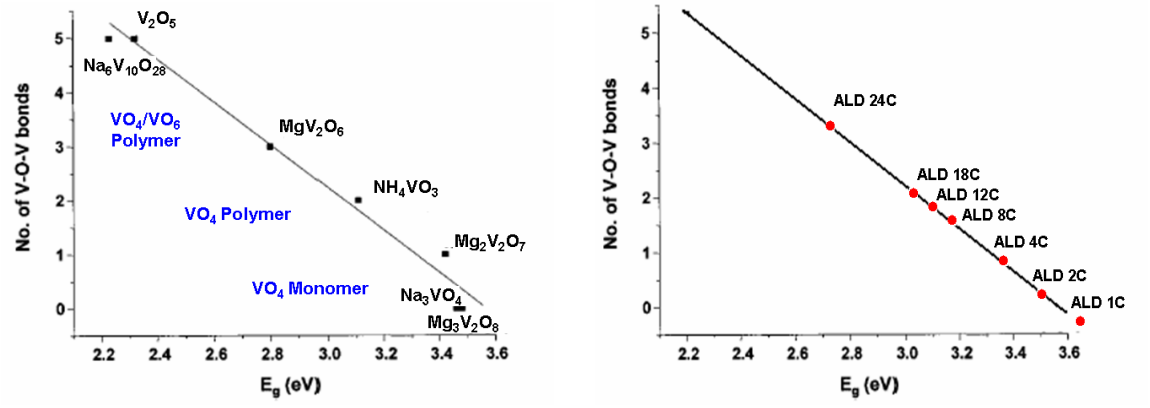

a. **b.**

Fig 6.4 The edge energies of the ALD VOx supported on the AAO membranes (b) compared to those of the reference compounds measured by Gao and Wachs (a) [61]

6.2.2 Analyses on the catalytic activity

The cyclohexane ODH reactions were carried out in the temperature range between 400 and 480°C at a constant reactant flow rate of approximately 10sccm/min. Very tiny conversions (0.1~0.5%) due to the background reactions were found under these conditions. The background has been subtracted from the catalysis test results when evaluating the performance of the VOx catalysts. The conversion curves measured on the series of ALD VOx samples are displayed in Fig 6.5. As we can see from these curves, at

the same reaction temperature, the conversion keeps going higher with the increasing loading of the catalyst, until a V surface density of ~16V/nm^2 (12 cycles of the ALD VOx) is reached. Beyond this point, further increase in the V loading does not lead to a higher conversion, which means that the saturated conversion is reached at the loading close to (≤) 16V/nm^2.

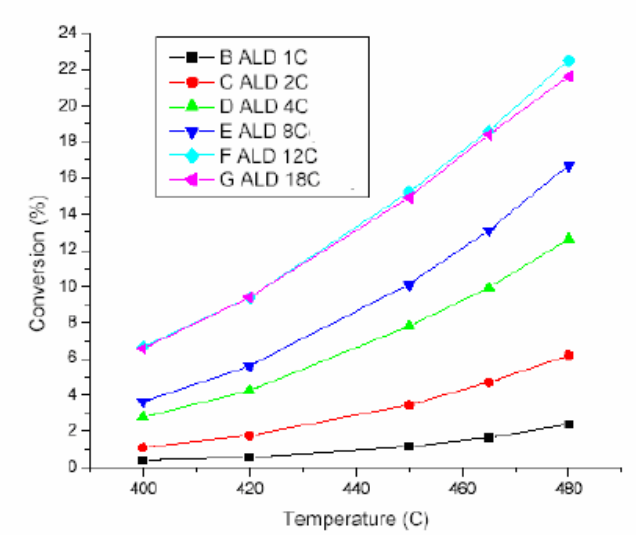

Fig 6.5 The conversions of the ALD VOx supported on the AAO membranes in the ODH of cyclohexane

The TOF of cyclohexane on these samples are calculated by normalizing the conversion data by the total amount of the supported vanadium measured with ICP. Fig 6.6 plots the calculated TOF of the different ALD samples at 450°C against the measured loading of VOx. Some interesting trends can be found in these TOF data: with increasing loading of the VOx, the TOF climbs up, stays constant, and finally goes down. The increments in

TOF are observed in the first 4 cycles of the ALD VOx loading and the TOF curve becomes almost flat as the number of ALD cycles is increased to 12. The transition point is close to 12 cycles where the TOF begins to drop. Normally a continuous decline in the TOF is expected at loadings higher than monolayer since at high loadings part of the catalysts will inevitably be buried and made unavailable for the reaction. The saturated conversion and the corresponding drop in the TOF observed on the sample with more than 12 cycles of ALD VOx is believed to be due to this effect. However, at loadings lower than 16V/nm^2 (1 to 12 cycles of the VOx ALD), the VOx species synthesized by the ALD technique are most likely to be in a highly dispersed form so that nearly all of them are available for the surface reactions. Furthermore, even if all the catalytic species are accessible, the TOF should at most be kept constant rather than go up with the increasing loading of the catalyst, provided that they bear the same catalytic properties. Therefore, the initial climbing in the TOF with increasing loading of the catalyst reflects the different chemical properties of the catalytic sites formed by different cycles of the VOx ALD.

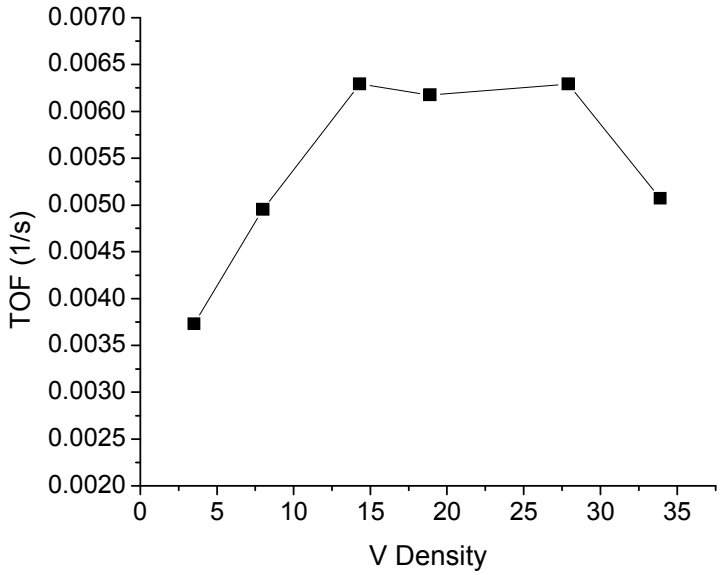

Fig 6.6 The TOF of the membrane supported ALD VOx samples at 450°C

Analyses on the UV-Vis spectra suggest that the VOx species formed by one cycle of ALD are mostly in the isolated state. The V-O-V bond connecting two adjacent V centers begins to form and gradually prevails on the surface as more cycles of VOx are put down by ALD. Apparently the presence of these V-O-V bonds makes two major changes to the catalyst: first, they replace part of the V-O-Al bonds so that the related chemical properties, such as the reducibility of the catalytic sites and the type and density of the surface functional groups, are affected; secondly, the adjacent V centers are brought closer and consequently a concerted reaction mechanism that involves the attendance of more than one V centers is more likely to take place. The promoted catalytic activities at high VOx loadings could be related to one or more of these effects.

The dependence of the catalytic activity on the domain size of VOx is not unique to the cyclohexane ODH reaction. In the ODH of propane, a similar correlation has been found by Iglesia and coworkers. [35.] In their report the different activities are attributed to the reducibility of the VOx species: since the dehydrogenation of the hydrocarbon involves the reduction-oxidation cycle of the V^{5+} center, the ease of reduction of the catalytic site will largely determine the activity of the catalyst. Therefore the polyvanadate domains, which have been shown to be more easily reduced than the monovanadate sites by TPR measurements, are more active in the dehydrogenation reactions. Because the ODH of cyclohexane and propane share many common features especially in the hydrocarbon activation step, the above explanation can also be applied to illustrate the observed dependence of the activity on the loading in the ODH of cyclohexane.

The density of the surface hydroxyl groups could also influence the catalytic activity. As is reflected in the change of the slopes in the ALD VOx loading curve (Fig 6.1), the density of the surface hydroxyl group on the ALD vanadia appears to be lower than that on the ALD alumina. Since the rise in the activity goes along with the decline in the density of the surface hydroxyl group, the presence of surface hydroxyls seems to have a negative effect on the catalytic activity. In the ODH reactions catalyzed by metal oxides, it is generally believed that the lattice oxygen in the catalytic site is responsible for abstracting the H atom from the hydrocarbon molecule. The lattice oxygen may lose part of its H abstraction capability once it has already bonded to H, as in the case of a surface

hydroxyl group. Because the surface OH groups may be able to turn off some of the catalytic sites by disabling their lattice oxygen, higher activities are expected on the samples with high loadings of the VOx, which have been shown to have relatively low surface hydroxyl group densities.

The fact that the V centers on the surface are brought closer at higher loadings may also help promote the catalytic activity. The shorter distance between adjacent V centers may affect the reaction rate through forming multi-adsorbed reaction intermediates, which are more firmly bonded to the catalytic sites and consequently less likely to desorb from the surface. Usually the first step in a surface reaction is the reversible adsorption of the reactant molecules onto the surface. In this step the chance of desorption could become smaller if the adsorbed species are more tightly attached to the surface. It is natural to expect that the multi-absorbed intermediates, if they exist, will bond to the surface more firmly than those anchored through a single site. If the adsorption of the hydrocarbon molecule onto the catalytic site is due to the interaction between a C atom and the V center, the spatial distance between adjacent V centers will largely determine the possibility of the formation of those multi-absorbed species. On the surface with the presence of the V-O-V bonds, the shortest distance between the two V centers is approximately 0.32 nm based on the crystallographic data of some di-vanadium compounds. [62] In comparison to this number, the average distance between the two isolated V centers next to each other is roughly 0.5nm at a surface density of $4V/nm^2$. The

C-C bond length in the cyclohexane molecule is 0.154 nm. The estimated V-C bond length is approximately 0.14nm based on the reported ionic radius of V^{5+} (0.072nm) and the covalent radius of C (0.07 nm). [63] From the above estimation we can find that the cyclohexane molecule can easily bond to the two vanadium centers in a V-O-V bond through a 1,2, 1,3, or 1,4 diadsorbed intermediate while it is impossible to do so with two isolated V centers. The multi-adsorbed intermediates will better hold the hydrocarbon molecules close to the catalytic sites and consequently facilitate the subsequent dehydrogenation process. In this reaction, the formation of these multi-adsorbed intermediates could also greatly affect the reaction path through facilitating multiple C-H breaking on the same catalytic site, which leads to the direct conversion from cyclohexane to benzene. Detailed analysis on this effect will be discussed in later paragraphs.

The reaction activation energies are obtained from the Arrenhius plots (Fig 6.7) using the conversion data over the temperature range of 400 to 480 °C. Since the ODH reaction rate shows a linear dependence on the concentration of cyclohexane, the reaction rate data at zero conversion (the original cycohexane concentration), which are determined by dividing the percentage of the un-reacted cyclohexane, are used in the Arrenhius plots. The activation energies of the series of ALD VOx samples ranged between 63 and 98 kJ/mol. Generally, the activation energy becomes lower with the increasing loading of VOx. This trend supports our conclusion that the polyvanadate domains are more reactive

than the isolated VOx sites in the activation of cyclohexane.

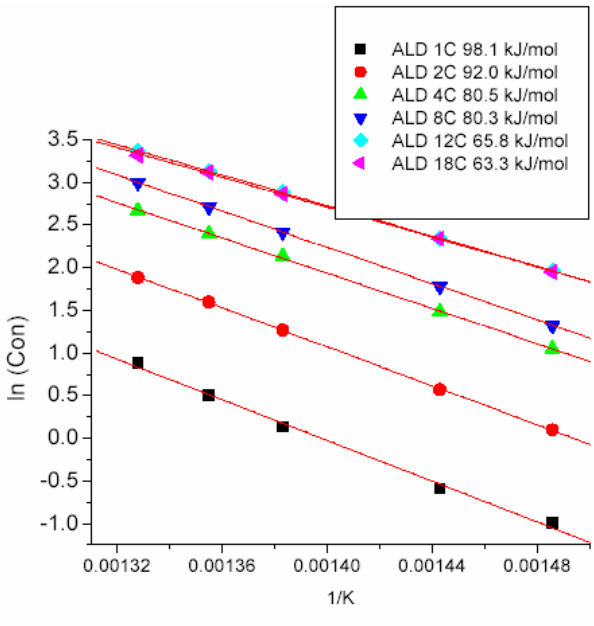

Fig 6.7 The Arrhenius plots of the ALD VOx supported on the AAO membranes

6.2.3 Analyses on selectivity and reaction paths

The product distribution (selectivity) patterns of the series of ALD VOx samples are list in Fig 6.8, from which some obvious trends can be found: as the conversion increases with elevated temperature, the selectivity to cyclohexene drops while the selectivity to benzene goes up. When different samples are compared at the same reaction temperature, the conversion becomes greater with increased loading of the catalyst, companied by a lower selectivity to cyclohexene and a higher selectivity to benzene. In all cases, the cyclohexane conversion and the selectivity to cyclohexene always go in the opposite directions. These trends reflect a typical hydrocarbon sequential oxidation pathway in

which the alkane is first oxidized to the alkenes and then further oxidized to the more stable deep oxidation products. On the other hand, the selectivity to COx (CO and CO_2) is almost constant despite the different reaction temperature or the loading of the catalyst, indicating that the formation of these most stable oxygenating species go though routes other than the consecutive reaction path. In the ODH of cyclohexane, the formation of cyclohexene and benzene is due to the breaking of multiple C-H bonds while the COx production is the result of C-C bond breaking or O insertion. The very limited selectivity to COx even at high cyclohexane conversions indicates that the VOx species supported on the AAO membranes are quite selective in catalyzing the C-H bond breaking process. The reason for the low selectivity to COx is perhaps related to the unique character of the membrane catalytic system, in which the potential for free radical gas phase reactions could be effectively quenched in the collisions with the pore walls so that the COx production from the heterogeneously induced homogeneous reactions in the gas phase is greatly reduced.

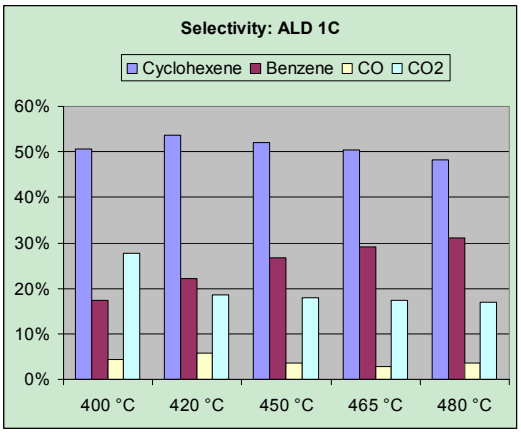

a.

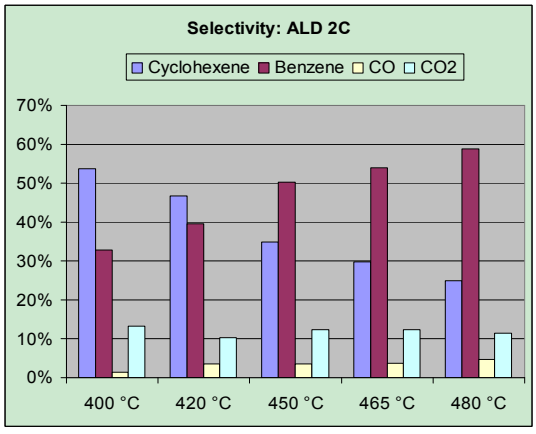

b.

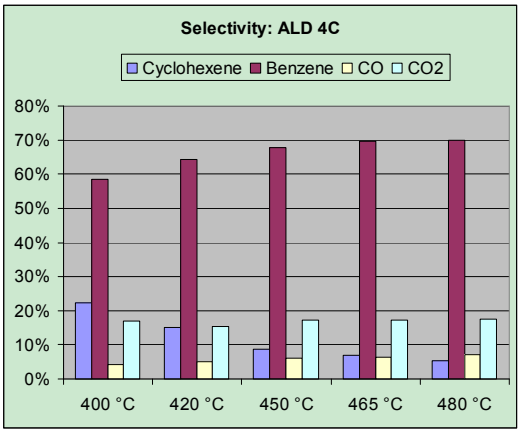

c.

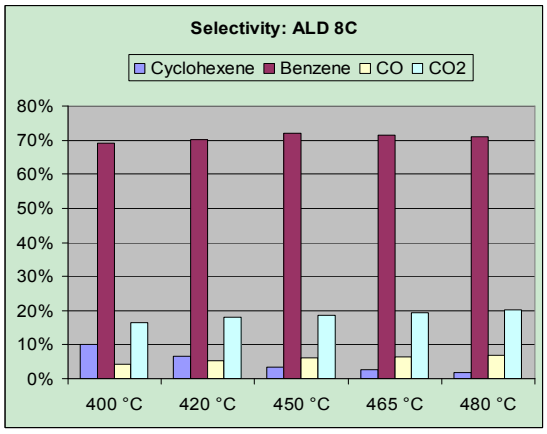

d.

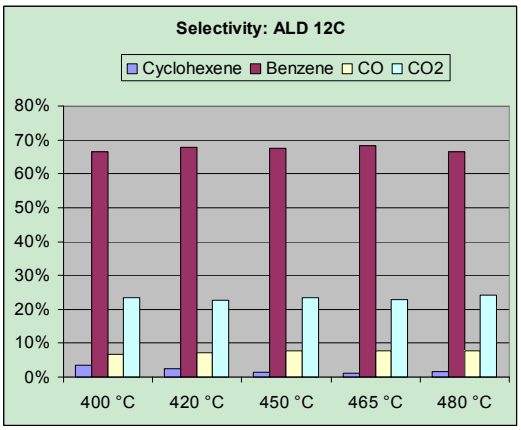

e.

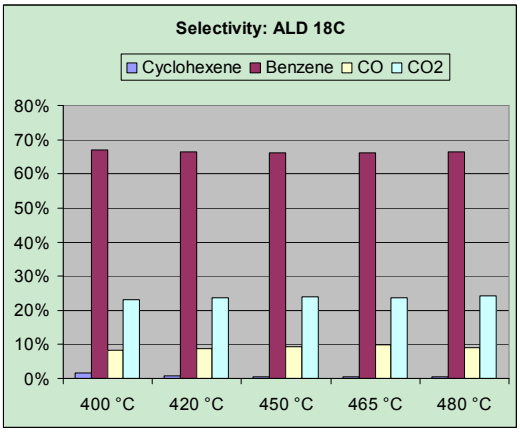

f.

Fig 6.8 The product distribution charts of the ALD VOx supported on the AAO membranes in the ODH of cyclohexane: a.) 1-cycle ALD VOx; b.) 2-cycle ALD VOx; c.) 4-cycle ALD VOx; d.) 8-cycle ALD VOx; e.) 12-cycle ALD VOx; f.) 18-cycle ALD VOx

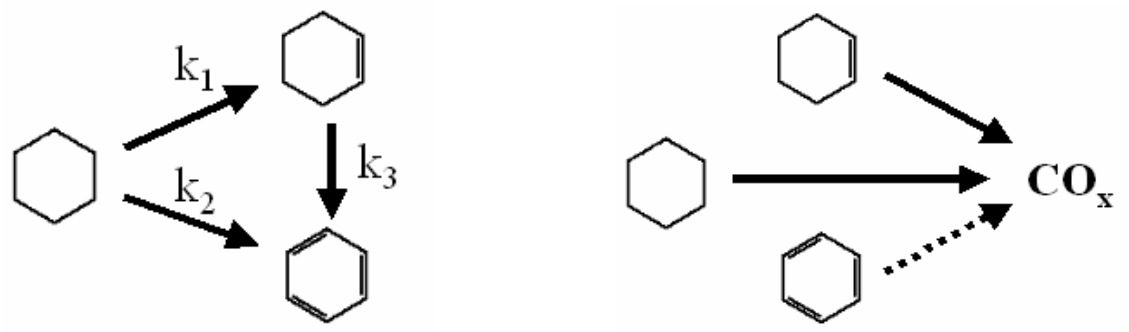

a. **b.**

Fig 6.9 The cyclohexane ODH reaction diagram: (a.) the C-H breaking process; (b.) the C-C breaking process

As is shown in Fig 6.9, in the ODH of cyclohexane the selectivity to cyclohexene and benzene is determined by the relative rate of converting cyclohexane to these two products (k_1 and k_2), and the rate of the further oxidation of cyclohexene (k_3). The conversion from cyclohexane to benzene via the formation and further oxidation of cyclohexene (the $k_1 \rightarrow k_3$ route) is a consecutive reaction path while the direct conversion from cyclohexane to benzene (k_2) is considered an independent parallel reaction. In this reaction it is likely that both the sequential path and the parallel path share a common reaction intermediate at some point: the initial dehydrogenation of cyclohexane on the catalytic site may form a structure close to the adsorbed olefin. It can either desorb from the surface and produce cyclohexene (the k_1 route), or lose another C-H bond and head for benzene (the k_2 route). Anything that increases the rate of k_2 or decreases the rate of k_1, or both, will lead to more benzene through the parallel reaction route. In the consecutive reaction route, anything increasing the rate of cyclohexene dehydrogenation

(k_3) will lower the selectivity to the olefin and consequently raise the selectivity to benzene.

Experimentally, the selectivity to cyclohexene appears to be influenced by many factors such as the reaction temperature, the reactant residence time (the reagent flow rate), and the VOx loading. In the ODH reactions of alkanes, the conversion is of primary importance in determining the selectivity because the partial oxidation product is very easy to be further oxidized so that the selectivity usually drops significantly with the increasing conversion. Other factors may affect the selectivity simply through influencing the conversion or may have some intrinsic effects on it. To better distinguish and analyze these effects, it is important to compare the selectivity at the same conversions. Fig 6.10 displays the C_6H_{10} selectivity versus C_6H_{12} conversion curves of the ALD VOx samples measured in the temperature range of 400 to 480 °C. Since in the ODH reactions a high selectivity to the partial oxidation product can always be achieved at very low conversions, it is meaningful to also analyze the yield to cyclohexene rather than the selectivity alone. The C_6H_{10} yield versus C_6H_{12} conversion curves are plotted in Fig 6.11. Fig 6.12 compares the effects of the reaction temperature and the reagent flow rate on the yield to cyclohexene for the selected ALD samples.

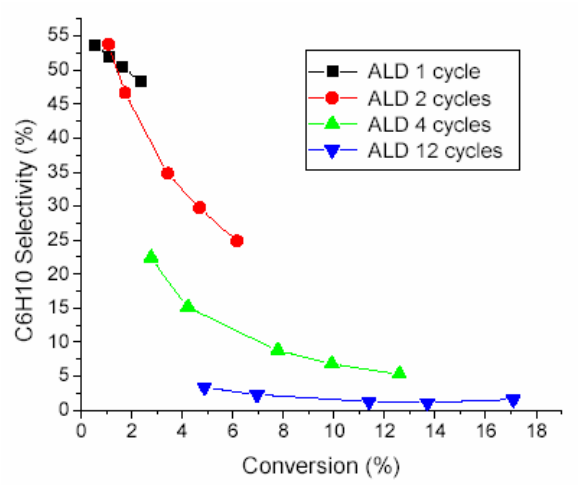

Fig 6.10 The C_6H_{10} selectivity vs C_6H_{12} conversion curve of the ALD VOx supported on the AAO membranes

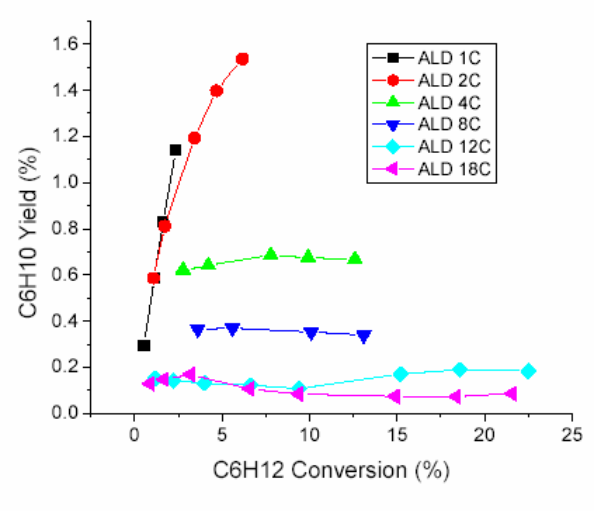

Fig 6.11 The C_6H_{10} yield vs C_6H_{12} conversion curve of the ALD VOx supported on the AAO membranes

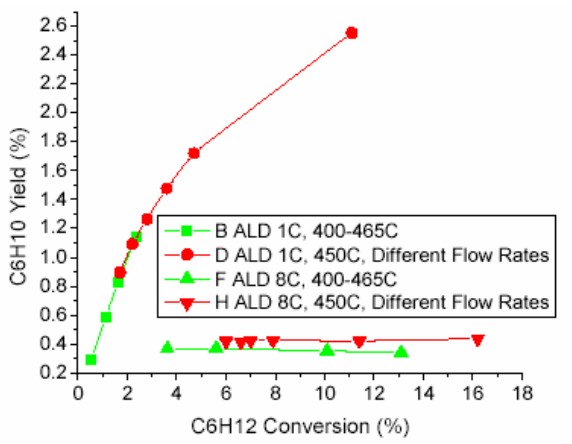

Fig 6.12 The C_6H_{10} yield vs C_6H_{12} conversion curves of the selected ALD VOx samples measured at different temperatures and at different reagent flow rates

When the membranes with the different VOx loadings are compared at the same C_6H_{12} conversions, the sample with a lower loading always shows higher selectivity or yield to C_6H_{10}. For the 1-cycle and 2-cycle ALD VOx samples, the yield to C_6H_{10} rises with the increasing conversion; while for the samples with higher loadings (≥ 4 cycles), the yield stays low and almost constant at all conversions. In Fig 6.12, the excellent matches between curves B and D and between F and H indicate that adjusting the reactant residence time or the reaction temperature has similar effects on the yield to cyclohexene through influencing the conversion. However, the loading of VOx seems to determine the selectivity/yield to cyclohexene through some unique effects other than the typical influence of the conversion. Since the form of the supported vanadium species gradually change from the isolated monovanadate sites to polyvanadate domains with the increasing number of the ALD VOx cycles, the observed trends in the selectiveity/yield

to cyclohexene clearly show that the isolated VOx sites facilitate the production of the olefin while the polymeric form of VOx mainly lead to the benzene formation.

It is possible that the dependence of the selectivity on the loading of VOx is related to the catalytic activities of the different forms of VOx. It has been shown previously that the polyvanadate domains have higher activities than the monovanadate sites in the ODH of cyclohexane. Accordingly, the decrease in the selectivity to cyclohexene may result from the promoted activity in the further conversion of this partial oxidation product (the k_3 route in Fig 6.9-a). Since the dehydrogenation process of cyclohexene is very similar to that of cyclohexane, a catalyst that is more active for cyclohexane oxidation is probably also more active for the reaction of cyclohexene. Plus, the weakest C-H bond in the cyclohexene molecule is much easier to break than that in cyclohexane, the dehydrogenation rate of the olefin could be much faster than that of the alkane molecule. Therefore, a lower selectivity to cyclohexene can always be found on a more active catalyst.

A more fundamental reason for the lower selectivity to cyclohexene on the samples with high VOx loadings is probably related to a so-called concerted reaction mechanism, which involves the participation of at least two V centers. In the cyclohexane ODH reaction, we notice that no cyclohexadiene, an intermediate between cyclohexene and benzene, has ever been detected. This fact implies that this partial oxidation product, if it

ever exists, probably never leaves the surface before it is further oxidized to benzene. However, the direct conversion from cyclohexene to benzene has to be hard on the catalytic site containing only one V center since such a site is not likely to be capable of abstracting all four H from cyclohexene and consequently be reduced during the process. Some kind of concerted reaction mechanism that calls for the attendance of more than one V center has to take over the job. With such a mechanism, the cyclohexene molecule may either bond to a polyvanadate domain and be fully oxidized to form benzene, or be partially oxidized on one site and then quickly bond to an adjacent site to go through further oxidations. In either case, the distance between adjacent V centers will largely determine the possibility of such a mechanism. We notice in the catalysis data of the 1 cycle ALD VOx sample (Fig 6.8-a) that the selectivity to cyclohexene is always high despite the reaction temperature or the cyclohexane conversion, which very well supports the point that the monovanadate sites are not good at converting cyclohexene to benzene. With the increasing loading of the catalyst, the V centers are brought closer and the polyvanadate domains are formed; as a consequence the olefin can easily be further oxidized to benzene over the adjacent V centers.

The direct conversion from cyclohexane to benzene (the k_2 route in Fig 6.9-a), which can cause a great loss in the yield to cyclohexene, may also play a major role in the production of benzene under some conditions. This process has to depend on the concerted reaction mechanism, since in this case all six H around the carbon skeleton

need to be pulled out on the same or adjacent catalytic sites. Likewise, the direct conversion to benzene is very likely to rely on the polyvanadate domains on the surface. As has been discussed before, due to the restrictions in the spatial separation between adjacent V^{5+} centers, the cyclohexane molecule can only form the multi-adsorbed reaction intermediate on the polyvanadate domains. These multi-adsorbed hydrocarbon species are most likely the precursors for the multiple C-H bond breaking process, which will lead to the direct conversion from cyclohexane to benzene. Similarly, cyclohexene may also be able to interact with the polyvanadate sites to form the multi-adsorbed intermediate, which could accelerate its conversion to benzene (through the k_3 route) and lead to the low selectivity to olefin.

To study the roles of the consecutive reaction route and the parallel routes in the ODH of cyclohexane and their relationship to the structure of the VOx catalyst, oxidation reactions using cyclohexene or benzene as the reactant were studied on two membrane samples with the different VOx loadings (2 cycles and 8 cycles of the ALD VOx). These reactions are run under exactly the same conditions of the cyclohexane ODH. The results of these tests are presented in Fig 6.13 and Table 6.3 (the 2 cycles ALD VOx), and Fig 6.14 and Table 6.4(the 8 cycles ALD VOx) respectively.

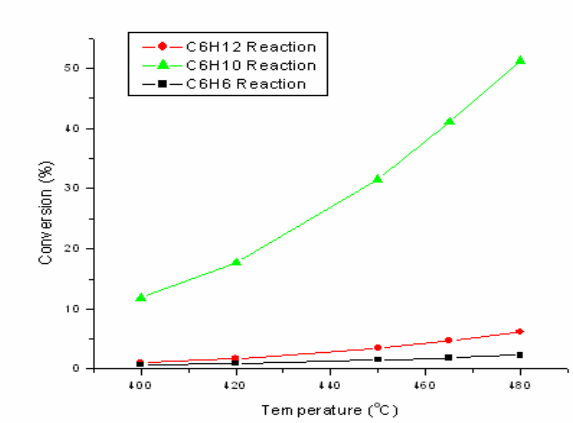

Fig 6.13 The conversions of C_6H_{12}, C_6H_{10} and C_6H_6 under the same experiment conditions over the 2-cycles ALD VOx supported on the AAO membrane

Product	C6H6	CO	CO2
400	77.1	3.9	19.1
420	77	4.5	18.5
450	77.4	5.2	17.4
465	77.6	5.7	16.7
480	77	6.1	17

a.

Product	CO	CO2
400	14.9	85.1
420	14.9	85.1
450	22.5	77.4
465	26.3	73.7
480	30.2	69.8

b.

Table 6.3 The selectivity in the oxidation reaction of C_6H_{10} (a.) and C_6H_6 (b.) over the 2-cycle ALD VOx supported on the AAO membrane

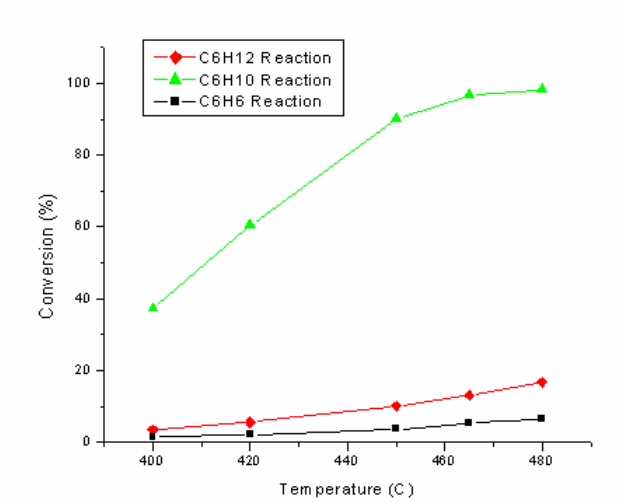

Fig 6.14 The conversions of C_6H_{12}, C_6H_{10} and C_6H_6 under the same experiment conditions over the 8-cycle ALD VOx supported on the AAO membrane

Product	C6H6	CO	CO2
400	76.8	4.3	18.9
420	76.4	4.9	18.7
450	75.1	5.6	19.3
465	74.8	6.2	19.1
480	74.5	6.6	18.8

a.

Product	CO	CO2
400	9.2	90.8
420	12.5	87.5
450	18.3	81.7
465	20.4	79.6
480	22	78

b.

Table 6.4 The selectivity in the oxidation reaction of C_6H_{10} (a.) and C_6H_6 (b.) over the 8-cycle ALD VOx supported on the AAO membrane

For both samples the rate of the cyclohexene oxidation is nearly ten times as high as that of the corresponding alkane reaction, which explains the slump in the selectivity to olefin with increasing conversion in the ODH of cyclohexane. Compared to the 2-cyle ALD

VOx sample, the sample with the higher loading (8 cycles of ALD VOx) shows higher activity (~ twice the TOF) in the temperature range of up to 450 C°, where the cyclohexene conversion is approaching 100%. As has been discussed before, at the VOx loading of 2 ALD cycles, a large fraction of the vanadium species supported on the membrane are still in the isolated state; while with 8 cycles of the ALD loading, polyvanadate domains become predominant on the surface. Therefore these results confirm the deduction that cyclohexene reacts quicker on polyvanadate sites. The conversions in the reaction of benzene are very low on both membrane samples, indicating that the consecutive reactions do not proceed further once benzene is formed. Consequently, the major source of the COx formation has to be C-C breaking during the oxidation of cyclohexane or cyclohexene.

From the conversion/selectivity pattern of the cyclohexene reaction, we are able to estimate the percentages of the reacted cyclohexane that go through the consecutive (k1 → k3) reaction path and the parallel (k2) path. If we assume a 100% consecutive path, in which the production of all the deep oxidation products (benzene and COx) inevitably go through the cyclohexene intermediate, the selectivity to cyclohexene appears in the cyclohexane ODH reaction has to be due to the un-converted olefin formed in the initial dehydrogenation step. Therefore this selectivity should be equal to 100% minus the olefin conversion measured in the cyclohexene reaction. As for the converted portion of cyclohexene, the selectivity to the further oxidation products will follow the pattern

measured in the reaction of the olefin. An estimated cyclohexane ODH selectivity pattern of the 2-cycle ALD sample based on such 100% consecutive path assumption is listed in Fig 6.15-a. The actual cyclohexane ODH selectivity pattern measured from the same sample is presented next to it (Fig 6.15-b) for comparison.

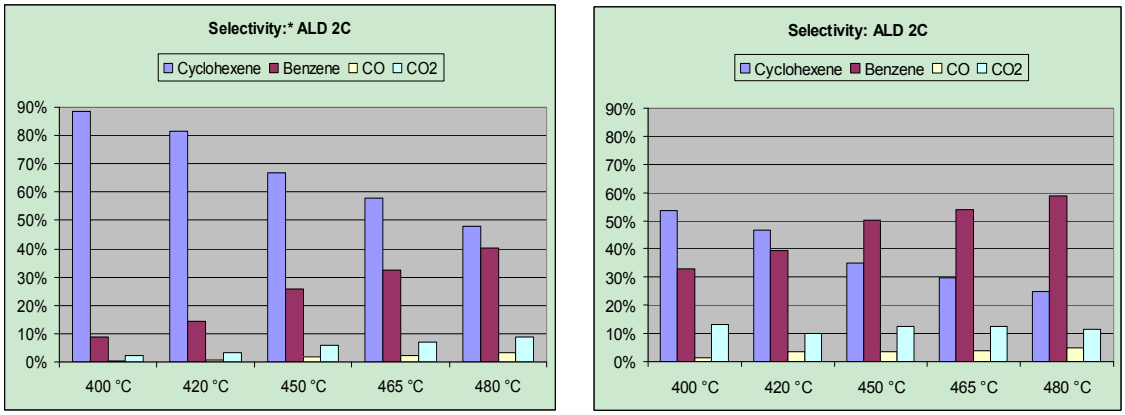

a. **b.**

Fig 6.15 The cyclohexane ODH selectivity pattern over the 2-cycle ALD VOx supported on the AAO membrane. a.) The estimated cyclohexane ODH selectivity pattern based on the 100% consecutive path assumption. b.) The actual cyclohexane ODH selectivity pattern measured from the reaction.

As we can see from the above graphs, the estimated cyclohexene selectivity based on such 100% sequential path consumption is usually higher than the actual olefin selectivity measured in the cyclohexane ODH reaction. The reason for the difference is most likely due to the direct conversion from cyclohexane to the deep oxidation products, or the

so-called parallel reaction routes, which greatly reduce the selectivity to the olefin. The predicted cyclohexene selectivity values in Fig 6.15-a can be brought down to match the actual values in Fig 6.15-b by multiplying a coefficient, which can be considered the fraction of the reacted cyclohexane that follows the sequential path. For this portion of the reacted cyclohexane, the product distribution in further oxidations will follow the pattern measured in the olefin reaction. Therefore the contributions to the selectivity to the deep oxidation products from the sequential path can be determined by multiplying the same coefficient to those selectivity values displayed in Fig 6.15-a. The resulting cyclohexane ODH selectivity pattern showing only the products from the consecutive path is displayed in Fig 6.16-a. Comparing this pattern to the actual selectivity pattern measured in the reaction (Fig 6.15-b), the fractions of the deep oxidation products formed by the direct oxidation of cyclohexane (through the parallel reaction routes) can be determined, as are represented by the green bars in Fig 6.16-b.

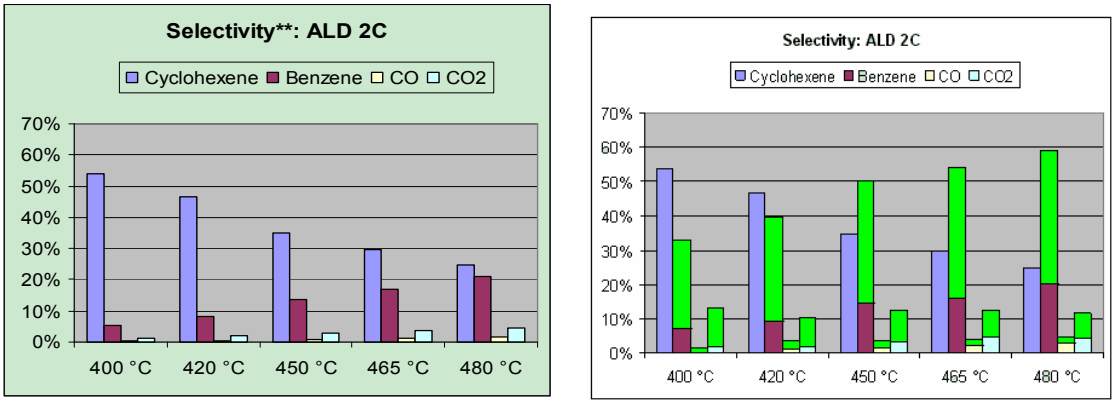

a. **b.**

Fig 6.16 The cyclohehxane ODH selectivity pattern over the 2-cycle ALD VOx supported on the

AAO membrane a.) The estimated cyclohexane ODH selectivity pattern showing only the products from the consecutive path. b.) The actual cyclohexane ODH selectivity pattern showing contributions from both the sequential path and parallel paths. The green bars represent the products from the parallel paths.

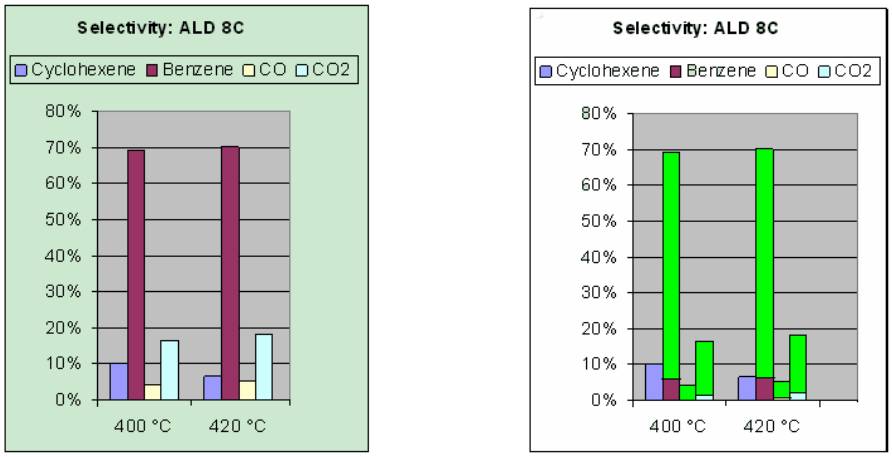

a. **b.**

Fig 6.17 The cyclohehxane ODH selectivity pattern over the 8-cycle ALD VOx supported on the AAO membrane. a.) The actual cyclohexane ODH selectivity pattern measured from the reaction. b.) The selectivity pattern showing contributions from both the sequential path and parallel paths. The green bars represent the products from the parallel paths

The same analysis has been applied to the 8-clcyle ALD VOx sample and the resulting selectivity pattern showing the contributions from the consecutive and parallel paths is displayed in Fig 6. 17. For this sample, the estimation is made only at relatively low reaction temperatures. At higher temperatures ($\geq$ 450°C) the conversion of cyclohexene is

so high that oxygen is completely exhausted. As a result, the reaction conditions of the alkane and the olefin ODH are no longer comparable therefore the above estimation method is not applicable. From Fig 6.16 and Fig 6.17, we can see that on the sample with a lower catalyst loading (2 cycles of the ALD VOx, 6V/nm^2), most of (60%) the reacted cyclohexane follows the sequential reaction path and only a small fraction (30%) is directly converted to benzene; while on the high loading sample (8 cycles of the ALD VOx, 14V/nm^2), majority (65%) of the reacted cyclohexane is directly converted to benzene through the parallel path. These observed trends suggest that it is the form or structure of the catalytic site that determines the reaction route. As is discussed in previous paragraphs, during the cyclohexane activation process, the multi-adsorbed intermediate could only be formed on polyvanadate domains containing the V-O-V bond, which is probably a most important step towards the direct conversion from cyclohexane to benzene. Additionally, these polymeric VOx clusters possess more lattice oxygen and have higher reducibility; therefore they are more likely to be capable of performing multiple C-H breaking on the same catalytic site and consequently facilitate the parallel reaction mechanism. .

Interestingly, the direct conversion from cyclohexane to benzene on the polyvanadate sites appears to require lower activation energy than does the dehydrogenation reaction towards the production of the olefin. Fig 6.7 clearly shows the trend that the reaction activation energy drops with the increasing loading of the catalyst. At the low loading, the

measured activation energy mainly represents the barrier towards the production of cyclohexene (the k_1 route), since the parallel route (k_2) is almost prohibited on the isolated VOx sites. While at the higher loading, the measured activation energy probably reflects more of the barrier of the direct conversion from cyclohexane to benzene since in this case it has become the major reaction route.

6.2.4 Effects of the support

In the alkane ODH reactions catalyzed by the vanadium containing compounds, it has been shown that the type of support plays a very important role in determining the catalytic performance. [34-36] Some researchers believe that it is the bridging O in the V-O-support bond that performs the rate determining H abstraction during the dehydrogenation process. [34] Changing the type of support is a convenient way to probe the functions of these V-O-Support bonds. In our studies, besides alumina, we also fabricated the AAO membranes with 1 nm ALD coatings of TiO_2 and Nb_2O_5. Two cycles of the ALD VOx were then loaded on top of the fabricated surface. The XRF measurements show that the surface vanadium densities on the TiO_2 and Nb_2O_5 coated membranes are 6.4 V/nm^2 and 8 V/nm^2 respectively. In the ODH of cyclohexane, the activities of the VOx supported on TiO_2 and Nb_2O_5 appear to be greatly enhanced. The TOF curves and Arrhenius plots of these samples are listed in Fig 6.18.

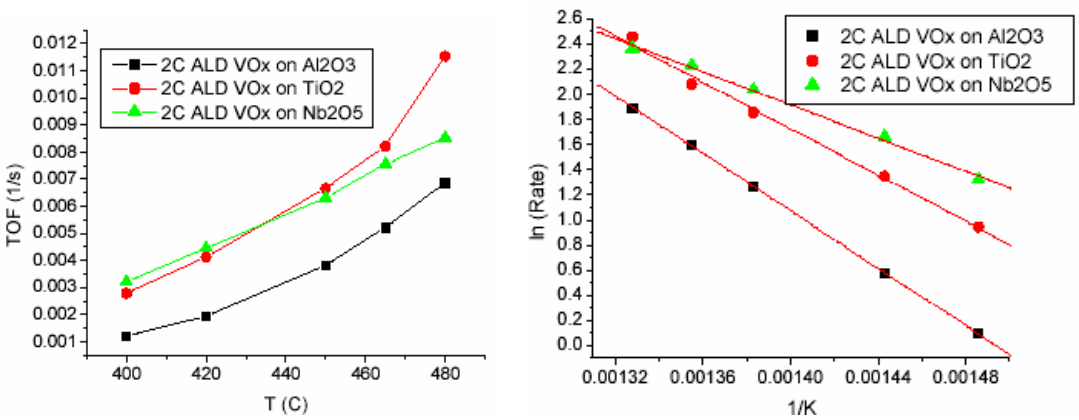

a. **b.**

Fig 6.18 The TOF (a.) and the Arrhenius plots (b.) of the 2 cycles of ALD VOx supported on the ALD Al_2O_3, TiO_2, and Nb_2O_5 fabricated AAO membranes

The TOFs of the TiO_2 and Nb_2O_5 fabricated membrane samples are approximately twice as high as that of the VOx supported on alumina. The reaction activation energies of the TiO_2 and Nb_2O_5 supported VOx are 72.3kJ/mol and 51.1 kJ/mol respectively, which are roughly 20kJ/mol and 40kJ/mol lower than that of the similar loading of VOx supported on alumina. The higher activity of the VOx supported on TiO_2 and Nb_2O_5 may be explained by the higher nucleophilicity or basicity of the O in the V-O-Support bond. Since the electro-negativity of Al^{3+}, Ti^{4+}, and Nb^{5+} increases in sequence $Nb^{5+} < Ti^{4+} < Al^{3+}$, [64] the electron density on the O in the V-O-Support bond is likely to be higher on the TiO_2 or Nb_2O_5 substrate. Therefore these O are possibly more capable of abstracting H from the hydrocarbon molecules. The fact that the catalytic activity is greatly affected by the type of substrate seems to support the point that it is the O in the V-O-Support bond that mainly performs the rate determining H abstraction in the dehydrogenation reaction.

Additionally, there could also be a cluster size effect: that is, compared to the case on the Al_2O_3 surface, bigger VOx domains could be formed on the surface of TiO_2 and Nb_2O_5, which will promote the catalytic activity. Since the surface of Al_2O_3 is more acidic than that of TiO_2 or Nb_2O_5, it could enable a better dispersion of the more basic vanadia species therefore the average VOx domain size on Al_2O_3 is probably smaller than that on the other two types of support. The measured UV-Vis absorption edge energies of the 2-cycle ALD VOx supported on the TiO_2 and Nb_2O_5 fabricated membranes are 3.25eV and 3.35eV respectively. Both these E_g values are lower than that of the 2-cycle ALD VOx supported on the Al_2O_3 membrane (3.48 eV), which indicates larger average domain sizes of the VOx supported on these substrates.

It is interesting to notice that the activities of the VOx at different loadings do not follow the expected sequence based on the analysis of electro-negativity. When the loading of the catalyst is low, the V species are attached to the alumina surface only through the V-O-Al bonds; while at higher loadings, the formation of the V-O-V bonds is somehow equivalent to the situation when V is supported on vanadia. The Sanderson electro-negativity of Al^{3+} (1.71 eV) is less than that of V^{5+} (2.56 eV), [64] which implies that the O in the V-O-Al bond should have a higher nucleophilicity, and consequently, a higher H abstraction capability, than that in the V-O-V bond. However in the catalysis tests, the very opposite trend is observed. This obscurity indicates that some factors other than the nature of the support, such as those discussed previously (the reducibility of the

VOx domains, the distance between the adjacent V centers, and the density of the surface hydroxyls), could also largely alter the H abstraction capability of the lattice oxygen in the dehydrogenation process.

In terms of the selectivity, both samples produce more than sixty percent of benzene at almost all measured temperatures/conversions. The selectivity to cyclohexene is low (<15%) and is not sensitive to the change in conversion. Compared to the 2- cycle ALD VOx supported on alumina, these samples show lower selectivity to cyclohexene and higher selectivity to benzene. The low selectivity to the olefin may be resulted from the promoted activity in the further reaction of the partial oxidation product due to the higher nucleophilicity of the O in the V-O-support bonds. In addition, since bigger VOx domains are likely to be formed on these supports, they could also greatly facilitate the benzene production and correspondingly lead to the loss in selectivity to cyclohexene.

Chapter 7

7. Other Topics Related to Nanostructured Catalytic Membrane Research

7.1 Catalytic Performances of the Vanadium Containing Organometallic Clusters Grafted on AAO Membranes

7.1.1 Introduction

The vanadium containing organometallic clusters were provided by Dr. Aswini Dash from Professor Tobin. J. Marks Group. These vanadium cluster compounds include Cp_2V, Cp^*_2V, and $V_4(\mu\text{-}O)_6Cp_4$. These compounds can react with hydroxyls on the surface of the AAO membrane and be attached to the surface (Fig 7.1). After calcination in oxygen, the organic ligands in the cluster will be burned away, leaving fully oxidized vanadium (V) oxides on the surface. Since the grafting process is based on the liquid phase reaction between the organometallic cluster and the surface hydroxyls, presumably the catalysts synthesized through this method can effectively prevent agglomeration and have a good dispersion on the surface. In addition, if a compound with multiple vanadium centers (such as the V4 cluster) is used in grafting, it is possible to synthesize well-defined isolated VOx sites, each containing a fixed number of vanadium atoms in the cluster, on the surface. As has been discussed before, these well-defined single site catalysts may

possess unique catalytic properties due to their unique structures.

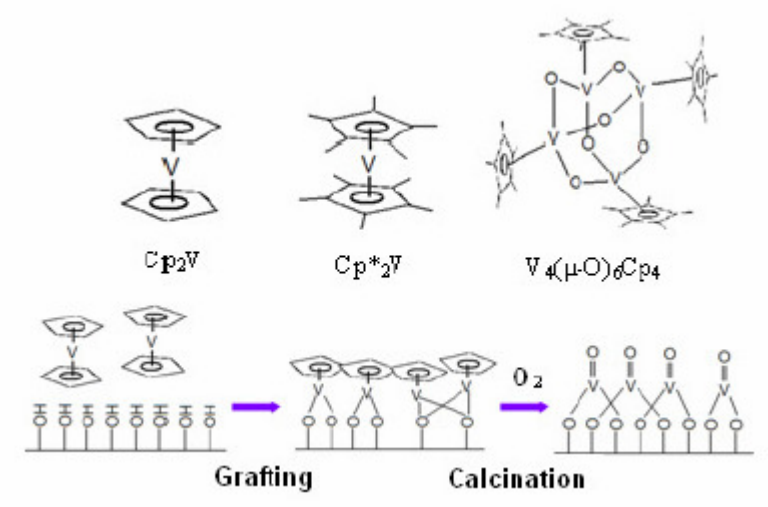

Fig 7.1 Organometallic V clusters and their grafting onto the AAO membrane

7.1.2 Results and Discussions

Experimentally, the cluster compounds were loaded onto the AAO membranes using methods described in Chapter 2 and were tested under the same conditions used for the ALD and impregnated VOx catalysts. Fig 7.2 lists the catalytic testing results from various organometallic cluster compounds grafted on the membrane. Table 7.1 shows the activation energy of these V cluster samples obtained from the Arrhenius plots.

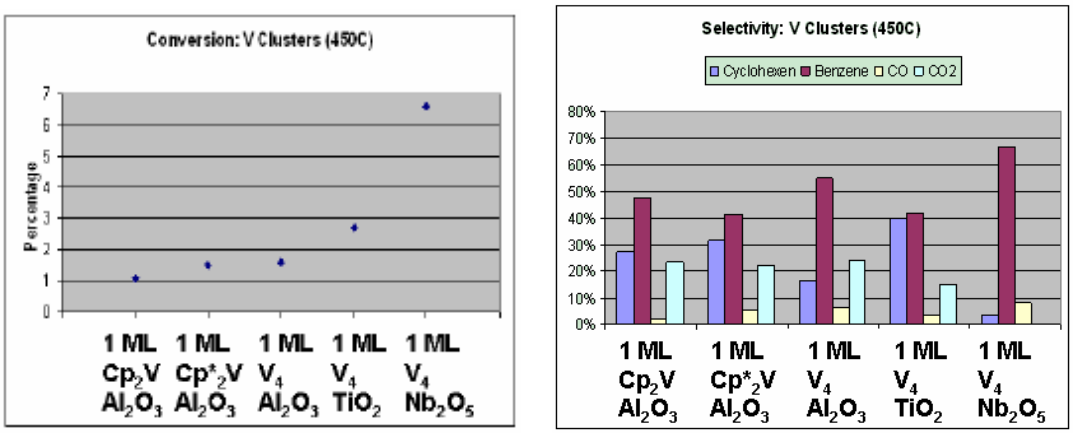

a. **b.**

Fig 7.2 The conversion (a) and selectivity (b) of V clusters supported on the ALD fabricated AAO membranes at 450 °C in the ODH of cyclohexane

V cluster	Ea (kJ/mol)
1 ML Cp_2V/Al_2O_3	82.7
1 ML Cp^*_2V/Al_2O_3	87.9
1 ML V_4/Al_2O_3	121.8
1 ML V_4/TiO_2	61.7
1 ML V_4/Nb_2O_5	65.3

Table 7.1 Activation energies of V clusters in the ODH of cyclohexane

Most of these V cluster samples have comparable catalytic performance to the impregnated VOx. Due to the low Tammann temperature of vanadium oxides, the

catalytic species may have a good mobility on the surface during the calcination, which may lead to a catalyst distribution similar to the situation when the catalyst is introduced by incipient wetness impregnation. [37] However, it turns out that the catalysis results obtained from V cluster samples are not as reproducible as those obtained from impregnated or ALD VOx samples. The poor reproducibility in catalysis data is due to the lack of control when loading the catalysts. As is revealed by XRF results, the amounts of vanadium loaded onto the membranes by grafting are largely different from sample to sample. Because these cluster compounds are sensitive to air and water, they have to be dissolved in an organic solvent (toluene) and the grafting has to be carried out in a glove box. Due to its hydrophobic nature, toluene will have difficulty entering the hydrophilic nanopores since it does not wet the surface of the membrane. [65] Furthermore, in a glove box it is hard to generate a vacuum to suck the solution into the nanopores. Consequently, a lot of the cluster compound will accumulate on the top surface of the membrane as the solvent evaporates. This leads to a poor distribution of the catalytic species on the surface of the membrane and the distribution state is hard to reproduce even if an equal amount of the cluster compound is introduced. In order to get more reproducible (or reliable) catalysis results with these metal clusters supported on the AAO membrane, the method to load the catalyst has to be improved to facilitate the contact between the organometallic clusters and the entire internal surface of the nanopores.

In spite of these limitations, the sample with monolayer $V_4(\mu\text{-}O)_6Cp_4$ supported on an

ALD TiO_2 fabricated membrane demonstrates some very interesting properties. Among all the V cluster samples, it shows the best selectivity to cyclohexene at a relatively high conversion. In addition, on this sample the selectivity to cyclohexene does not decrease dramatically with the increasing conversion (Fig 7.3). This sample also has the lowest activation energy (61.7kJ/mol) in its class. The XRF measurement indicates that the V density on this sample is only approximately 3.2V/nm^2, which means that this sample is most active in that it has a very high TOF.

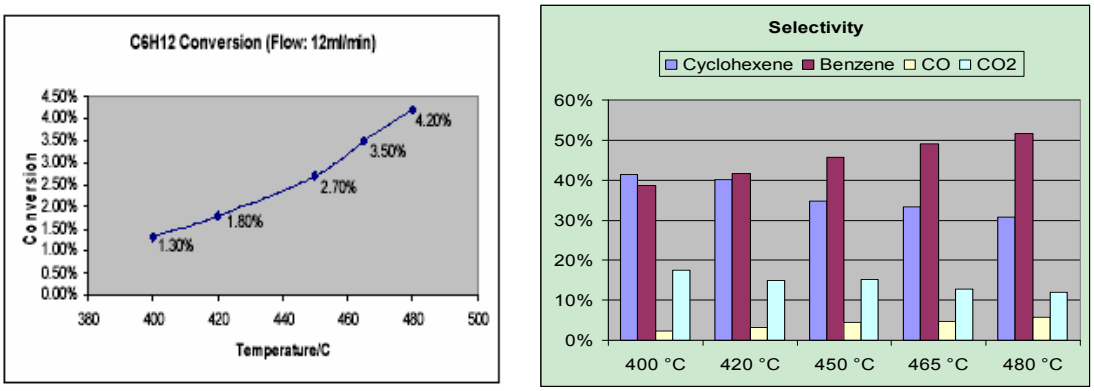

a. **b.**

Fig 7.3 The conversion (a) and selectivity (b) of 1 ML of $V_4(\mu\text{-}O)_6Cp_4$ cluster supported on the TiO_2 fabricated AAO membrane in the ODH of cyclohexane

As has been discussed in Chapter 6, TiO_2 substrate has the effect of promoting the catalytic activity and lowering the activation energy. The TOF and activation energy data of the V_4/TiO_2 sample are comparable to those of the other types VOx supported on TiO_2. In most cases the trade-off of this increase in activity is the remarkable decrease in the selectivity to cyclohexene. Nevertheless, from this example we learn that a low loading

of VOx supported on TiO_2 substrate might give the best balance between activity and selectivity to the olefin. Besides, the unique structure of the VOx transformed from the V_4 cluster may also have some contributions to the high selectivity to the olefin. To better understand this interesting effect, more control experiments as well as characterizations are needed to study the catalytic properties of VOx supported on the surface of TiO_2 at low loadings and the structure of these VOx generated from V_4 clusters.

7.2. Asymmetric Catalytic Stripes inside the Nanopores

7.2.1 Introduction

Numerical simulation of the diffusion pattern of the reactant molecules inside the nanopore on the AAO membrane indicates that the number of collisions between the reactant molecules and the pore walls is a function of the position along the pore axis. [13] Since in the membrane reactor all the reactant molecules are forced to flow through the nanopores, there are two possibilities once a reactant molecule enters a nanopore: 1). it passes through the nanopore and reaches the other side of the membrane; 2.) it is bounced back in a collision with the pore wall and will re-enter at a later time. The transmission probability f_t, which is defined as the probability that a reactant molecule can pass the entire length of the channel and reach the other side of the membrane once it enters the nanopore, is determined by the aspect ratio (L/d) of the pore:

$$f_t = \frac{\#\text{of particles that travel through the pore}}{\#\text{trials at the beginning of the pore}}$$

$$f_t = \frac{3L}{4d} \qquad 7.1$$

Based on the transmission probability, an estimation of the number of collisions between the reactants and the pore walls along the axial direction of the nanopore can be made by theoretical calculations considering the contributions from reactants that pass through the channel and from those that re-enter the channel. One important conclusion drawn from the results of such calculations is that the collisions between the reactants and the pore walls are much more frequent near the entrance of the channel than on the exit end of the nanopore (Fig 7.4). If an asymmetric catalytic structure can be made with catalytic species located only near one end of the nanopore, its catalytic performance could be significantly different between the two situations when the reactant is forced to enter the nanopores from one side and when it is introduced from the other side. A schematic description of this experiment can be found in chapter 1 (Fig 1.2-b). Catalytic results from such experiments may be a valuable test of theoretical predictions regarding the location of catalytic transformations in the pores.

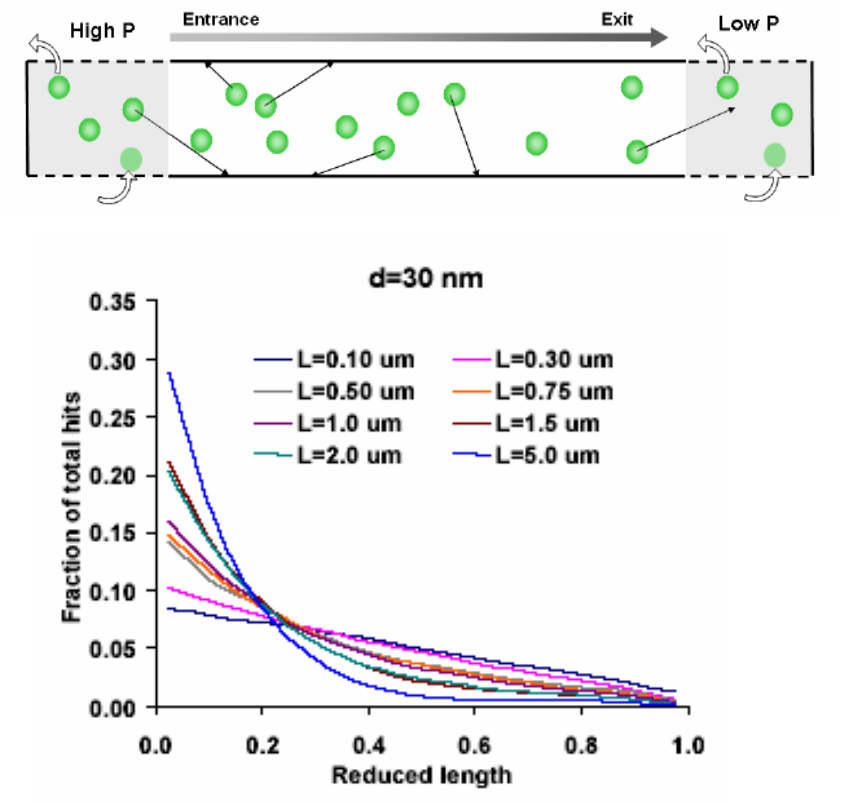

Fig 7.4 Simulation results on the fraction of hits on the different location of the pore walls [13]

7.2.2 Experimental, Results and Discussions

Asymmetric catalytic structures can be made using the ALD technique. By sealing the membrane in a VCR or VCO fitting, it is possible to expose only one side of the membrane to the ALD precursors. With such a configuration the catalyst will start to be deposited on the pore walls from the exposed end of the channel. The exposure time to the precursors determines how deep they can diffuse into the nanopores. When the exposure time is kept short enough, the precursors can only reach a certain depth below the top surface of the membrane and thus the asymmetric catalytic structure is made. The EDAX characterization along the axial direction of the nanopore shows that the catalyst

is only deposited on the pore walls within 5 microns from the exposed ends of the pores. In order to test the performance of the asymmetrically loaded catalytic stripe, the reaction system is modified accordingly so that the flow direction through the membrane reactor can be conveniently switched during the experiment (Fig 7.5).

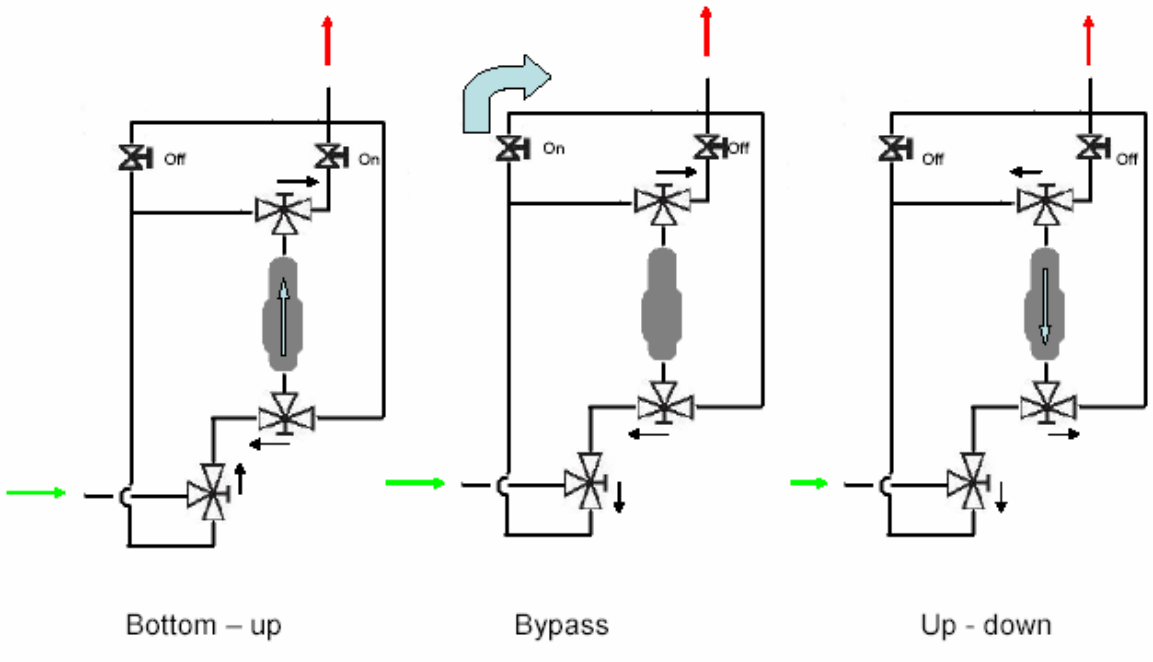

Fig 7.5 Control the direction of reactant flow through the membrane reactor

Fig 7.6 shows the results of such a test in which the catalysis data were collected when the reactants flow through the reactor in both directions. Interestingly, no significant difference in catalytic performance (conversion or selectivity) has been found between the two situations. This result indicates that some factors might have been neglected in the simulation model.

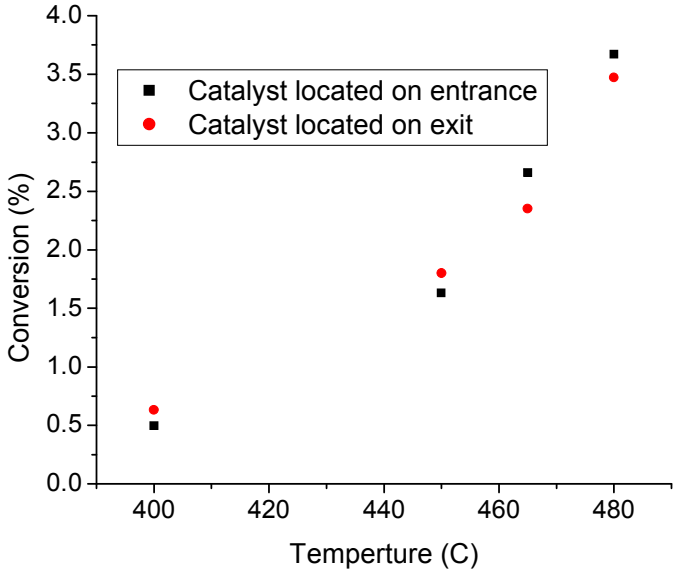

Fig 7.6 Effects of the reactant flow direction on the conversion of a membrane sample with asymmetrically loaded catalytic stripe

As we can find from the above simulation model, when counting the number of collisions on the pore walls, no contribution from the molecules re-entering the nanopore from the low pressure side has been considered. This is reasonable for a specific nanopore. Considering the mean free path of the reactant molecule which is much greater than the diameter of the nanopore, the reactant molecule has a very small chance to re-enter the same pore once leaving it from the exit. However, there is still a good chance that it is bounced back in a collision with another molecule in the gas phase. Such backward movement may cause the reactant molecule to enter another nanopore on the membrane and experience more collisions with the pore walls. Therefore, it seems that the simulation model needs to be modified to include the contribution from the collisions due to the molecules re-entering the nanopores from the downstream (low pressure) side.

With such consideration, the number of hits on the pore walls will mainly concentrate on both ends of the nanopores; and this conclusion is in agreement with the above catalysis experiment results.

Chapter 8

8. Counting the Active Sites through Partially Poisoning the Catalyst in a Heterogeneous System

8.1 Introduction

The titration poisoning of catalysts has been used in both homogeneous and heterogeneous systems for the purpose of counting the active sites. [66, 67] Generally, such poisoning experiments involve the introduction of an inhibitor, which interacts with the active species at a certain stoichiometric ratio and thus makes part of the catalytic sites inactive. The number of active sites can be counted by relating the amount of the introduced poison and the reduction in the catalytic activity. By monitoring the change in the activity while introducing different types of inhibitors, one can possibly determine the nature of different active sites (for example, the Bronsted and Lewis acid sites) in the system. [68] Traditionally, titration poisoning has been carried out in batch reactors for liquid (homogeneous) or liquid/solid (heterogeneous) systems. It's application in the gas/solid heterogeneous reactions carried out in flow reactors has not been fully developed. The poisoning method has been used in a similar but much more inconvenient manner for gas/solid systems, where the poison was introduced onto the catalytic surface ex-situ by incipient wetness impregnation and the partly poisoned catalyst was then tested in heterogeneous reactions. [69] On the other hand, the operando poisoning of Pt/alumina

catalyst by organosilicon compounds during the total oxidation of hydrocarbons has been intensively studied; however, the poisoning mechanism is not based on the direct chemical reaction with the catalytic sites and thus not applicable for counting the active sites on the surface. [70-73] Therefore, there is a need to extend the application of titration poisoning to gas/solid reactions in flow reactors so that the surface active sites in these systems can be conveniently counted.

8.2 Discussion

In the poisoning experiments, hexamethyldisiloxane is used as the poison compound to react with a supported vanadium oxide catalyst in the oxidative dehydrogenation (ODH) of cyclohexane. The proposed surface reaction mechanism corresponding to this poisoning process is presented in Fig 8.1. With such a mechanism, each poison molecule will react with one V^{5+} center on the catalytic surface and deactivate it. Therefore the surface active sites can be counted by correlating the reduction in catalytic activity and the poison compound introduced into the system. However, it is hard to directly detect the gas product from the proposed surface reaction because of the interference from the background ODH reaction. On the other hand, a possible indirect method to testify this mechanism is to run ICP on the completely poisoned membrane samples, from which a relationship between the V and Si atoms attached to the surface can be found. By comparing the Si/V ratios measured on samples exposed to excess amounts of the poison, we can also find out whether or not such surface reaction is specific for V^{5+} centers. (If

the reaction is specific for V^{5+} centers, it is very likely that the measured Si/V ratio stays constant despite the excess amount of the poison introduced; otherwise, we would always see an increasing Si/V ratio as more poison compound is introduced.)

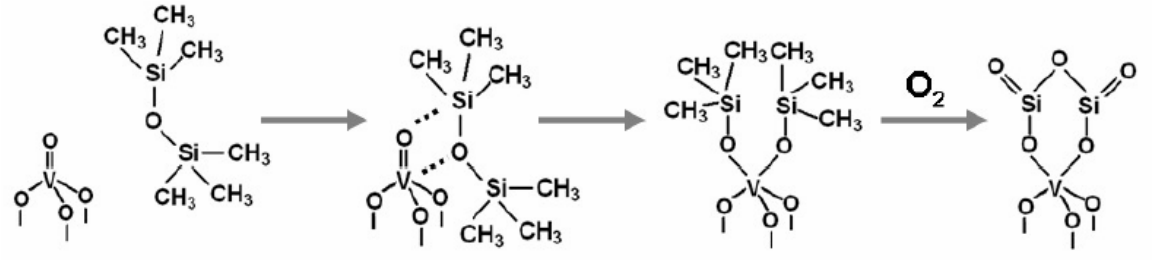

Fig 8.1 The proposed poisoning mechanism of the supported VOx

The detailed instrument setup and procedures of the poisoning experiment have been described in chapter 2. The reaction is carried out in the sealed membrane flow reactor, where the straight one-dimensional channels on the AAO membrane can greatly facilitate the contact between the poison compound and the catalytic surface. For the titration poisoning experiment carried out in a flow system, a sufficient contact between the poison molecules and the active sites is of great importance, since it determines the shape of the poisoning curve from which the information about the number of surface active sites is drawn.

After each poison injection, the activity of the catalyst is continuously monitored over a period of time until it does not change any further. During this process, the activity may drop first and then gradually recover, depending on the residence time of the poison

compound in the catalytic layer and the nature of the chemical reactions between the poison and the surface active sites. Fig 8.2 displays the change in the catalytic activity in the ODH of cyclohexane after the first injection of the poison compound, where a sudden drop in the activity was observed first and then it gradually recovered until finally a steady state is reached. The reaction temperature does not influence the effectiveness of poisoning. However, it influences the rate of the poisoning process in that the steady state can be reached faster when the poisoning experiment is carried out at a higher temperature.

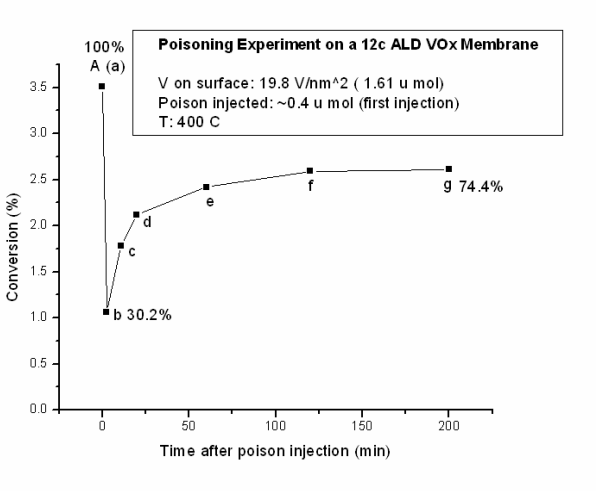

Fig 8.2 The change in catalytic activity after a dose of poison injection

Consecutive injections of the poison compound into the reactor can result in continuous reduction of the catalytic activity. A poisoning curve showing the decrease in the activity of the vanadium oxides in the ODH of cyclohexane with the increasing amount of the poison introduced is displayed in Fig 8.3. All the data points on the curve are taken after the steady state has been reached. Unlike traditional titration processes, the obtained

poisoning curve is not linear, which is probably a typical phenomenon for the titration in a flow reactor, where the chemical equilibrium cannot be reached due to the limited residence time of the poison compound in the catalytic layer.

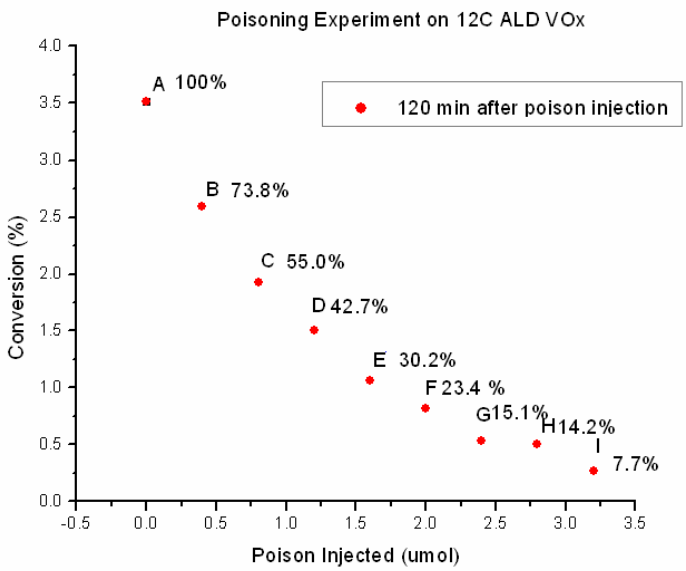

Fig 8.3 The titration poisoning curve on 12C ALD VOx

Fig 8.4 plots the logarithm of the conversion versus the number of poison injections using the data points in Fig 8.3. A nice linear correlation can be found between these two variables, indicating that there is an exponential relationship between the catalytic activity and the amount of poison introduced into the system. For example, the curve in Fig 8.3 can be expressed as Con = (3.7%) × 0.73^{n}, where 3.7% is the initial conversion before any poison injection and n stands for the number of injections. The meaning of this poisoning function is that only 73% of the catalytic activity remains after each injection of an equal amount (~0.4 μmol) of the poison into the system. This exponential correlation can be explained by the limited residence time of the poison compound in the

flow reactor and the gradual decrease in the number of the active sites due to the poisoning of the catalyst. During the poisoning process, the average number of collisions between the poison molecules and the pore walls is nearly constant during their residence in the reactor. The poison molecule will react with the catalytic site and deactivate it once an effective collision occurs. When the poison is introduced for the first time, nearly all such effective collisions can lead to the deactivation of active sites. However, in consecutive poison injections, the chance of surface reaction will become less and less since a fraction of the active sites have already been deactivated. In another word, although the total number of collisions with the pore walls is still the same, the collisions in some regions will be ineffective with respect to deactivating the catalytic sites since no more active sites are available there; and the area of such regions become bigger and bigger as the poisoning goes on. The exponential correlation properly reflects the reaction between the surface active sites and the consecutively injected poison compound in the flow reactor. It is possible to use a circulation system to extend the residence time of the poison compound in the catalytic layer, which can facilitate the complete consumption of the poison in each injection so that a more linear titration poisoning curve can be obtained. Simply reducing the flow rate during poisoning will increase the residence time of the poison compound in the catalytic later, which could also facilitate contact with the catalytic surface and lead to a more linear poisoning curve.

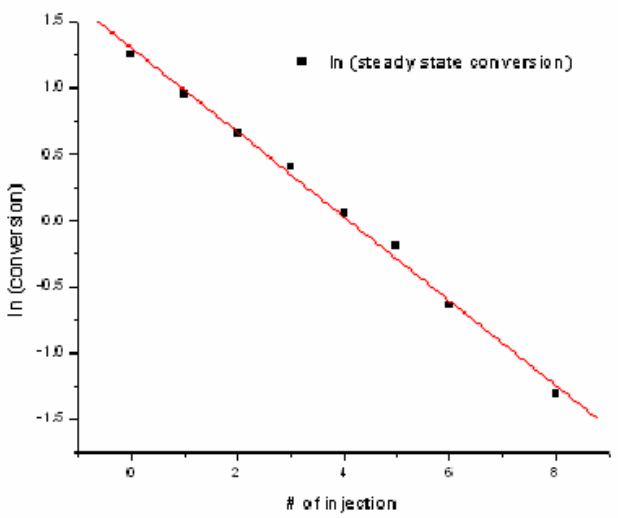

Fig 8.4 Logarithm of the titration poisoning curve where a linear relationship is evident

Estimation on the number active sites can be made using the poisoning function. For example, in the above experiment, 0.4 μmole of the poison compound kills 27% of the catalytic activity during the first poison injection. Therefore the total amount of the active sites in the catalytic layer is estimated to be 0.4÷0.27 = 1.48 μmole. The XRF measurement (calibrated by ICP) on this sample shows that the total amount of vanadium loaded is 1.42 μmole. The measured amount of vanadium is in excellent agreement with the estimated value from the titration curve. As a result, for this sample each V center is probably a distinct active site, which also reflects the excellent dispersion of the catalytic species as synthesized by ALD. In another poisoning experiment carried on a sample using the grafted $V_4(\mu\text{-}O)_6Cp_4$ cluster as the catalyst precursor, the poisoning function is expressed as Con = 10.9% × 0.67^n (Fig 8.5). Since 0.2 μmole of the poison is used in each injection, the total amount of active sites in this sample is estimated to be 0.2÷0.33 =

0.60 μmole. According to the XRF measurement, the amount of vanadium put onto this sample is 0.90 μmole. Therefore in this sample nearly one third of the vanadium species is inactive, which is probably because of the formation of V_2O_5 particles on the surface due to the limitation of the catalyst loading method. This could also be interpreted in terms of each poison molecule deactivating more than one V^{5+} center: since the adjacent V^{5+} sites are presumably closer to each other as they are introduced onto the surface by grafting of the cluster compound, the poisoning of one V^{5+} site could possibly influence the activities of its adjacent sites through some steric or chemical effects. This might also imply that the V centers synthesized by grafting of the cluster compound have some unique catalytic properties: in the ODH reactions, they are more likely to catalyze the hydrocarbon conversion with more than one V^{5+} center working simultaneously on each reactant molecule.

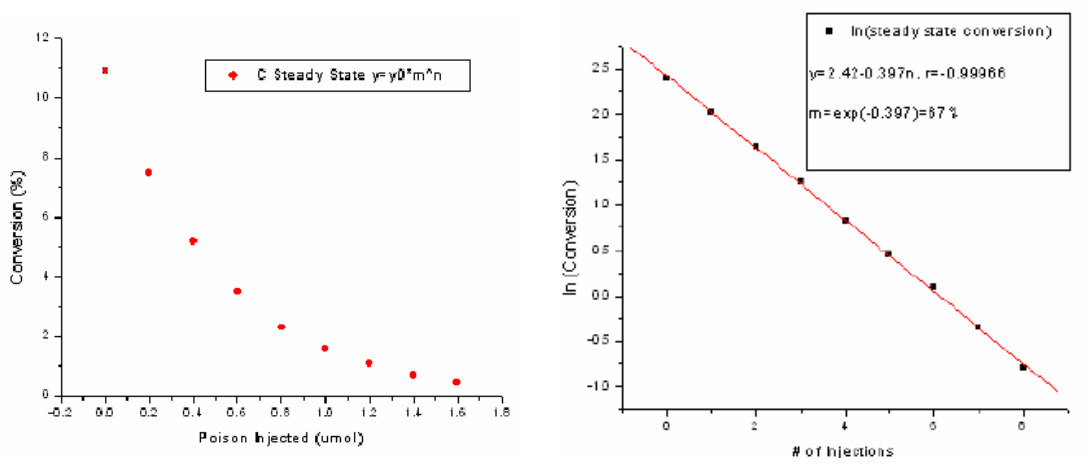

a. **b.**

Fig 8.5 The titration poisoning curve on the $V_4(\mu\text{-}O)_6Cp_4$ cluster

There are two premises of using the poisoning curve to estimate the number of active sites. First, the consumption of the poison in the first injection has to be complete. The un-reacted poison compound should not show up in the composition analysis of the reaction products. Correspondingly, the reduction in the activity should not be too much, say for example, more than 50%, so that all the poison molecules can have a good chance to react with the surface active sites. Therefore a smaller amount of the poison is preferable for each injection. On the other hand, an amount too small will require many injections and consequently take a very long time to obtain the entire titration curve. It is recommended that six to eight poison injections be applied altogether to deactivate most of (>95%) of the surface active sites. Secondly, in the poisoning process an exponential poisoning function has to be obtained, which means that a linear correlation between the logarithm of activity and the number of poison injection has to be found. If the actual poisoning curve deviates much from the exponential function, the above analyses are no longer valid and therefore cannot be used to estimate the number of active sites on the surface.

As has been discussed in previous chapters, in the oxidative dehydrogenation of cyclohexane catalyzed by supported vanadium oxide catalysts, both the isolated monovanadate sites and the polyvanadate domains may be present on the surface. The former sites are believed to be less active but more selective to cyclohexene, the desired partial oxidation product in this reaction; the latter sites are more active but they greatly

facilitate the production of unwanted deep oxidation products (benzene and COx). During the poisoning process, the polyvanadate sites are likely to be killed first because of their higher reactivity; and at the same time the selectivity to cyclohexene might be promoted. Fig 8.6 and Fig 8.7 display the selectivity and the yield to the different products during the poisoning process. As we can see from these graphs, with an increasing amount of the poison introduced, the selectivity to cyclohexene becomes higher and those to the deep oxidation products become lower; the yield to cyclohexene is almost constant during the poisoning process while those to benzene and COx progressively decreases. In such reactions although the poisoning cannot help increase the yield to the more valuable partial oxidation products, it can effectively prohibit the production of the undesired deep oxidation products by preferably disabling the more active but less selective sites. The applicable aspect of this finding is that selective poisoning is promising for preventing the waste of reactants and reducing the need for separating the reaction products.

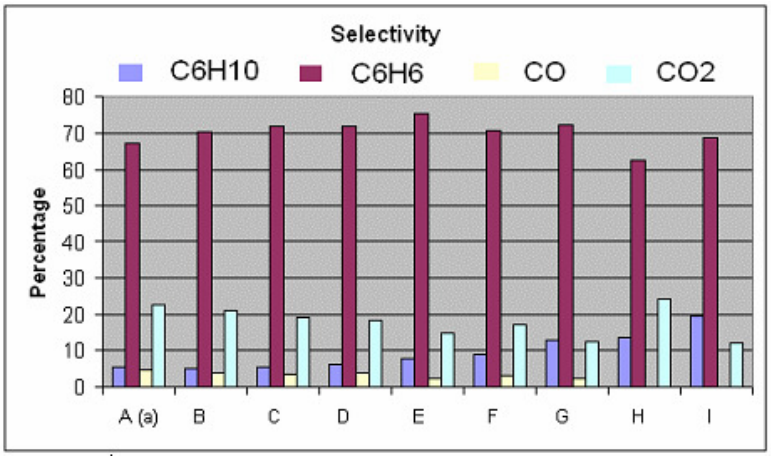

Fig 8.6 The change in selectivity during the poisoning process

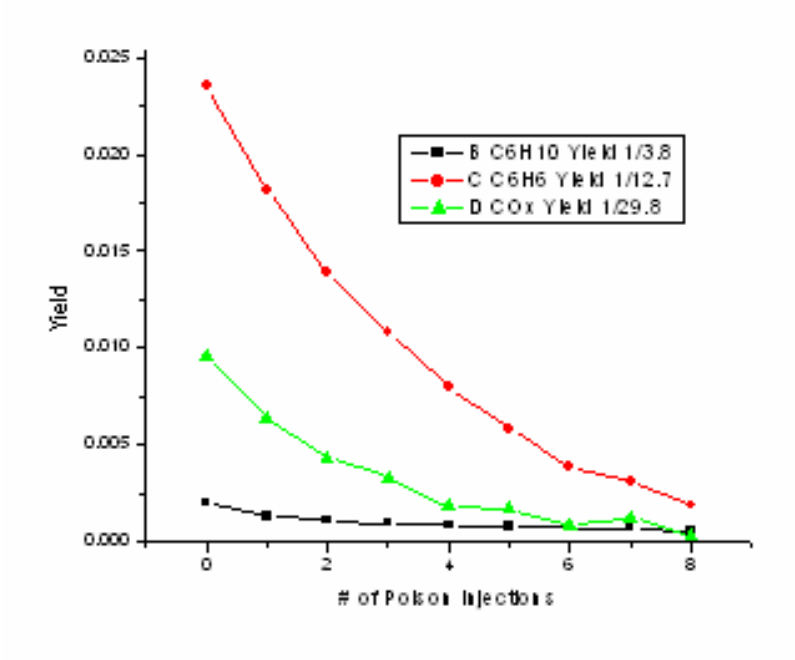

Fig 8.7 The changes in yields to different products during the poisoning process

Chapter 9

9. Summary

This thesis describes the design and application of a novel catalytic system based on the nano-structured AAO membrane. The AAO membrane consists of an assembly of identical pores having nanometer dimensions that span a flow reactor so as to produce an array of nanoreactors. This configuration results in more uniform and tunable contact times than are possible with a conventional fixed bed powder catalyst. The open, one-dimensional channel structure of the AAO membrane facilitates the deposition of coatings and catalytically active materials by ALD. With the combination of AAO and ALD, we are able to precisely control the pore size and shape, the pore wall composition, and the catalyst distribution in the membrane catalytic system.

The arrays of nanoreactors on the AAO membrane make a promising, highly selective catalytic system for some sequential reactions. When the reactants flow through the nano-pores, the limited thickness of the film may dramatically reduce the contact time between reactants and catalyst so that undesired over reactions can be limited to a great extent. In the oxidative dehydrogenation of alkanes to olefins, the application of the membrane catalytic system can effectively separate the partial oxidation products (olefins) before the thermodynamic equilibrium is reached.

The AAO membrane has been successfully mounted in an aluminum ring support by

forming the membrane in the center of an aluminum disc. The membrane connects seamlessly to the aluminum ring so that an airtight seal can be formed between the AAO membrane and a conventional flow reactor by using the supported membrane as a gasket in a standard Swagelok VCR fitting. The straight nanopores on the AAO membrane function as an array of nanoreactors as the reactant flows through them. Attaching catalysts to the walls of the nanopores turns the AAO membrane into a unique catalytic system. These catalytic membranes are stable up to a pressure differential of 11 Psi at temperatures up to 550 °C.

The membrane catalytic system has been compared to a conventional powder bed in the ODH of cyclohexane catalyzed by supported vanadium oxide. In this reaction the membrane system has demonstrated better activity as well as selectivity to the partial oxidation product. These results show that the membrane effectively reduces the residence time of the initial product in the catalytic layer so that the chance of over reaction is largely prohibited. Homogeneous reactions, which lead to the formation of COx, are also largely eliminated with the membrane system because of quenching of the free radicals inside the nanopores. The membrane catalytic system can help make full use of the catalyst in that with the flow-through mode the possibility of bypass from the catalytic pores has been eliminated and all of the catalyst is available for the reaction.

Both mass flow and diffusion contribute to the mass transfer through the nanopores on the AAO membrane. For the dimensional scale of these nanopores, Knudsen diffusion is

the predominant transport mode. The Knudsen diffusion constant is estimated and compared to the mass flow factor. The result shows that mass transfer inside these nanopores is close to the mixed flow model.

The catalytic membranes are prepared by loading the VOx catalysts onto the surface of the AAO using either incipient wetness impregnation or ALD. The XRF measurements on these catalytic membranes indicate that approximately 1/4 monolayer of the VOx is loaded onto the surface of the membrane in each ALD cycle using vanadium oxytriisopropoxide /hydrogen peroxide and water as the precursors. The 1-cycle, 2-cycle, and 4-cycle ALD VOx samples show UV-Vis absorption edge energies similar to the monolayer, 2 layers, and 4 layers wet impregnated VOx, implying that the structure of the catalytic sites are nearly the same on each pair of such membranes.

In the ODH reaction of cyclohexane, the membranes with the ALD VOx show much higher TOF than those with the impregnated VOx, which reflects the better dispersion of the catalytic species synthesized by ALD. With increasing loading of the catalyst, the ALD samples exhibit a rising tendency in the catalytic activity while the activities of the wet impregnated samples remain unchanged. Estimations of the fraction of the catalytically active dispersed VOx on the wet impregnated samples are made by comparing the TOF of the pair of impregnated and ALD samples showing a similar UV-Vis absorption edge energy. The results indicate that on these samples more of the

VOx are in the form of the non-active crystalline V_2O_5 at higher loadings.

VOx catalysts are also synthesized by grafting vanadium containing organometallic clusters (Cp_2V, Cp^*_2V, $V_4(\mu\text{-}O)_6Cp_4$ or $V_4(\mu\text{-}O)_6Cp_4^*$) onto the AAO membrane. In the ODH of cyclohexane, most of these cluster compounds have comparable catalytic performance to their wet impregnated counterparts. The dispersion of the VOx loaded by grafting is not as good as those by the ALD technique, because the toluene solutions of V clusters have difficulty wetting the entire surface of the AAO membrane. However, a cluster sample with a small amount of V_4 grafted on the TiO_2 fabricated membrane shows high selectivity to cyclohexene at relatively high conversions, which might reflect the unique catalytic properties of the VOx prepared from V_4 clusters.

In the membrane catalytic system, the cyclohexane ODH reaction over ALD VOx is found to be almost first order for the hydrocarbon and zero order for oxygen. The observed reaction orders are in agreement with the Mars-Van Kereven redox mechanism, which is typical for the ODH of alkanes over supported metal oxide catalysts. The activation energies of the ALD and impregnated VOx supported on the AAO membranes are comparable to those reported values of the VOx supported on γ alumina. These results imply that the chemical properties of supported VOx are not altered by the AAO scaffold or the ALD loading technique. Therefore ALD can be applied as an alternative method to prepare supported catalysts.

VOx catalysts of different structures are synthesized on the surface of AAO membranes by performing cycles of VOx ALD. In the UV-Vis spectra of these membrane supported catalysts, red shifting of the absorption edge energies with the number of ALD cycles reveals that the predominant form of the supported VOx transforms from monovanadate sites to polyvanadate domains as the loading increases. In the ODH reaction of cyclohexane, a rise in the catalytic activity (TOF) and a decrease in the activation energy is observed with increased loading of the catalyst, implying that the polyvanadate domains are more active than the monovanadate sites. The enhanced activity at higher loadings may be due to a higher reducibility of bigger VOx clusters, the lower density of the surface hydroxyl groups, the smaller distance between adjacent V centers, or a combination of these effects. The selectivity to cyclohexene drops dramatically as the VOx loading increases. Compared at the same conversion, the samples with higher VOx loadings always show lower selectivity to cyclohexene than those with lower loadings. Since the activation process of cyclohexene, a consecutive step in the ODH of cyclohexane, is similar to but easier than that of the alkane, the catalyst which is more active for the reaction of cyclohexane is probably also more active for the reaction of cyclohexene. A concerted reaction mechanism, which requires the presense of at least two V centers, may greatly facilitate the production of benzene on the samples with polyvanadate sites.

The reaction network for cyclohexane ODH is analyzed by comparing the oxidation of cyclohexane, cyclohexene and benzene under the same experimental conditions. It is found that both the sequential and parallel paths exist in the cyclohexane oxidation process. The formation of the deep oxidation products, benzene and COx, can proceed through either the sequential path or the parallel paths, depending on the structure of the supported catalysts. Large domains of VOx appear to facilitate the direct conversion from cyclohexane to the deep oxidation products (the parallel route) while the sequential path is favored on the isolated VOx sites.

The type of support also appears to have significant effects on the properties of the catalyst. VOx supported on ALD TiO_2 and Nb_2O_5 fabricated membranes are almost twice as active as those supported on the Al_2O_3 membrane. At the same time, much lower selectivity to cyclohexene is obtained on these samples. These dramatic differences in the catalytic performance may be due to the different nucleophilicity of the O in the V-O-Support bond, which could determine the ease of H-abstraction in the hydrocarbon activation process. Additionally, since surface acidity may influence the dispersion of the supported VOx, larger domains can form on the surface of TiO_2 or Nb_2O_5, which would promote the catalytic activity and greatly reduce the selectivity to the olefin.

The nano-structured catalytic membrane also provides a platform for using a poisoning

method to count the number of active sites in a gas/solid heterogeneous system. In the poisoning experiment hexamethyldisiloxane is introduced to react with and to deactivate the supported vanadium oxide catalyst in the oxidative dehydrogenation (ODH) of cyclohexane. The surface V centers are counted by correlating the reduction in catalytic activity and the poison compound introduced into the membrane catalytic system. A non-linear titration poisoning curve is obtained by continuously injecting the poison into the flow reactor. This curve has been found to follow an exponential function, which is probably typical for the titration process in a flow reactor where chemical equilibrium can not be reached. Information about the number of active sites can be drawn by analyzing such a titration poisoning curve. On an ALD VOx sample, the estimation on the number of V centers using this method is in excellent agreement with the result of XRF measurement.

References

1. T. Kuo and J. Xu, *Journal of Vacuum Science & Technology B*, **24(4)**, 1925-1933 (2006)

2. http://www.whatman.com/products/?pageID=7.57.293

3. http://www.superiormetals.us/anodized-aluminum-applications.htm

4. A. R. Walpole, E. P. Briggs, M. Karlsson, E. Palsgard, P. R. Wilshaw, *Materialwissenschaft und Werkstoffechik,* **34**, 1064-1068 (2004)

5. H Masuda, M Satoh, and M Satoh, *Appl. Phys.Lett*, **71**, 2770-2772 (1997)

6. Gao T, Zhang J, and Zhang J, *Appl. Phys. A*, **74**, 403-406 (2002)

7. K. Nielsch, F. Muller, A. P. Liand U. Gosele, *Adv Mater*, **12(8)**, 582-586, (2000)

8. Goodwin, J. G., Jr., Kim, S. & Rhodes, W. D. *Catalysis*, **17**, 320-347 (2004)

9. Weitkamp, J., Ernst, S. & Puppe, *Catalysis and Zeolites*, 327-376 (1999)

10. Roy, S., Raju, R., Chuang, H. F., Cruden, B. A. & Meyyappan, *Journal of Applied Physics,* **93**, 4870-4879 (2003)

11. G. Patermarakis, *J of Catalysis* **147** 141 (1994)

12. Li J, Xu J, and Xu J, *Nature*, **402**, 253-254, (1999)

13. S.E. Albo, L.J. Broadbelt, R.Q. Snurr, *AIChE J.* **52**, 3679-3687 (2006)

14. S. M. George, A. W. Ott, and J. W. Klaus, *Journal of Physical Chemistry*, **100**, 13121-12131 (1996)

15. J. W. Elam, M. D. Groner, and S. M. George, *Review of Scientific Instruments*, **73**, 2981-2987 (2002)

16. J. W. Elam, Z. A. Sechrist, and S. M. George, *Thin Solid Films*, **414**, 43-55 (2002)

17. J. A. McCormic, B. L. Cloutier, A. W. Weimer and S. M. George, *Journal of Vacuum Science*

& Technology A, **25(1)**, 67-74 (2007)

18. M. Ritala, M. Leskela, *Handbook of Thin Film Materials*, Ed. H.S. Nalwa, **1**, 103-159 (2002)

19. M. Leskela and M. Ritala, Thin Solid Films, **409**, 138-146 (2002)

20. M Lashdaf, T. Hatanpaa, A. O. Krause, J. Lahtinen, M. Lindblad, and M. Tiitta*, Appl. Catal. A*, **241**, 51-63 (2003)

21. http://www.es.anl.gov/Energy_systems/Atomic_Layer_Deposition/Index.html

22. Cicente Cortes Corberan, *Catalysis Today*, **99**, 33-41 (2005)

23. E. A. Mamedov, and V. Cortes Corbeberan, *Applied Catalysis A*, **127**, 1-40 (1995)

24. H. H. Kung, *Adv. Catal*., **40**, 1-23 (1994)

25. *Kirk-Othmer Encyclopedia of Chemical Technology*; Online ed. Wiley-VCH: Weinheim, (2002)

26. M. M. Bhasin, J. H. Mccain, B. Vora, T. Imai, and P. R. Pujado, *Appl. Catal. A*, **221**, 397-419 (2001)

27. I. Wiehe and F. E. Herkes, *CATTECH*, **7(6)**, 234-236 (2003)

28. J. Dubios, *Catal. Today*, **99(1-2)**, 5-14 (2005)

29. F. Canvani, F. Trifiro, *Catal. Today*, **24(3)**, 307-313 (1995)

30. L. Leveles, *Ph. D Thesis, Netherlands Institute of Catalysis,* Enschede, Netherlands, (2002)

31. P. Mars and D. W. van Krevelen, *Spec. Suppl. To Chem. Eng. Sci*., **3**, 41 (1954)

32. L. Ovens, and H. H. Kung, *Journal of Catalysis*, **144**, 202-213 (1993)

33. K. Chen, A. Khodakov, J. Yang, A. T. Bell and E. Iglesia, *J. Catal*., **186**, 325-333 (1999)

34. Khodakov, A., B. Olthof, Bell, A. T., Iglesia, E. (1999). *J. Cata.,* **181**: 205 (1999)

35. K. Inumaru, M. Misono, and T. Okuhara, *Applied Catalysis A*, **149**, 131-149 (1997)

36. I. E. Wachs, and B. M. Weckhuysen, *Applied Catalysis. A, General*, **157**, 67-90 (1997)

37. L. E. Briand, O. P. Tkachenko, M. Curaya, X. Gao, I. E. Wachs and W. Grunert, *J. Phys. Chem. B*, **108(15)**, 4823-4830 (2004)

38. G. Centi, *Catal. Letters*, **22(1-2)**, 53-66 (1993)

39. R. K. Grasselli, D. L. Stern, J. G. Tsikoyiannis, *Appl. Catal. A*, **189(1)**, 9-14 (1999)

40. F. Cavani, and F. Trifiro, *Catal. Today,* **51(3-4)**, 561-580 (1999)

41. F. Cavani, N. Ballarini, and A. Cericola, *Catal. Today*, **127(1-4)**, 113-131 (2007)

42. R. Burch, and E. M. Crabb, *Appl. Catal. A*, **100(1)**, 111-130 (1993)

43. L. D. Schmidt, J. Siddall, and M. Bearden, *Aiche J.*, **46(8)**, 1492-1495 (2000)

44. A. Beretta, L. Piovesan, and P. Forzatti, J. Catal., **184(2)**, 455-468 (1999)

45. A. Beretta, E. Ranzi, and P. Forzatti, *Chemical Engineering Science*, **56,** 779-781 (2001)

46. K. Sato, M. Aoki, and R. Noyori, *Science*, **281**, 1646-1647 (1998)

47. W. Yao, Y. Chen, M. Liang, H. Fang, Z. Yan, H. Wang and J. Wang, *Journal of Molecular Catalysis: A*, **246**, 162-166 (2005)

48. M. Panizza, C. Resini, G. Busca, E. F. Lopez and V. S. Escribano, *Catalysis Letters*, **89**, 199-205 (2003)

49. H. Masuda, and K. Fukuda, *Science*, **268** 1466-1467 (1995)

50. J. Elam, J. Libera and M. Pellin, unpublished results

51. O. Jessensky, F. Muller and U. Gosele, J. Electrochem. Soc., **145**, 3735-3740 (1998)

52. G. D. Sulka and K. G. Parkola, *Electrochimica ACTA*. **52(5)**, 1880-1888 (2007)

53. G. Xiong, J. Elam, H. Feng, C. Y. Han, H. H. Wang, L. Iton, L. Curtiss, M. Pellin, M. Kung, H. Kung and P. Stair, *J. Phys. Chem. B,* **109 (29)**, 14059 -14063 (2005)

54. Y. Du, W. L. Cai, C. M. Mo and J. Chen, Applied Physics Letters, **74**, 2951-2953 (1999)

55. Stair, P., Marshall, C., Xiong, G., Feng, H., Pellin, M., Elam, J., Curtiss, L., Iton, Ll, Kung, H., Kung, M., Wang, H. –H, *Topics in Catalysis*, **39**, 181-186 (2006)

56. M. Y. Sinev, L. Y. Margolis and V. N. Korchak, Russian Chemical Reviews, **64**, 349-364 (1995)

57. Octave Levenspiel, *Chemical Reaction Engineering*, **3rd Ed**. (1997)

58. G. Gutierrez and B. Johansson, *Physical Review B*, **65**(10), 104202-104211 (2002)

59. J. Elam, G. Xiong, C. Y. Han, H. H. Wang, J. P. Brirell, U. Welp, J. N. Hryn, M. Pellin, T. Baumann, J. Poco and J. Satcher Jr., *Journal of Nanomaterials*, **2006**, 1-5 (2006)

60. A. Dejoza, J. M. Lopez, F. Melo and I. Vazquez, *Ind. Eng. Chem. Res*., **36**, 2588-2596 (1997)

61. X. Gao and I. E. Wachs, *Journal of Physical Chemistry: B*, **104**, 1261-1268 (2000)

62. R. Gapal, and C. Calvo, *Acta. Crystallogr., Sect. B: Struct. Sci*., **30**, 2491 (1974)

63. R. Shannon, *Acta. Crystallogr., Sect. A: Found. Crystallogr*. **32**, 751 (1976)

64. R. T. Sanderson, *Journal of Chemical Education*, **65**, 112 (1988)

65. R. Redon, A. V. Olmos, M. E. Mata-Zamora, A. O. Medrano, F. R. Torres and J. M. Saniger, *Rev. Adv. Mater. Sci*., **11**, 79-87 (2006)

66. J. V. Sinisterra, F. Garcia-Blanco, M. Iglesias and J. M. Marinas, Reaction Kinetics and Catalysis letters, **27**, 263-267 (1985)

67. J. Mejzlik, M. Lesna and J. Kratochvila, *Advances in Polymer Science*, **81**, 83-120 (1986)

68. D. C. Calabro, J. C. Vartuli and J. G. Santiesteban, *Topics in Catalysis*, **18**, 231-242 (2002)

69. A. Larsson, J. Einvall, A. Anderson and M. Sanati, *Energy & Fuels*, **20**, 1398-1405 (2006)

70. R. H. Savage, *Journal of Chemical Physics*, **16**, 237-240 (1948)

71. M. Matsumiya, W. Shin, F. Qiu N. Izn, I. Matsubara and N. Murayama, *Sensors and Actuators B: Chemical*, **96**, 516-522 (2003)

72. M. Rahmani and M. Sohrabi, *React. Kinet. Catal. Lett*., **86**, 397-405 (2005)

73. M. Rahmani and M. Sohrabi, *Kinetics and Catalysis,* **47**, 891-900 (2006)

Curriculum Vitae

PERSONAL INFORMATION

Name	Hao Feng
Date of Birth	Oct 6, 1979
Place of Birth	Shaanxi, China
Nationality	China

EDUCATION

Ph.D. in Chemistry, Northwestern University, Dec 2007, Evanston, IL
Dissertation: "Nanostructured membrane catalysis"

B.S. in Chemistry, Peking University, June 2002, Beijing, China.

EXPERIENCE

2002-2007 Research Assistant, Northwestern University, Evanston, IL
Adviser: Professor Peter C. Stair

Studied the cyclohexane oxidative dehydrogenation (ODH) reaction over vanadium oxide catalysts supported on nano-structured porous alumina membranes. Demonstrated the advantages of the membrane catalytic system in terms of the better activity and selectivity.

Explored the kinetics and mechanism of the cyclohexane ODH reaction. Investigated the factors influencing the catalytic performances and optimized the reaction system.

Developed the device for the mass-production of porous alumina membrane supports. Designed the membrane flow reactor towards the application of the membrane support as a potential highly efficient and selective catalytic system.

2003-2004 Research Assistant, Argonne National Laboratory, IL
Adviser: Dr Hsien-Hau Wang

Synthesized and characterized the nano-porous alumina membranes and other novel nano-structures based on these membranes.

1998-2002 B.S. Thesis Research, Peking University, Beijing, China
Adviser: Professor Zhongfan Liu

Worked on the CVD synthesis, purification, characterization, chemical fabrication and assembling of single-wall carbon nanotubes.

PATENTS/PUBLICATIONS

Counting the Number of Active Sites and Enhancing the Catalytic Selectivity through Partially Poisoning the Catalyst in a Heterogeneous System, Feng, H., T. J. Marks and P. C. Stair, **US Patent Application in Process.**

Towards Nano-Reactor Arrays: Nano-Structured Membrane Catalysis, Feng, H., J. W. Elam, H. –H. Wang, L. A. Curtiss, M. J. Pellin and P. C. Stair, *Chemistry of Materials,* 2007. **To Be Submitted.**

Oxidative Dehydrogenation of Cyclohexane over Vanadium Oxide Catalysts Supported on the Nanoporous Alumina Membrane, Feng, H., J. W. Elam, J. Libera, M. Kung, H. Kung and P. C. Stair, *Journal of Catalysis,* 2007, **To Be Submitted.**

Structure-Function Relationship of the Vanadium Oxide Catalysts Supported on the AAO Membrane, Feng, H., J. Libera, J. W. Elam, M. J. Pellin, M. Kung, H. Kung and P. C. Stair, *Journal of Catalysis,* 2007, **To Be Submitted.**

Novel, Uniform Nanostructured Catalytic membranes, Stair, P. C., C. Marshall, G. Xiong, H. Feng, M. J. Pellin, J. W. Elam, L. Curtiss, L. Iton, H. Kung, M. Kung, and H. –H. Wang, *Topics in Catalysis*, 2006, **39**(3-4): p. 181-186.

Effect of Atomic Layer Deposition Coating on the Surface Structure of Anodic Aluminum Oxide Membrane, Xiong, G., J. W. Elam, H. Feng, C. Y. Han, H. –H. Wang, L. E. Iton, L. A. Curtiss, M. J. Pellin, M. Kung, H. Kung, and P. C. Stair, *Journal of Physical Chemistry* B, 2005. **109**(29): p. 14059-14063.

ABSTRACTS/PRESENTATIONS

"Nano-structured Membrane Catalysis in the ODH of Cyclohexane", H. Feng, J. Libera, J. W. Elam, M. J. Pellin, H.-H Wang, H. Kung, M. Kung and P. C. Stair, ***234th American Chemical Society National Meeting,*** Aug 2007, Boston, MA.

"Vanadium Oxide Catalysts in the AAO Scaffold", H. Feng, J. Libera, J. W. Elam, M. J. Pellin, H.-H Wang, H. Kung, M. Kung and P. C. Stair, ***International Symposium on Relations between Homogeneous and Heterogeneous Catalysis,*** Jul 2007, Berkeley, CA.

"Nano-structured Membrane Catalysis", H. Feng, J. W. Elam, M. J. Pellin, H. Kung, M. Kung and P. C. Stair, ***20th North America Catalysis Meeting,*** Jun 2007, Houston, TX.

"Preparation and Application of the Nano-structured Catalytic Membranes", H. Feng, J.

W. Elam, M. J. Pellin, and P. C. Stair, (oral and poster presentations, winner of the student poster award), ***Gordon Research Conference on Catalysis***, Jun 2006, New London, NH.

PROFESSIONAL ACTIVITIES

American Chemical Society
Chicago Catalysis Club